PORE PRESSURE PREDICTION AND DIRECT HYDROCARBON INDICATOR: INSIGHT FROM THE SOUTHERN PLETMOS BASIN, OFFSHORE SOUTH AFRICA.

A Thesis in Applied Geology (Petroleum Geology Option)

BY

AYODELE OLUWATOYIN LASISI

Submitted in Fulfilment of the Requirements for the Degree of Magister Scientiae (MSc.) in the Department of Earth Sciences,

University of the Western Cape,

CapeTown, South Africa.

Supervisor: **Dr. Mimonitu Opuwari.**

Co-supervisor: **Prof. Jan Van Bever Donker.**

June, 2014

DECLARATION

I declare that my research work titled “Pore Pressure Prediction and Direct Hydrocarbon Indicator: Insight from the Southern Pletmos, Bresdasdorp Basin, Offshore South Africa” is my own work, that it has not been submitted before for any degree or examination in any other university, and that all the sources I have used or quoted have been indicated and acknowledge by means of complete references.

Oluwatoyin L. AYODELE. June, 2014.

……

Signature

ACKNOWLEDGEMENT

My greatest thanks go to God almighty for his provision, gift of life, and strength during the course of my study. My sincere appreciation goes to my supervisor, Dr. Mimonitu Opuwari for his constructive criticism, proof reading, advise, patience and support throughout the period of this research, may God almighty bless you. I also wish to express my unflinching thanks to Professor Jan Van Benker Donker, co-supervisor, department of Geology for his time, patience in proof reading this work as well as his invaluable advice and creating a condusive atmosphere in writing this thesis.

My sincere gratitude goes to the Inkaba-ye Africa for sponsoring my studies through its scholarship scheme. However, special thanks go to Petroleum Agency, SA for providing the data used for this research work.

I would also express my appreciation to Dr. Oluwaseun Fadipe, for his financial support, provoking comments and the time spent to review the chapters of this thesis. Also, Mr. Chris Samakinde (MSc), for his assistance in reviewing the chapters as well. Special thanks go to my fellow post graduate students in Lab 59 & 60, mostly Haajierah Mosavel for the motivation and assistance rendered during the course of this research, Moses Magoba, Hakundwi Mandende, Senzanga Khona, Sedzani Nethenheni for creating an enabling environment to the success of this study and Buhle Ntshele the dearest one.

More gratitude goes to my fellow brothers and friends Dr. Agbele Kehinde, Mr. Ayodele Egunlusi (Pharmacist), Mr. Tosin Aina (Mphil), Mr. Seyi Abegunde. The list is endless I am only human to leave out some names.

Finally, I want to appreciate the effort of my Mom, Stella Ayodele for her spiritual prayer support and encouragement, May God almighty grant you long life (amen). I also thank my siblings for their support throughout this endeavour.

.

Contents

List of Figures

List of Table

List of Appendices

ABSTRACT

An accurate prediction of pore pressure is an essential in reducing the risk involved in a well or field life cycle. This has formed an integral part of routine work for exploration, development and exploitation team in the oil and gas industries. Several factors such as sediment compaction, overburden, lithology characteristic, hydrocarbon pressure and capillary entry pressure contribute significantly to the cause of overpressure. Hence, understanding the dynamics associated with the above factors will certainly reduce the risk involved in drilling and production. This study examined three deep water drilled wells GA-W1, GA-N1, and GA-AA1 of lower cretaceous Hauterivian to early Aptian age between 112 to 117.5 (MA) Southern Pletmos sub-basin, Bredasdorp basin offshore South Africa. The study aimed to determine the pore pressure prediction of the reservoir formation of the wells. Eaton's resistivity and Sonic method are adopted using depth dependent normal compaction trendline (NCT) has been carried out for this study. The variation of the overburden gradient (OBG), the Effective stress, Fracture gradient (FG), Fracture pressure (FP), Pore pressure gradient (PPG) and the predicted pore pressure (PPP) have been studied for the selected wells.

The overburden changes slightly as follow: 2.09g/cm3, 2.23g/cm3 and 2.24g/cm3 across the selected intervals depth of wells. The predicted pore pressure calculated for the intervals depth of selected wells GA-W1, GA-N1 and GA-AA1 also varies slightly down the depths as follow: 3,405 psi, 4,110 psi, 5,062 psi respectively. The overpressure zone and normal pressure zone were encountered in well GA-W1, while a normal pressure zone was experienced in both well GA-N1 and GA-AA1.

In addition, the direct hydrocarbon indicator (DHI) was carried out by method of post-stack amplitude analysis seismic reflectors surface which was used to determine the hydrocarbon prospect zone of the wells from the seismic section. It majorly indicate the zones of thick hydrocarbon sand from the amplitude extraction grid map horizon reflectors at 13AT1 & 8AT1 and 8AT1 & 1AT1 of the well GA-W1, GA-N1 and GA-AA1 respectively. These are suggested to be the hydrocarbon prospect locations (wet-gas to Oil prone source) on the seismic section with fault trending along the horizons. No bright spot, flat spot and dim spot was observed except for some related pitfalls anomalies.

Keywords: Pore pressure, Hydrocarbon, Direct Hydrocarbon Indicators (DHIs), Seismic, Amplitude, Reservoirs, Disequilibrium, Compaction, Bright spot, Flat spot and Dim spot, Overburden, Fracture gradient, Fracture pressure, Bredasdorp basin, South Africa.

CHAPTER ONE

1.1: Introduction

Bredasdorp Basin of the passive continental margins of South Africa has experienced incessant hydrocarbon exploration due to its' economic importance to the country, therefore much attention is increasingly laid down on the petroleum system processes of the basin for the economic viability of the basin. Petrophysica properties are very important in assessing hydrocarbon accumulation potential of a reservoir rock and must be evaluated to determine the hydrocarbon in place before any decisions are made. This study involves the pore pressure prediction from well logs and seismic data to evaluate the pore pressure condition, the direct hydrocarbon indicator from seismic data to delineate the prospect zone of the hydrocarbons potential reservoir in Bredasdorp basin. Exploration in South Africa began in the 1940s by Geological Survey of South Africa. The exploration activity in 1981 and 1991 advanced to 181 exploration wells drilled, with the Bredasdorp Basin being of primary focus resulting in several oil and gas discoveries (Petroleum Agency SA, 2004/5). However, The Pletmos Basin is proven to have working petroleum systems with numerous oil shows, mature oil- to wet-gas prone source rocks and good quality reservoir sandstones.

However, determining the overpressure zone prior to drilling of reservoir is quite essential for the petroleum industries. Success in drilling, and reservoir depletion procedures are all affected by presence of overpressure strata. Thus, for successful drilling of reservoir wells, it is extremely important to estimate the pore pressure conditions of a given well. The appraisal of the pore pressure will be utilized for mud weight and the casing design, because if the mud weight is not designed for the right pore pressure, hazards such as blowout due to "kicks" and loss of circulation may happen. Likewise, wellbore dependability issues, for example, borehole breakout or stuck pipes might be avoided based on good estimation of pore pressure prediction. Direct hydrocarbon indicator (DHI) has been successfully used in petroleum

industry to search and locate hydrocarbon deposit in a thin bed by means of seismic reflection coefficient inherently changes. This is due to differences in the acoustic impedance of the hydrocarbon bearing zone which occur when gas-oil replace the small intervening spaces of brine water in existing reservoir.

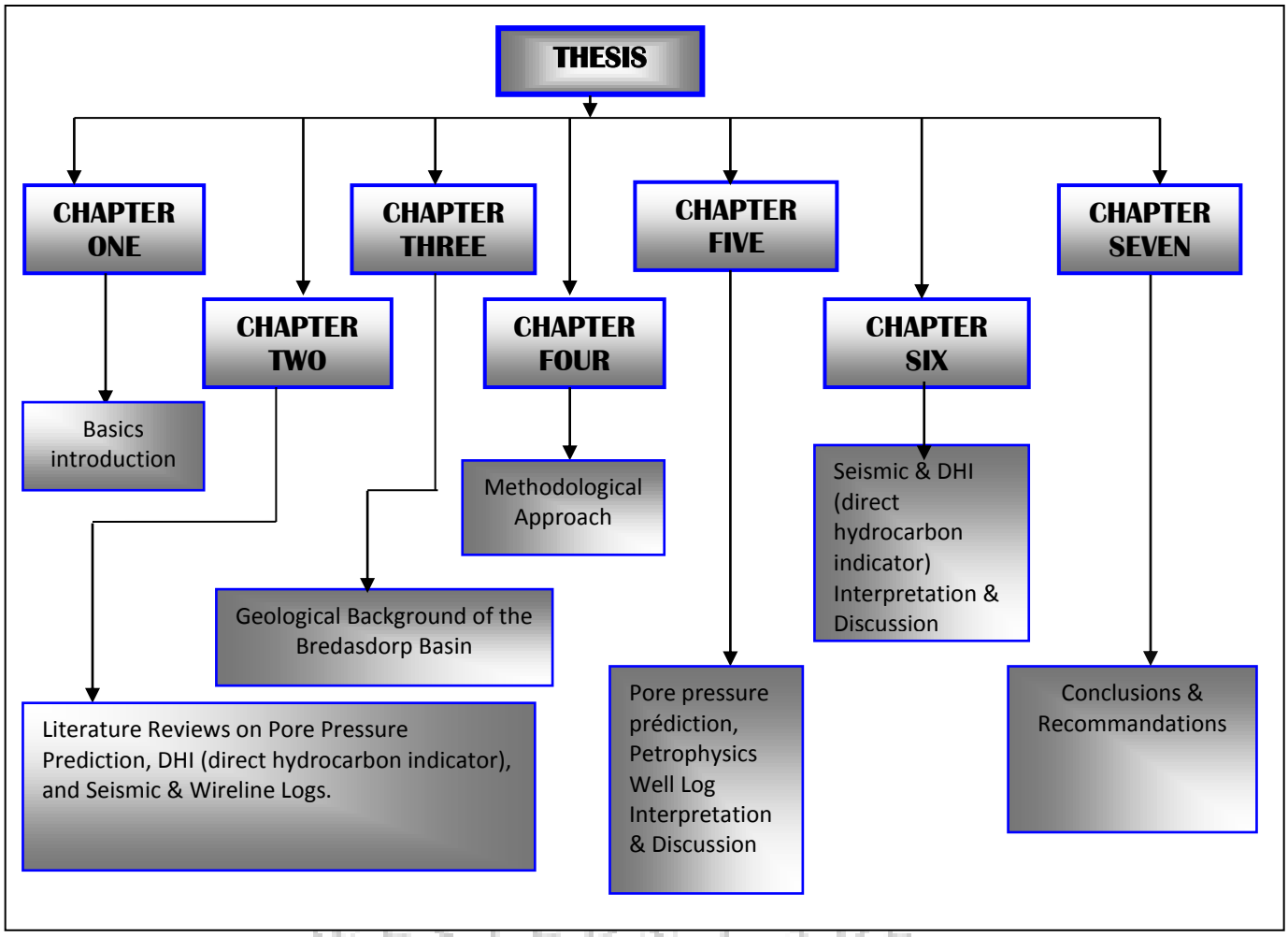

Figure 1: Frame work diagram of the thesis.

1.2: Aims

This study aimed to investigate the pore pressure prediction of sub-surface overpressure zones reservoir of some selected drilled wells Ga-N1, Ga-W1 and Ga-AA1. In order to avoid risk of blow-out and other drilling hazards in Pletmos, Bredasdorp Basin, Offshore South Africa. The geological features such as bright spot, dim spot and flat spot as well as sand region will be

adequate examine to locate the possible of hydrocarbon prospects on seismic section for the selected well.

1.2.1 The objective of the study

The main objective is to accurately predict the pore pressure conditions of the selected wells Ga-N1, Ga-W1 and Ga-AA1 located at the Southern Pletmos sub-basin Bredasdorp Basin offshore South Africa. The three wells serve are deep-water exploratory wells, which has been drilled to depths of (3205 m, 3320 m and 3560 m), respectively. The formation of interest for the study wells are within the Lower Cretaceous period (Hauterivian to early Aptian) between 112 to 117.5 (Ma). Understanding the pore pressure conditions will in drilling plan for safety, economically and efficiently drilling the wells required to test, produce oil and natural gas accumulations. Also, to have a proper casing points and design adequate casing programmed for the well to effectively drill and maintaining well control during and completion operation. Well control activity such as lost circulation, formation fluids kicks, surface blowout and underground blowout can be avoided with the uses of accurate pore pressure prediction.

In addition, the direct hydrocarbon indicator (DHI) interpretation will be carried out by means of using Post-stack amplitude analysis seismic reflectors surface (bright spots, dim spot and flat spot as well as sand region). Through the horizon picking from the seismic based on well tops. This will be used to delineate possible of hydrocarbon prospects locations on the seismic section for wells in the basin.

1.3: Scope of work

The scope of work is as follow: **Section 1: Pore pressure prediction analyses.**

- Well logs interpretation.
- Pore pressure prediction determination by establishing Eaton's pore pressure prediction methods of resistivity with depth-dependent normal compaction trend line to analyze:
- Pore pressure gradient calculation.
- Calculation of the pore pressure.
- Calculation of the overburden gradient stress relationship.

- Calculation of the effective stress.
- Calculation of the fracture pressure effects
- Development and estimation of the resistivity shale effects.
- Calculation of the fracture gradients.
- Calculation of the fracture pressure.
- Calculation of the mud weight.
- Development of the Normal conductivity (compaction) Trend-line (NCT).
- Result and conclusion of the Eaton's pore pressure prediction methods using formation resistivity measurements.
- Establishments of the interval velocity transit time (DT, sonic log) to predict the formation pore pressure condition from the seismic.
- Establishment of the tomography grid map from the seismic to delineate the layered model of the pore pressure image.

Section 2: Direct hydrocarbon indicator (DHI).

- The Post-stack amplitude analysis seismic reflectors surface extraction techniques will be used to validates the direct hydrocarbon indication, (DHI).
- Identification of bright spot, flat spot and dim spot as well as Sand region by means of horizon picking to delineate the possible presence of hydrocarbons location on the seismic section.
- Horizons picking interpretation.
- Amplitude extraction grids maps of the horizons generation to delineate the bright spot, flat spot, dim spot and the Sand region on geometry of the basin.
- Time grids map of the horizon used to delineate the depth variation across the horizon.

1.4: Local geology of study areas.

The study area focuses on the Pletmos Basin as one of the five sub-basins in the Outeniqua Basin off the south coast of South Africa and covers approximately 18000km^2. The Outeniqua Basin is bounded to the west by the Columbine-Agulhas Arch, to the east by the Port Alfred Arch and to the south by the Diaz Marginal Ridge as indicated in the figure 1.4a It comprises a series of rift sub-basins which are separated by fault-bounded basement arches comprising Ordovician to Devonian metasediments of the Cape Supergroup. The Southern Pletmos sub-basin, the survey confirmed the presence of large dome structures within the synrift succession along the periphery of the basin.

Sediment thicknesses up to 9000 m have been mapped adjacent to basin-bounding faults. However, the study area is bounded in the west and east by geographical co-ordinates as indicate in Table 1 each of the well Ga-AA1, Ga-W1 and Ga-N1 studied are located within Block 11a Ga-gas-field of the basin.

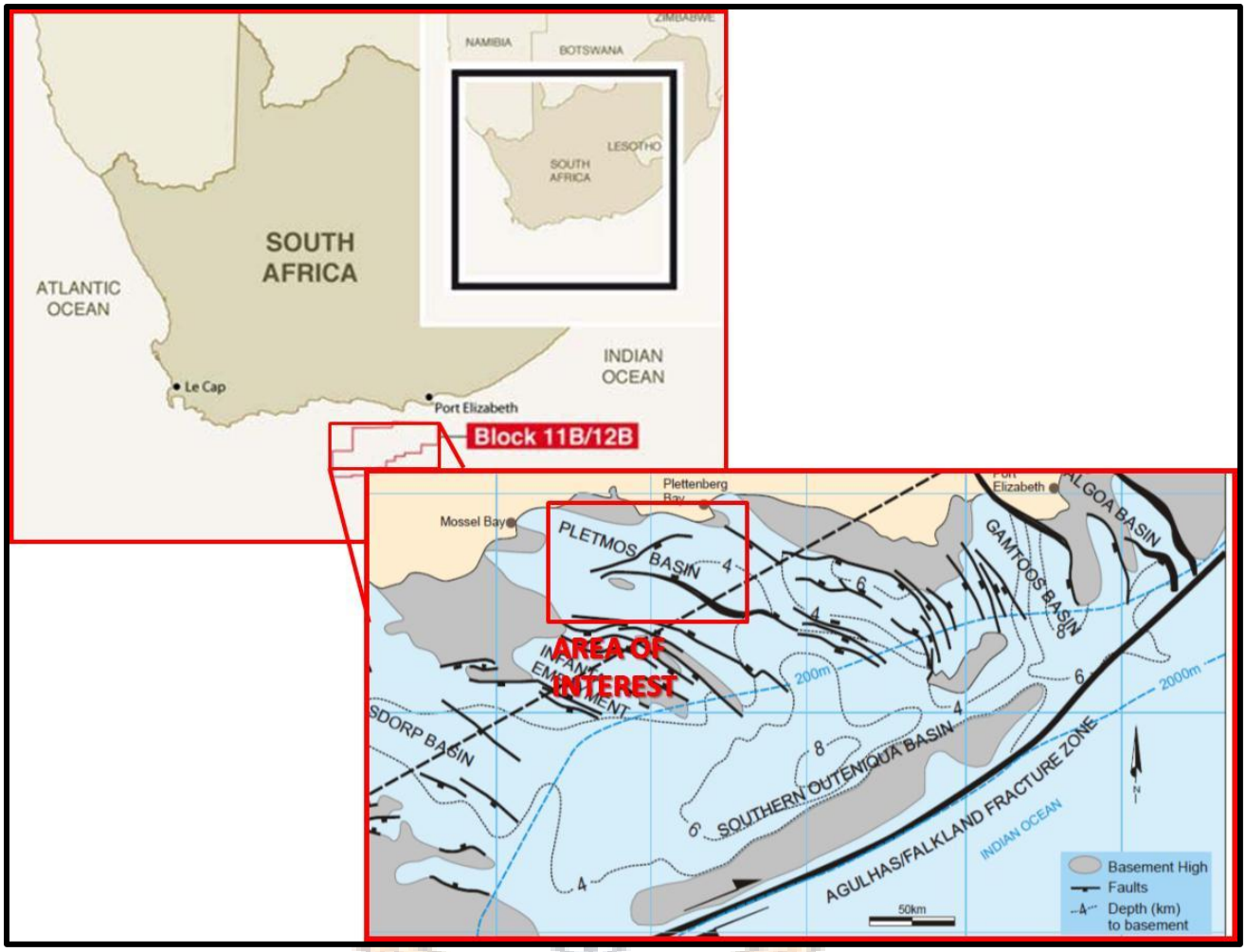

Figure 1.4 a. The map showing the locality of the Pletmos sub-basin and the block of the study well.

Table 1 : Showing the name and location of the well.

Well Name	Location	UTM Format	Depth (M)	Total Depth Drilled (meters)
GA-AA1	Lat: 34°39'32" S	620571.9 E	3860 m	3776 m
	Long: 28°18'57" E	3836003.6 N		
GA-N1	Lat:34°41'15.82" S	700232.7 E	3205 m	3184 m
	Long:23°11'8.99"E	3840588.4 N		
GA-W1	Lat:34°35'38.37" S	706643.3 E	3320 m	2495 m
	Long:23°15'11.74"E	3830327.5 N		

1.5: Exploration and production history on pletmos basin, (block 11 a)

SOEKOR (Southern Oil Exploration Corporation), the state owned oil and gas Exploration Company, (petroleum oil and Gas Corporation of South Africa) discovered gas and oil deposits offshore in Pletmos basin Block 11a in the Bredasdorp Basin. The records show that Ga-gas field of the Pletmos basin majorly Ga-A1 was the first borehole in the Pletmos basin drilled in 1968, which produced gas at potentially commercial rates (22million cf/d) from the synrift shallow marine sandstones and fracture quartzite basement of Ordovician to Devonian age. However, records shows that more than forty wild cats, mostly on synrift structures, have been drilled throughout the Pletmos Basin and Infanta embayment north of the Southern Outeniqua Basin. The gas flow rates between “24 and 5’’ million cf/d with minor amount of NGL (natural gas liquid) were measured. Sandstones from 1,565 - 2,500 ms subsea have porosities of up 25%, averaging between 11% to 18% and the permeabilities which range between 10 and 100 mD, with a maximum of 450mD, (SOEKOR), for instance, a test performed within the fractured Table Mountain group quartzite basement flowed 11 million cf/d of gas. Borehole drilled in the southern Pletmos Basin intersected gas-saturated sandstones within the synrift succession. It shows a large percentage of the dry gas in synrift reservoir has been derived by up-dip

migration from early-rift shales (Kimmeridgian) lyin within the Southern Outeniqua Basin. This area is regarded as a major hydrocarbon kitchen with multiple drift source rocks lying within the oil window.

The hydrocarbon prospects of the Pletmos Basin, in the early cretaceous, synrift sequence, good reservoir are expected within deep marine fan and channel sandstones in the Southern Outeniqua Basin. However, some good quality wet gas to oil-prone shales is postulated to occur at the base of the aggradation infill succession over the Southern Outeniqua Basin. Source shales varying from the dry gas to wet gas and oil have been encountered in the southern Pletmos Basin and Plettenberg graben which are presently fall in the wet gas-to oil maturity window. However, in the mid of post rift sequence in the cretaceous, wet gas to oil-prone source shale have been intersected in the southern Pletmos Basin are expected to follow the established regional trend of improvement in quality and thickness towards the Southern Outeniqua Basin.

CHAPTER TWO

LITERATURE REVIEW:

2.0: Introduction:

This chapter offers the background information relating to overpressure formation and it effect to drilling operations in Oil and gas industries. Mindful effort is made to the use of definitions and explanations mostly recognized among the professionals in the oil and gas industries. Also, the chapter begins with basic commonly terminology used by pore-pressure professionals, with an overview of understanding of mechanisms that causes overpressure in the subsurface.

The review also focused on Pore pressure, direct hydrocarbon indicator (DHI), Seismic data and Geophysical well log (wireline logs). These was carried out in order to gain the knowledge of pore pressure prediction methods and the direct hydrocarbon indicators in determining the lithology fluid content that are likely filled with hydrocarbon location based on seismic reflectance of amplitude such as bright spot, flat spot and the dim spot in the selected wells. This chapter also showing the example of over pressure from around the world, and collective used overpressure estimation and detection approaches are describe in this section as follow order.

2.1: Basic terminology:

2.1.0 Pressure:

Pressure is defined as the expression of a force exerted on a surface per unit area, is a scalar quantity and fundamental physical value which presented with a single value in each location. The standard unit of pressure is Pascal (Pa), which equivalent to one Newton per metre squared (N/m^2 or $N .m^{-2}$). Pressure generally has only a real meaning for fluids not solids. In a porous media, pressure is often term as the pressure within the fluids in the pore, i.e the pore pressure which generally increased with depth.

2.1.1: Hydrostatic pressure:

Hydrostatic pressure is the pressure applied by static column of fluid with a reference depth, which dependent on the formation fluid density, typically water or brine, and the true vertical height of the column of fluid. In real sense, atmospheric pressure also subsidized to the hydrostatic pressure, but has a relatively small value which often neglected without showing any important error. Hydrostatic pressure can be calculated as follow by the expression below:

$Ph = pgH$……equation (2.0)

Where Ph is the hydrostatic pressure, p is the average density of the fluid, g is the acceleration due to gravity and the H is the vertical height of the column water. This equation can as well expressed as the rate at which hydrostatic pressure changing with depth i.e., the hydrostatic pressure gradient as expressed in the equation below:

$\delta Ph/\ \delta H = pg$……equation (2.1)

However, for this project, the density value of water 1.025 g/cc (0.433 psi/ft) used as the average formation water density.

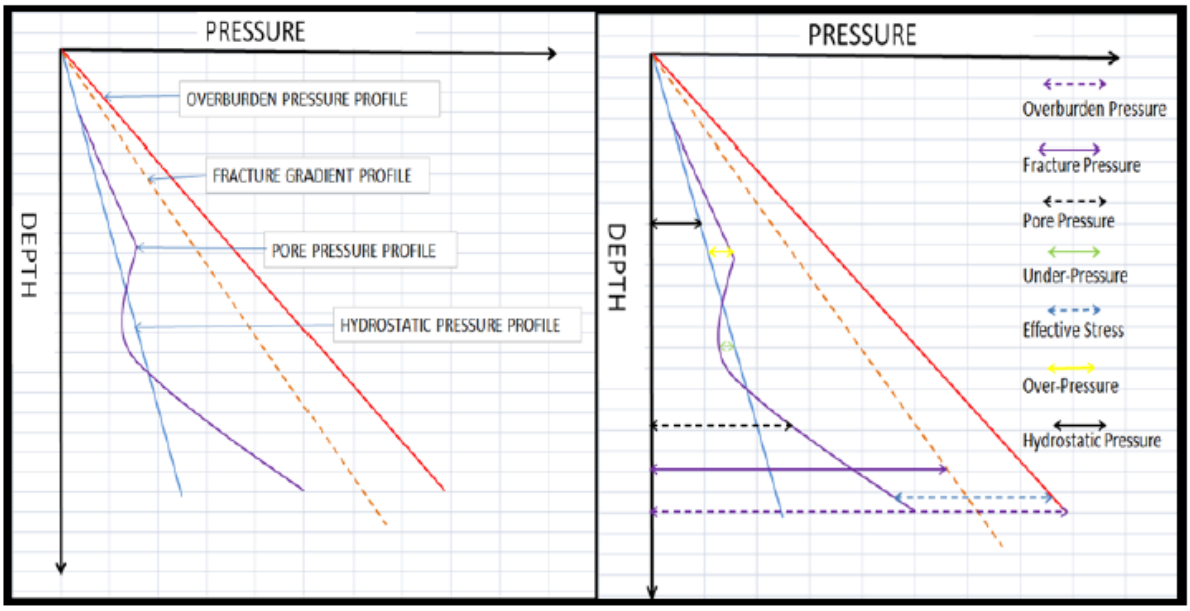

Figure 2.1 showing the diagram pressure- depth plot with the sketch of typical terminologies used in pore pressure prediction.

2.1.2.Overburden pressure:

The Overburden pressure also regarded as the overburden, lithostatic or the vertical stress, is the pressure applied at specific depth by the weight of the overlying sediments with the containing fluids. In over-all, when the density data are unobtainable or untrustworthy, an overburden gradient of 1 psi/ft is often used as default. But with the availability of data's, more accurate evaluation based on the lithology and density tied with information of local geology is desirable. For the overburden estimation of this project, the mudline density is 1.06 g/cc. In contrast, the bottom-hole densities range at 2.3g/cc. The highest contest with overburden evaluation is the any huge gaps in the data and the extrapolation of density data from underneath in the shallow section of the well where density was not logged.

The overburden stress, S_V, is calculated by using this expression below:

Sv = ρbZ……equation (2.2)

Where ρb is the average formation bulk density and the Z' is the thickness of vertical overlying sediment.

The bulk density is the density of the whole rock, i.e., the matrix and the fluid inside the pores. This is expressed as follow:

$\rho b = \rho m(1-\varphi) + \rho f \varphi$……equation (2.3)

Where φ the porosity is expressed as a fraction, ρf is the formation fluid density, and ρm is the matrix formation density.

2.1.3 Pore pressure:

Pore pressure is defined as the pressures of the fluid occupied in the pore spaces of sediments or any other rock matrix (Mouchet and Mitchell, 1989). It's also known as the formation pressure. Pore pressure can be estimated ramblingly by comparing expected normal and actual density, neutron, sonic, or resistivity responses from the wireline logs. In addition, direct measurement of pore pressure can only be anecdotal through measurement of pressure within the adjacent permeable beds or from the indirect indication such as caving, gas, mud weight or even the rate of penetration (ROP) while drilling.

However, pore pressure prediction is major components of exploration risk analysis. The knowledge of formation pressure is very important in the evolution of oil and gas field. Understanding of the reservoir formation pore pressure is an essential mechanism for the

petroleum Geologist to determine the potential traps, seals, mapping of hydrocarbon migration pathway, analysing trap configuration and basin geometry as well calibration for basin modelling. Also predrill pore pressure prediction is major criteria for engineers to ensure the safe drilling plan and economic subsurface drilling by mean of using right appropriate mud weight, borehole stability, rig selection and casing program to be optimised.

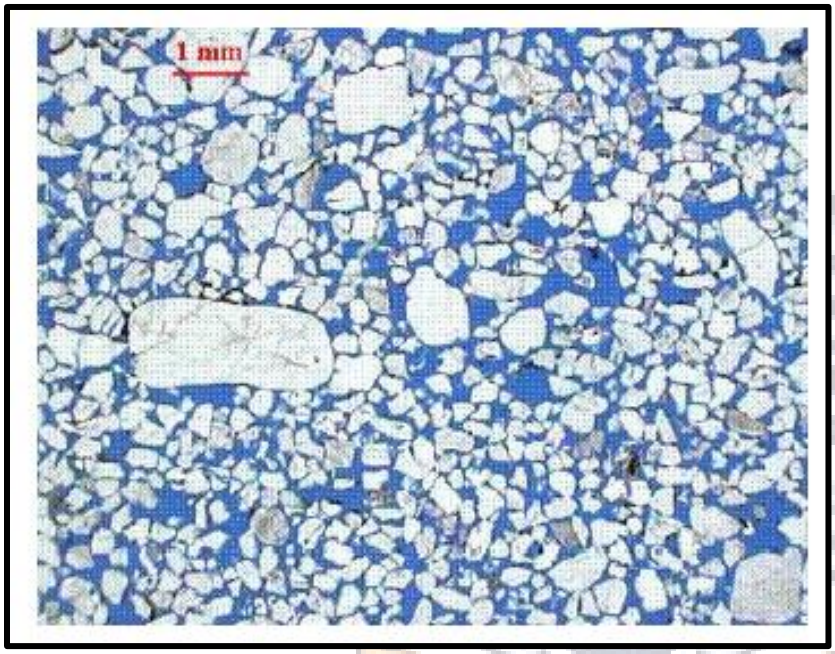

Figure 2. 2. Showing thin section of Sandstone. The pore pressure is the pressure in the pore space (blue colour) Taken from; Kvam O. 2005.

2.1.4 Normal hydrostatic formation pressure:

The normal hydrostatic formation pressure occurs when the pore pressure profile parallels to the hydrostatic profile as expressed in figure 2.1. This pore pressure can be regarded as normal formation pressure. Abnormal formation pressure observed as the formation pressure is higher (overpressure) or lower (underpressured) than hydrostatic pressure.

2.1.5. Overpressure :

Overpressure occurred when the formation pressure, Pf, surpasses the hydrostatic pressure at the same depth, this type of formation is known as overpressured formation, and overpressure OP, is equivalent to the excess pressure as expressed below:

$OP = Pf - Ph$……equation (2.4)

Where OP, overpressure, Pf, formation pressure and Ph, hydrostatic pressure.

2.1.6 Underpressure:

An underpressured zone occurred when the formation pressure is less or less than hydrostatic pressure at the same depth, classically originated from pressure depletion in reservoir during production.

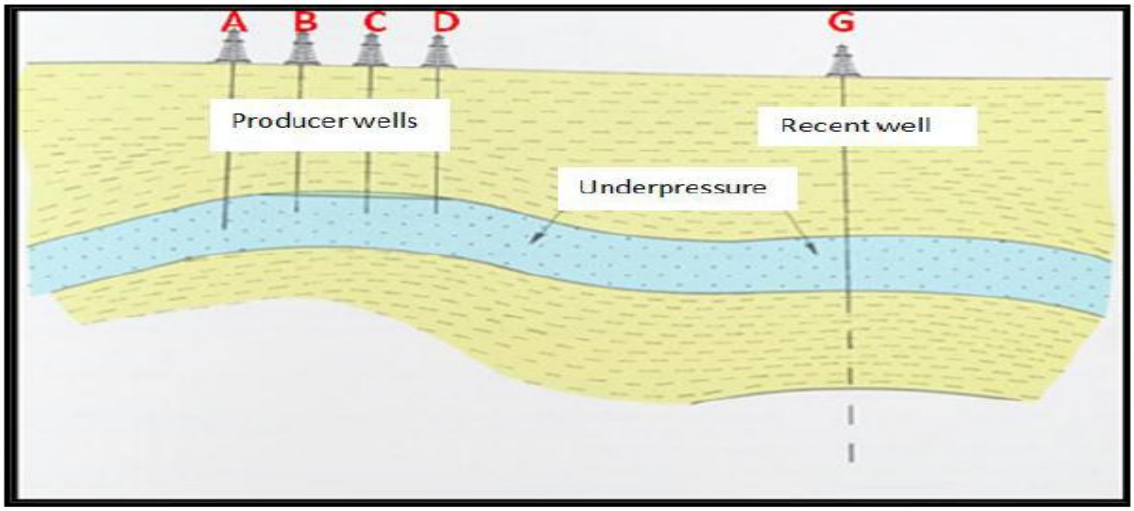

Figure 2.3 showing an example of underpressured as a result of reservoir depletion. Well A, B, C and D have been producing for a while, without pressure maintenance such as any injectors. If a new well such as well G, drilled along the same reservoir will be underpressured.(Taken from tp://faculty.ksu.edu.sa/shokir/PGE472/Lectures/Abnormal%20pressure.pdf. Access on 15th April, 2013.

2.1.7. Vertical effective stress:

The difference between the overburden stress and the formation pressure is known as the vertical effective stress,∂v. It cannot be directly measured, but estimated by means of using Terzaghi's equation as expressed below:

$\partial v = Sv - Pp$.....equation (2.5)

Where ∂v effective stress, Sv is overburden stress and the Pp formation pressure.

2.1.7.1. Minimum horizontal stress:

The minimum horizontal stress, Sh, is measured during the leak-off- test (LOT) under the casing shoe once each section of the hole drilled (Mouchet & Mitchell, 1989). It is expected to obtain the minimum mud pressure to hold an open fracture in the formation. There is regularly an interval of open hole of 3 – 5 m depth at the base of the casing shoe in a compacted formation, and the Leak-off-test (LOT) is usually run typically in this section of the hole in order to select a suitable mud weight to drill the next section. The drilling mud is pumped directly in to the well while the well is shut in, with the pressure on the wellbore increased. The pressure which increased with time is being monitoried as indicated in the figure 2.4. The fracture pressure occurs at point B, i.e., showing the pressure at which the mud occupies the formation – hereafter the pressure dropped. The leak-off pressure (LOP) acquired during the LOT shows the maximum mud weight that can be safely used to drill the succeeding section of the hole deprived of tensile disaster in the formation.

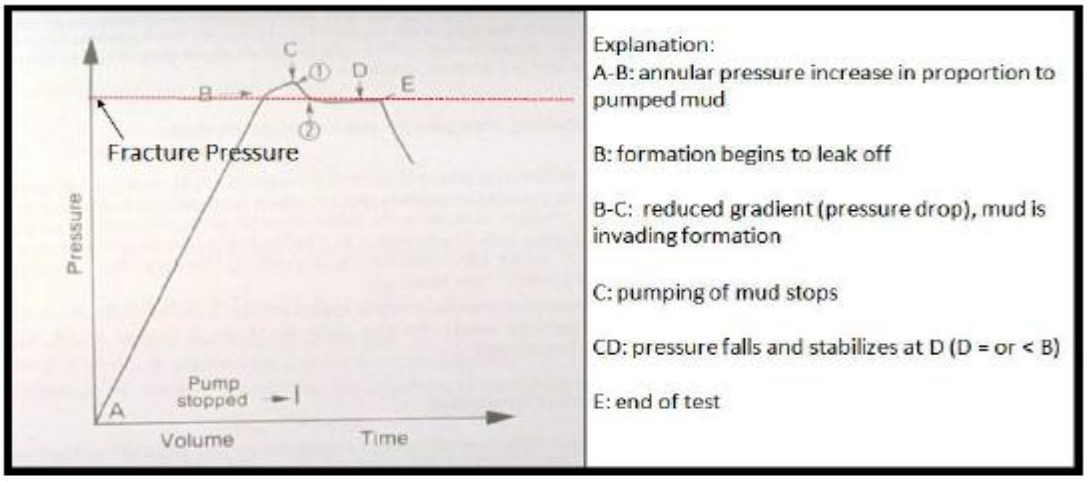

Figure 2.4 showing example of LOT pressure-time profile. After (Mouchet & Mitchell ., 1989).

In addition, the formation integrity test (FIT) is another test similar to that of LOT leak-off-test in both technique and purposed, but, during the formation integrity test (FIT) the pressure or the mud-weight will increased to pre-determined value, deprived of the formation to leak off or fracture.

There are some of the empirical methods recommended in the literature in a way to evaluate the minimum horizontal stress. Yoshida et al., (1996) in his survey for drilling engineers in operating companies, resolved that the Matthews & Kelly (1967), Eaton (1975), and Daines (1982) methods are the most popular, but the Eaton's methods and the Matthews and Kelly (1967) are the most general accepted used.

2.1.7.2 Maximum horizontal stress:

The maximum horizontal stress S_H cannot be determined directly from the well during the drilling; it can be determined from the borehole breakouts on image logs or calliper logs, provided with calliper of four arms or more. In a basin that is highly affected by tectonic, the information of maximum horizontal stress is highly required in relevant accurately determine the mean stress and to obtained a reasonable estimate of pore pressure in tectonically active setting by mean of valuing mean effective stress from porosity logs (Goulty., 2004).

2.1.7.3 Supercharging:

The supercharging is typically displayed as a very high pressure rate in a dataset of wire formation test (WFT) dimension and likely to occur in low permeability region, where drilling mud has been are injected forcefully into the formation while drilling.

2 . 2 Over pressure (abnormal pressure) generation mechanisms:

Dickinson (1953) studies in the Gulf of Mexico (GOM) labelled an overpressure zone as imperfect dewatering. The word disequilibrium compaction, or compaction disequilibrium, has subsequently being coined for Dickinson's mechanism, which is believed to be the most common mechanism of the overpressure generation in young, and fast buried sequences of sediments with mud-rich at depth down to ~ 2km . Different additional mechanisms of overpressure generation have been subsequently subjected for both Gulf of Mexico and the other basins in the world. However, recent research shows that on overpressure generation mechanisms can be classified into two classes such as firstly, loading mechanisms, which mainly associated to stress, secondly, the fluid expansion mechanisms (Swarbrick et al., 2002). Also hydrocarbon buoyancy is another source of overpressure generation mechanism in a hydrocarbon accumulation in reservoir.

2. 2 .1 Loading mechanisms:

Loading mechanisms occur as a result of pore fluids which resist to escape fast enough from the sediment thereby stay in hydrostatic equilibrium as increasing in compressive stress applied there by leads to generate an overpressure. The overpressure can occur by disequilibrium compaction as a result of increasing in overburden stress as the sediment is being buried. Also increasing in tectonic stress is the other parts of loading mechanism which can generate an overpressure, which normally act in a horizontal plane supposing the vertical stress is the principal stress.

2. 2. 2 Disequilibrium compaction:

The disequilibrium compaction mechanisms of overpressure generation mostly occur in Neogene and Quaternary basins of rapid rate of sedimentation with low permeability sediment. In older basins, owing to the momentary nature of pressure, overpressure can merely be conserved in thick, low permeability rock, due to the excess pressure which dispels with time (Swarbrick & Osborne, 1998; 2002). During the deposition in young basins, the overlying sediment weights end compacted and expels fluid from the underlying deposited sediments. However, the inability of the pore fluid to be expelled quickly in order to have retention of pore pressure in a hydrostatic level, this leads to increases in overburden which supported by the pore fluid and results in increasing the pore fluid pressure. As a result of this situation, the sediments will have a higher porosity (i.e. less compacted sediments) than it else would require at the same depth. Using relative example from Jurassic shale offshore mid-Norway and Miocene shale in the Lower Kutai Basin, (Goulty et al., 2012) compete that disequilibrium compaction is merely active to depths where the temperature ranges ~ 100^0C, below which chemical compaction occur, mainly liberated of effective stress. In such a structure, where there is no horizontal drainage, the fluid expelled velocity relatively to the matrix is directed by the Darcy's equation expressed as follow:

$V = -(kpfg/\mu)\, d(OP)/dZ$ ……equation (2.6)

Where k is the permeability sediments, μ is the viscosity of the pore water, pfg is the formation pore pressure and gravity; $d(OP)/dZ$ is the overpressure gradient.

2. 2 .3 Tectonic compressional stress:

This mechanism is comparable to the process accountable for generating overpressure by disequilibrium compaction, but in this situation the loading occur due to additional horizontal compressive stress produced by tectonics. Examples of this mechanism are found in geologically younger region of the Earth's crust such as, Rocky Mountains, USA; mountain chain in Indonesia (Agip manual, 1980).

2. 2 .4 Unloading mechanisms:

Unloading mechanisms regarded as decrease in the effective stress, either by a reduction in limiting or by an increase in pore pressure. Limiting stress is compact by exposure, and restricted the fluid from escape may result in overpressure formation. However, fluid expansion mechanisms is another type of unloading mechanisms which normally formed where the rock matrix limits expansion of inward fluid or an inner increased in fluid volume. These group examples include hydrocarbon generation, I.e; the cracking of oil and bitumen to gas, clay diagenesis, and the aquathermal expansion (Bowers, 1995; Swarbrick & Osborne, 1998;

2 .2. 5 Hydrocarbon generation (kerogen maturation):

The hydrocarbon generation are highly dependent on time and the temperature which are the kinetics of it reaction (Swarbrick et al., 1998, 2002). Kerogen maturation pays a major role in overpressure formation by forming the lower density fluid from the higher density kerogen. Except adequate fluid is expelled, the porosity will not be reliable with the predictable amount of compaction at a given depth. However, the conversion of kerogen to lighter hydrocarbon probable to occur at depth of 2 - 4 km at temperature of 70 – 120^{0}C (Tissot et al., 1987). For instance the act of bacteria at shallow depth on organic materials can yield biogenic methane. Assume such methane is produced within a sealed structure, the pore pressure will increase. If this kind of shallow depth methane is expected while drilling, result may be disastrous, mostly in offshore drilling where blow-out preventers (BOPs) are lacking in the area of shallow section drilling. However, with the use of seismic, high resolution seismic data can disclose shallow gas dangers predrill (Mouchet & Mitchell, 1989).

2. 2. 8 Aquathermal expansion:

Barker (1972) reported that thermal expansion of pore water results in increasing in pore pressure. The idea built on the expansion of water when heated, and thus these occur in a closed seal structured it will produce further pressure. The major weakness of aquathermal expansion as a result of overpressure requires a very effective or perfect seal to be effective, a situation that is near to unbearable (Daines, 1982; Luo & Vasseur, 1992). include the link between the increase in temperature and viscosity reduction, thus, hence increased fluid expulsion, and the changes into the hard overpressure zone suggested of some permeability (Mouchet & Mitchell, 1989).

2. 2. 9 The cracking of oil and bitumen to gas:

This process is called thermochemical cracking which are highly depend on temperature and depth is another process of hydrocarbon generation which contribute to overpressure formation. This includes the converting of a heavier product to a lighter product, and the conversion ranges maximum at ~ 100^0C (e.g Mouchet & Mitchell, 1989). Barker (1990) proposed that the conversion of oil-bitumen to gas befalls at depth of 3.0 – 3.5 km and temperature at 90 – 150^0C.

2. 2. 10 Clay diagenesis:

Water is discharge during smectite dehydration and through the transformation of smectite to illite. The smectite dehydration occurs with discharge of water in pulses (Power, 1969; Burst, 1969). According to Swarbricks et al.; (1998; 2002), the quantity of water produced from the process is slight and could not produce a significant overpressure. In addition, Colton-Bradley (1987) observed that the dehydration process affected by overpressure with the rates of slowing down. However, Lahann (2002) and Lahann & Swarbrick (2011) have contended that smectite-illite transformation contains structure work wearying in the process by which the illitized mudrock compacts to lower porosity at a given effective stress level. Therefore the mudrock inclines to compact on smectite-illite transformation, provided the expulsion of excess water. In the region where the expulsion of water is withdrawn by low permeability, such region can developed an over pressure. Water is also discharge during the transformation of

kaolinite to illite (Bjorlykke, 1998), which assumed can add to overpressure as for the smectite-illite transformation (Lahann & Swarbricks, 2011). However, change of smectite – illite needs the existence of potassium and could begin at temperature of 65 – 70^0C (Freed & Peacor, 1989). Bredehoeft et al. (1988), in Swartbrick el al., (2002) noted that no change in smectite to illite ratio in overpressured strata of the Caspian Sea Basin, at 6 km depth with temperature of 96^0C, this may owing to the absence or low amount of potassium.

2 .2. 11. The characteristic of the overpressure:

As earlier discussed in the section 3.0, above that overpressure generation mechanism can be grouped into two such as loading burial mechanism or tectonic compressive stress which resulted in overpressure generation mechanisms by disequilibrium compaction; also the unloading process which leads to reduction of the effective stress that acting on the sediments, gas generation, horizontal transfer and the transformation of the clay minerals (Swarbrick et al., 2002; Lahann & Swarbrick, 2011). These two classes of overpressure generating mechanisms generate difference characteristic styles in wireline logs and cross plot. This section will show the common methods to indicate the causes of the overpressure either by loading mechanism or unloading mechanism. During the burial of sediments, sediments compacted rapid as a result of the overlying weights acting upon with the decreases in porosity, and increases in resistivity, sonic velocity and density. With the increase in depth, the compaction rate reduces. The normal compaction trend (NCT) for porosity logs while the pore pressure is at hydrostatic state could be affected by the transformation of clay minerals in adding more to mechanical compaction processes (e.g., Dutta, 1987, Bower, 2001; Lahann, 1998). If the normal compaction trend (NCT) deviated towards the higher porosity, is an indication of undercompaction as shown in figure 2.5. Apparent deviation may also occur from (NCT) normal compaction trend as a result of lithology differences.

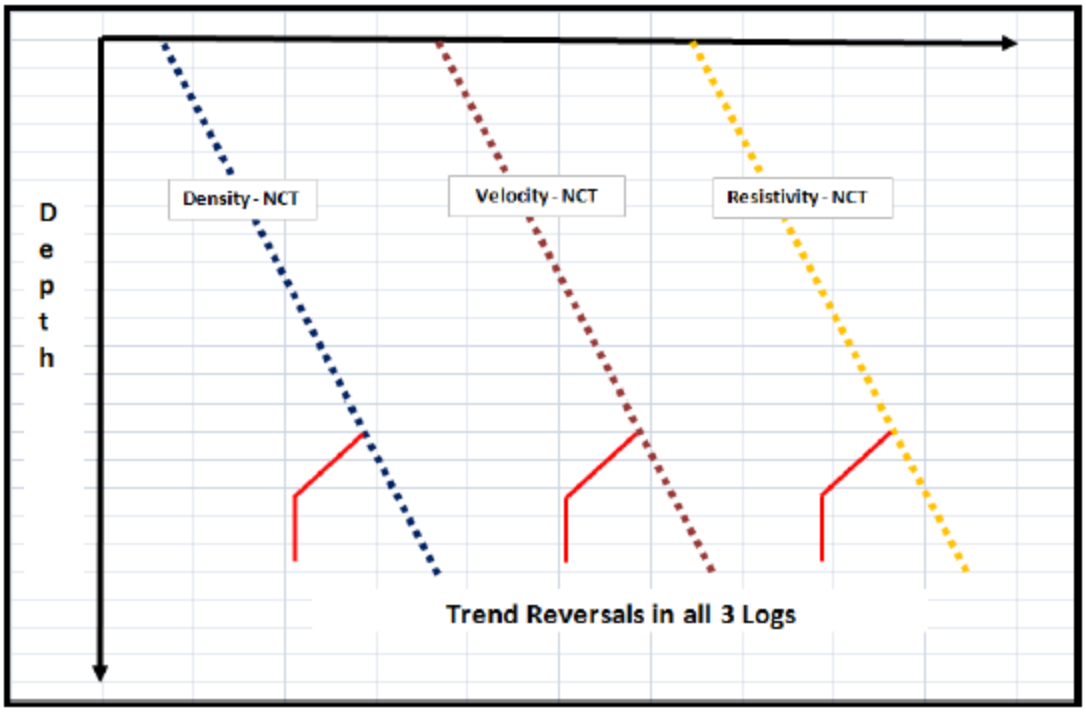

Figure 2.5: Showing illustration trend reversal of density, velocity and resistivity versus depth.

As regards to unloading overpressure mechanism, overpressure formed as result of fluid expansion or reduction in porosity. The pore pressure could increase rapidly more than the overburden thereby resulted in decreasing of effective stress with the increase in depth which usually indicated as velocity reversal (Bower, 2001). Katahara (2003) discovered that in an unloading mechanism there is great significant decrease in velocity of sediment with large decrease in effective stress, nonetheless having unaffected density i.e. unloading have no effect on density; however, there is great effect in velocity and resistivity reversal. Bower (1995, 2001), Katahara (2003) and Ramdhan & Goulty (2010) have used related plots of depth against density, porosity sonic velocity and the resistivity to deduce the presence of overpressure as a result of unloading. The figure 2. 3 shows the reversals of velocity and resistivity but no significant shows on density plot.

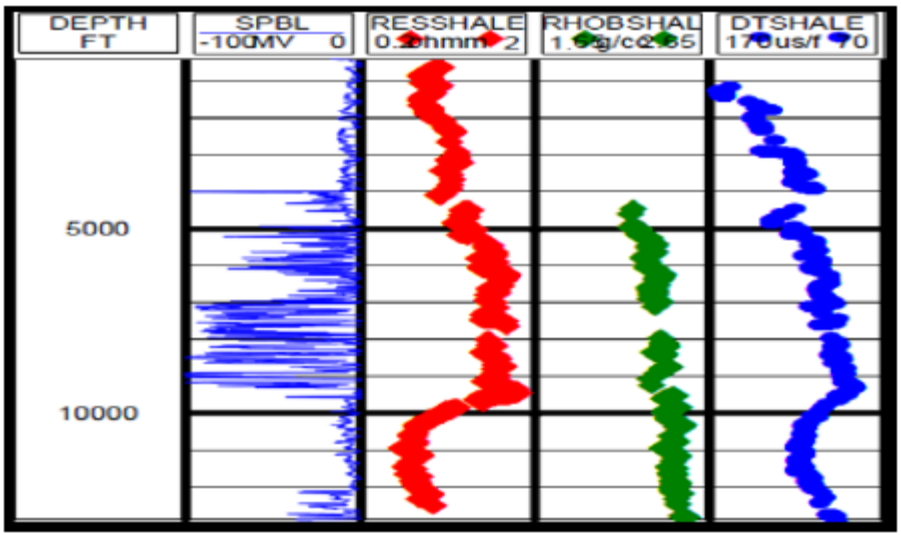

Figure 2. 6: Showing no reversal in density (green), & reversal in resistivity (red) and sonic (blue) in dense mud rock sequence. Taken from (Katahara (2003).

This idea has enable Bowers & Katsube (2002) to study the performance of the storage and the connecting pores of mudrocks under stress. They discovered that the connecting pores containing a low rate of ratio and mechanically flexible, however, the storage pores have higher ratio rate and somewhat stiff as show in the figure 2.4. However porosity sediments are tremendously looks like storage pores, thus bulk density logs response are controlled by the conduct of the storage pores, while the opening of connecting pores has no effect on bulk density, but have effect on the sonic and electrical properties. In conclusion, the density logs response in fluid expansion or unloading mechanism is minimal or absent, while there is significant response from sonic and resistivity logs.

2. 3 . The methods of estimating overpressure zones:

This section will describe three major methods commonly used to determine the overpressure zone in sedimentary basin such as follow: first of all, the pore pressure estimation by quantitative methods, mostly the equivalent depth method, Eaton's (1975) method, and Bowers' (1995) method; secondly, the direct measurements of pore pressure estimation using wireline formation testing equipment tools (WFT), such as RDT, MDT, RCI, and XFT, thirdly, is the drilling operation method to detect the overpressure formation, such as the rate of penetration (ROP), drilling exponent, D, gas cutting or caving, drag and torque methods.

However, the quantitative method of pore pressure estimation from wireline logs entails the formations of (NCT) normal compaction trend for every type of logs used for the work done. The normal compaction trend (NCT) must normally recognise at the shale interval of sparkling. In addition, shale pressure prediction built on the theory that the shale pressure is at the equilibrium with pressure in the interval of the attached sand, but, this assumption is regardless, not true always. However, this section would discuss a bit details on normal compaction trend (NCT) hypothetical bases in pore pressure prediction or estimation.

The compaction of the sediments is a utility of mean effective stress and the differential stress (Goulty, 2004), but out-dated methods have usually been practical on the assumption that the porosity is a role of vertical effective stress. The creation of normal compaction trend (NCT) for the logs types sensitive to porosity is built on the anticipation of linear, logarithmic, and exponential or power law function connection in the mudrocks as a resolution of depth. For instance, normal compaction trend could be established for sonic velocity or transit time, resistivity, and density as a role of depth.

Therefore, determination should be made in picking cleanest shale for the analysis by using normal compaction trend (NCT), for instance, gamma-ray logs response with one or two thresholds. (Matthews, 2004) cautioned must be made in selecting clean shale, thus limiting the data density. Ramdhan & Goulty (2010, 2011) considered using the combination of neutron and density logs in identify clean shale, with > 18% of NPHI – DPHI as their cut-off threshold.

Bowers (2001) shows that Gardner's shale line works better in shale density greater than 2.1 g/cc, but commonly overrated shale density near to mudline. However, proposed that the lower bound shale line remain use in combination with Gardner's upper bound trend. The Gardner's shale-line velocity to density relationship can be expressed as follow:

$Vp = (pb/0.23)$ ……equation 2.7

Where Vp is the velocity in ft/s, pb bulk density units are g/cc. But, Bower (2001) proposed the lower bound in case of sonic velocity in shale having same units for velocity and density as show in the relationship below:

Vp = 4790 + 2953 $(pb - 1.3)^{3.57}$……equation 2.8

2. 3. 1 Normal compaction trend (nct) from porosity logs:

The normal compaction trend (NCT) can be estimated with the uses of either linear or exponential form of Athy's (1930) equation as follow below:

$\varphi = \varphi_o - cz$ …… ……Athy's linear equation 2.9.

$\varphi = \varphi_o \exp(-cz)$……Athy's exponential equation 2.10.

Where φ_o is the initial surface porosity (%), c is the compaction constant (m -1), z is the depth (m) and φ is the porosity (%).

Issler (1991) observed that the commonly used is the Athy's exponential form, and he effectively used the Athy's linear form equation in other compacted region of Beaufort-Mackenzie Basin of Northern Canada. Conferring to Issler neither of the equations fits impeccably for whole data range every time there is presence of overpressure. However, Issler now suggested improved form of the equation at certain depth intervals. Dutta (2000) improved Athy's (1930) equation as expressed below:

$\varphi = \varphi_o \exp(-k\sigma)$……equation 2.11

Where k is the coefficient which correlated to bulk density of the sediment as well the density of the pore water, and σ is the effective stress.

However, other form of similar computation of NCT for porosity transform that can as well be plotted against the depth or the effective stress, are presented below. Also depend on the available log types.

2. 3. 2 Normal compaction trend (nct) from sonic (Δt)logs:

Ramdhan & Goulty (2011) used this equation expressed below where the sonic transit log is available.

$\Delta t = (\Delta t0 - \Delta tm)\exp(-bz) + \Delta tm$……equation 2. 12

Where Δt is the transit time; $\Delta t0$ is the initial surface transit time; Δtm regarded as matrix transit time; while b; is the compaction constant (m -1) and Z regarded as the depth (m).

2. 3. 3 Normal compaction trend (nct) from resisitivity logs:

This can be expressed based on the equation below according to (Ikon's RockDoc training manual).

$R = R_0\exp(bz)$……equation 2.13

Where R is the resistivity; R_0 is the initial surface resistivity; z is the depth (m) and the b; is the compaction constant (m-1). From, Ikon's RokDoc training manual).

2. 3. 4 Normal compaction trend (nct) from density logs:

The normal compaction trend (NCT) can be created and estimated from the density by mean of using Athy's (1930) or using the converted equation (2.15), of density to porosity through this equation shown below:

$\varphi = \frac{\rho m - \rho b}{pm - pf}$……equation 2.14

Where σ is the porosity (fraction); pm is the matrix density; pb is the bulk density; and pf is the fluid density in (m). However, the limitations of normal compaction trend (NCT) due to the method to the prediction of the formation pressure have been stated by many researchers. For instance, normal compaction trend (NCT) do not sufficiently describes the following: The horizontal transfer, shallow overpressure, even the choice of the curve at the shallow section of the hole (Swarbrick, 2001); the difference of the shale mineralogy (Swarbrick, 2001; Alberty & Meclean, 2003); the needed of using the three main principal stress (Swarbrick, 2001; Alberty & Mclean, 2003; Goulty, 2004); The expansion of the fluid contribution to the overpressure (Osborne & Swarbrick, 1997; Swarbricks et al., 1998 in Swarbrick, 2001); as well the chemical compaction at depths greater than 2 – 4 km (Goulty et al., 2012).

2. 4. The estimation of the ovepressure from wireline logs methods:

The Eaton's (1975) and Bowers (1995) are the most used common methods of equivalent depth for the quantitative evaluation of pressure. However the selected choice to be used depends on the analyst. The data needed for each method are described in the table below:

Table 2.1: Showing the types of data used for different methods of estimation of overpressure or pressure prediction from wireline logs.

		Methods			
		Eaton	Equivalent Depth Method	Bowers	D-xc
Data	Interval Velocity (seismic)	Yes	Yes	Yes	
	Sonic (DT)	Yes	Yes	Yes	
	Resistivity	Yes			
	Conductivity	Yes			
	Density/Porosity		Yes		
	ROP_normarlized	Yes	Yes		Yes
Calibration Types					
	Data		Quality		
	RFT, MDT,RCI, FMT, etc.		HIGH		
	DST		MODERATE		
	Kick		Low		

2. 4. 1 Equivalent depth method of Overpressure estimation:

This method built on statement that each points on the logs takes an equivalent point on the normal compaction trend (NCT). For instance, the figure 2.9 shows how the response of logs at 700ft depth equivalent as 400ft depth. At the point noted the pore pressure is hydrostatic, the vertical effective stress also expected to be equivalent to those depth, hence, thus the pore pressure can be predictable as long as the vertical effective stress owing to the overburden weight could be estimated from the density information.

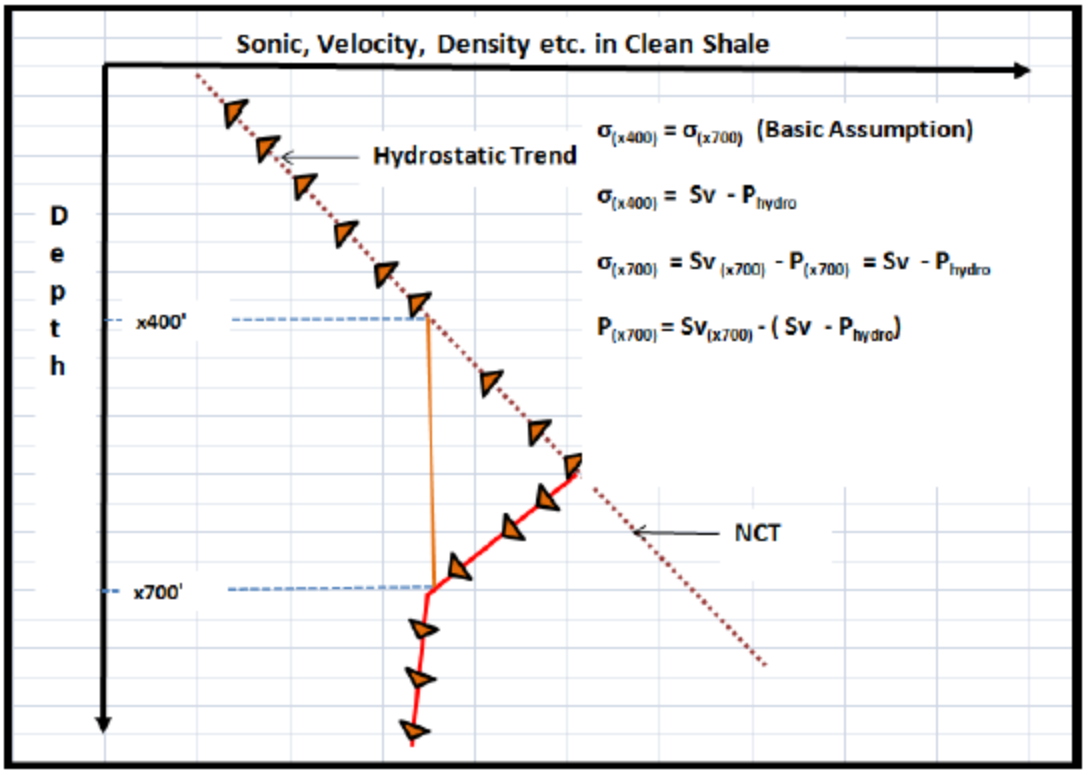

Figure 2. 7 : Schematic of the equivalent depth method for pore pressure prediction.

Bower (2001) revealed that, where mechanism apart from disequilibrium compaction occurred i.e., the unloading mechanisms, the equivalent depth method below- predicted pressure.

2. 4. 2 The eaton's method of estimating pore pressure prediction :

The Eaton's methods of the predicting pore pressure based on the links that pressure is associated with variance between the overburden and the effective stress product i.e, (the normal pressure region) and the logs ratio value right from the reversal with the value of logs on the estimating normal trend. However, based on the work done by Yoshida et al., (1996) according to his survey of the frequently drilling engineers at GoM, decided that, most of the operating companies are solely depend on the history of offset wells with the seismic for predicting pore pressure. Nevertheless, most of the noted predictions methods are the Hottman and Johnson (1969), Eaton's (1975) together with Equivalent depth method. Though, Eaton's method, sometime by exponent modification is commonly used for pore pressure prediction. Examples of the Eaton's equation mostly used are listed below.

2. 4. 2. 1 Eaton's method using sonic log:

$Pp = Sv - \{ (Sv - Ph) * (\Delta t_{norm} / \Delta t_{obs})^3 \}$……equation 2.15

Where Pp is the pore pressure; Sv known as vertical stress; Ph is the hydrostatic pressure; Δt_{norm} is the sonic velocity on the normal trend; and Δt_{obs}

In another way, it can be re-written as:

$Pp = Sv - \{ Sv - Ph) * Vp_{obs} / Vp_{norm})^3 \}$……equation 2.16

Where Vp_{obs} is the observed velocity; Vp_{norm} is the normal trend velocity.

2. 4. 2. 2 Eaton's method using resistivity log:

$Pp = Sv - \{ (Sv - Ph) * (R_{obs} / R_{norm})^3 \}$ ……equation 2.17

Where R_{obs} is the observed resistivity, R_{norm} is the resistivity on normal trend.

2. 4. 2 .3 Eaton's method using DX or DXC exponent:

$Pp = Sv - \{ (Sv - Ph) * (DX_{obs} / Dx_{norm})^3 \}$……equation 2.18

DX_{obs} is the DX observation, and the $Dx_{norm.}$

2. 5. The Method of Estimating Pore Pressure during Drilling:

2. 5 .1 Rate of Penetration (ROP): This is one of the methods used to detect the overpressures zone in the reservoir. The rate of penetration (ROP) is a clue to observe the quickness at which the bit drills through an interval. Supposed, by keeping drilling parameters constant, the rate of penetration (ROP) would decrease with depth as a result of increased in the compaction of the rock with depth. Thus, increased rate of penetration (ROP) or form of deviation along the trend of increased may be possibly being as a result of undercompaction which usually related to overpressure. Nevertheless, as a result of the parameters such as weight on the bits (WOB), hydraulics, revolutions per minutes (RPM), and mud weight which are not always kept constant during the drilling, thereby enhanced ROP to increased or decreased independent of the state of the sediment compaction. However, normalized rate of penetration are commonly used whenever it accessible in combination with other indicators, this provides accurate means of deducing undercompaction during the drilling. Such example of normalized rate of penetration (ROP) comprises of D-exponents.

2. 5. 2. D -exponents as normalization to rate of penetration (POR):

Forgotson (1969), proposed the shortest use of drilling rate of penetration (ROP) in predicting geopressure, mainly comparing rate of penetration (ROP) to geopressure (Fertl & Timko, 1971). As mention earlier that some parameter such as mud weight, bits size (types, wear, and the hydraulic), weight on the bits (WOB) and revolution per minute (RPM) can as well caused increased or decreased in rate of penetration, in order to avoid the effect of hole disorder as well, the drilling parameter conditions and rate of penetration has to be normalized. However, one example of normalization is the D-exponent (Dx).

The D-exponent (Dx) was established by Jordan and Shirley (1966), based on the following equation below:

Dx = $\{log\ (R\ /\ 60N)\}\ /\ log\ (12W\ /\ 10^{6}B)$ ……..equation 2.22

Or it can as well express as follow:

R/N = a $(W/B)^{d}$……equation 2.23

Where R is the drilling rate in (ft/hr), N is the speed of the rotary in (RPM), W is the weight on the bit (pounds), B is the bits diameter in (inches), a' is regarded as the lithology constant and the d is the compaction exponent.

However, Dx-exponent is dimensionless and as well sensitive to variance pressure, therefore it can be used as tools for the adjustments of the mud weights as the drilling progresses. Above all, at a constant lithology and hydrostatic pore pressure, Dx-exponent is usually expected to increase with depth, but indicate decreasing with depth at overpressure region, as shown in the figure 2.11 below. Nevertheless, Dx-exponent does not adjusted for mud weight, the rate of penetration decrease as a result of increasing the mud weight while drilling thereby increased in Dx- exponent this enhanced difficulty in interpretation in such circumstances. Furthermore, the corrected D-exponent (Dxc) is related to Dx in code but through normalization for mud weight. Though, hydraulics, lithology, bit (type and wear) and the compaction are not corrected (Agip, 1980).

Some of the factors needed to note when using of Dxc (Dx-correction) for pressure detection as a follow:

- By using only trend in shale.
- The trends usually change with bit as hole size change.
- The section should not be used with controlled drilling or sliding.
- By drilling with roller cone bits, the trend shows more consistences.
- It can be used in combination with other indicators.
- By mean of it deviation from normal trend, is an indicative of transition zone.

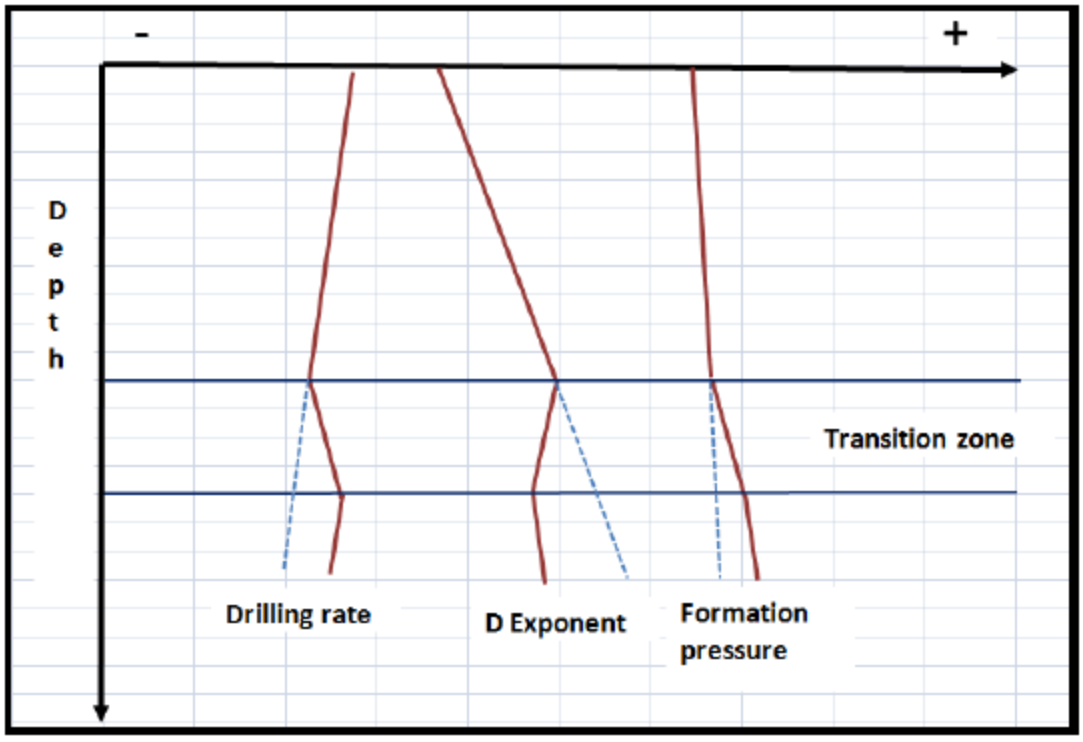

Figure 2. 8: Showing Schematic of drilling rate response, Dx, as well as Formation pressure.

In addition, others related normalization for rate of penetration such as gas show, and mudweight.

Gas shows: Gradually increase in trip gas (TG), background gas (BG) as well as connection gas (CG) are all likely indicating underbalance drilling (UBD) conditions and must be examined before the drilling advanced. In most of time, it needed to circulate out the gas by mean of circulating bottom up (CBU) as well increased the mud weight. However, on lowest drilling, the equivalent circulation density (ECD) is adequate high usually to balance the pore pressure and production of the gas from the formation. By stopping the circulation, the equivalent static density (ESD) is usually lower than the equivalent circulation density (ECD), however, supposing the equivalent static density (ESD) lower as compared to pore pressure, the liberated and the gas produced move in to the mud thereby indicate an increased in trip gas, (TG), back ground gas (BG) and the connection gas (CG). If this situation is not checked, with the connection of each pipe, more dilution of the mud by connection gas (CG) will result reduction in mud weight thereby gradually higher of connection (CG) gas is recorded.

The Mud weight: With the addition of constant mud weight being injecting into the hole , supposing the mud weight moving out is lower than that of the move in, it is usually an indication of underbalanced.

2. 6. Prediction of pore pressure from geophysical wireline logs data.

Predicting abnormal pressure from geophysical data, most of the methods of predicting reservoir overpressure used the following phenomena such as; lower bulk densities (thus, lower seismic velocity), higher porosity, higher reservoir temperature and lower stress. There are two major types of approach for predicting pore pressure and the effective stress, which are based either on empirical relationship derived from statistical data and case histories or laboratory measurement and rock physics model. However, most methods used seismically derived velocities as way of prediction. The sonic velocities are calibrated against velocity derived from the sonic log and petrophysical measurement, under a normal pressure condition, in an absence of hydrocarbon saturation, sonic velocities increases with depth and any major trace of deviation from this is considered to be abnormal pressure or others anomalies such as saturation with gas). In general, formation pressure that deviates from hydrostatic pressure at a similar depth is considered as an abnormal pressure, which is indicated by significant change in the sonic velocity with depth. This change can result from difference origin such as lithology, hydrocarbon saturation, and formation temperature and formation pressure. Table 2.3 below indicate how exact types of measurements at difference stage of well development are employ to predict reservoir pressure using geophysical data (Dutta, 1987).

Table 2.2: The geopressure prediction techniques adapted by (Dutta, 1987).

Development Stage	Source of data	Pressure indicator
Prior to drilling	Surface geophysical methods (gravity and 2-D,3-D, 3-C and Seismic	P- and S- waves velocity, density and porosity.
During drilling	Drilling mud parameters	Mud gas cutting, Pressure kicks, Flow line temperature, Pit-level, Total pivot volume, Hole fill-up, and Mud flow rate.
	Shale cutting parameters	Bulk density, Shale formation factor, Volume, Shape, Size and %Shale.
	Correlation between new and existing well	Drilling data
After drilling	Surface and sub-surface geophysical data (VSP, cross well, 4D,3C) petrophysical data	P-and S-waves velocity, density, porosity, downhole gravity: sonic, resistivity density and neutron.
During testing and completion	Monitoring pore pressure variation in short zone	Repeat formation test (RFT), Drilling stem test (DST), Pressure bombs, and 4-D seismic.

Geophysical well logging is very necessary because geophysical sampling during the drilling (cutting sampling) brings a very impressive record of the each lithology formation encountered, however, wireline geophysical well logs are recorded when the drilling tools are no longer in the hole. There are many models of wireline loggings tools designed to handle specific logging restrictions. The classifications based on their principle of logging tools and the usage i.e. to measure physical parameters and the deductions made from them such as follow:

- **Based on operational principle: wireline logs can be classified as:**
  - Electrical logs: Spontaneous Potential (SP) and Resistivity logs.
  - Nuclear or Radioactive logs: Gamma ray (GR), Density and Neutron logs.
  - Acoustics log: Sonic logs.
- **Classification based on usage**
  - Resistivity logs: Deep-resistivity logs, Induction, Laterolog.
  - Lithology logs: Spontaneous potential and Gamma ray
  - Porosity logs: Sonic, Density and Neutron logs.
  - Auxiliary logs:, Bit Size logs, Caliper, Dip meter.

In addition, for the purposed of this study, a few logging tools such as gamma ray (GR), resistivity log, sonic log, neutron log and density log have been selected for short description of their distinctiveness.

2. 6. 1. Gamma ray logs:

Gamma ray logs are strictly designed to measure the natural radioactivity in formation. The radiation generated from the naturally-occurring radioactive elements such as uranium, thorium and potassium. The number of the elements of the naturally occurring gamma ray in the formation is measured and distinguished between elements of parent and daughter products of the three main families. In sediments, due to the radioisotopes of the clay content, the gamma ray log usually reflects clay contents as a result of potassium, thorium and uranium. Potassium feldspars, volcanic ash, and some salt rich deposits containing potassium (e.g. potash) may as well give a significant gamma-ray reading.

However, shale-free sandstones and carbonates have low concentrations of radioactive element and give low gamma-ray readings. API (America Petroleum Institute) is the standard units of measurements gamma-ray. Gamma-ray logs are quantitatively used to derive shale volume, to correlate, suggest or predict facies and sequences and to identify lithology (shalyness) also spectral gamma-ray can be used to derived qualitatively, radioactive mineral volume and more accurate shale volume, indicate dominant clay minerals types and also depositional environments.

Gamma ray log is usually preferred to spontaneous potential logs for correlation purposes in open holes nonconductive borehole fluids, for thick carbonate intervals, and to correlate cased-hole logs with open–hole logs.

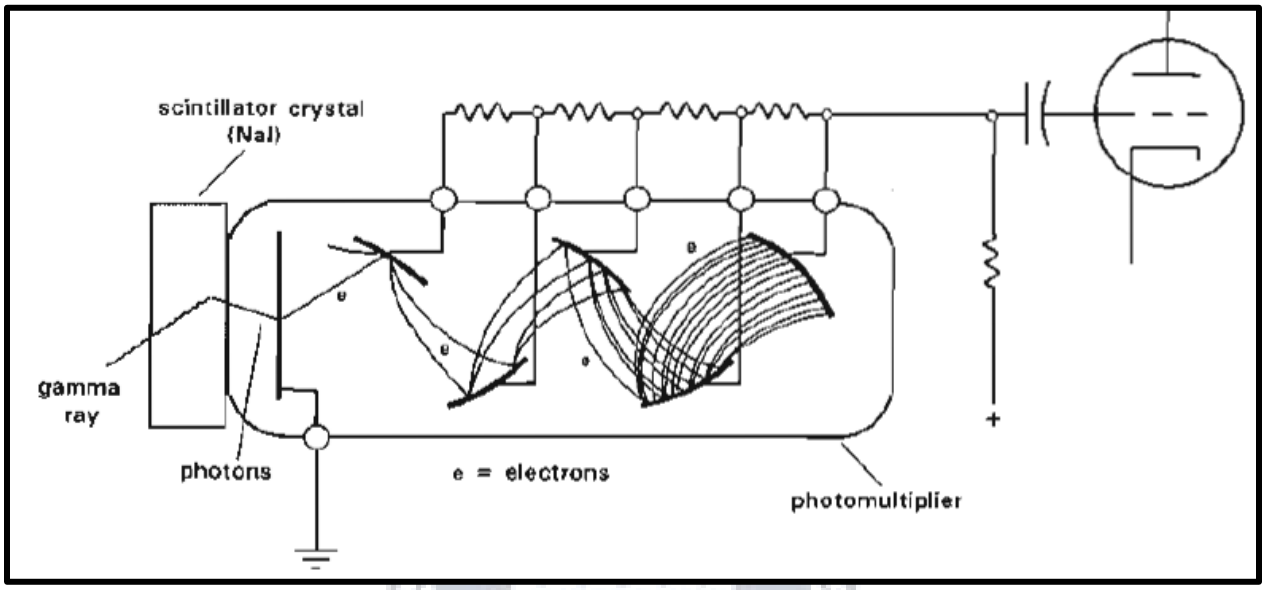

Figure 2. 9: Showing gamma-ray tools (modifies by Serra, 1979).

2. 6. 2. Resistivity logs:

Resistivity logs are designed to measured formation resistivity, i.e the resistance to the passage of an electric current. Hydrocarbons do not conduct electric current (infinitely resistitive). Resistivity is usually low in porous formation containing salty water also, resistivity mostly high in the same formation containing hydrocarbon, with this method employed by resistivity logs, therefore, high resistivity value can be used qualitatively to indicate a porous formation and hydrocarbon bearing formation. In addition, formation resistivity can be in determining information on lithology, texture, facies, and overpressure and source rock.

The limitation, resistivity tool could only function in borehole containing conductive mud, such mud mixed with salt water, and could not be run in oil based mud or fresh water based muds. Induction logs contrary are mostly effective with non-conductive mud, oil based or fresh water based and they cannot be ran in wells with salt water based muds.

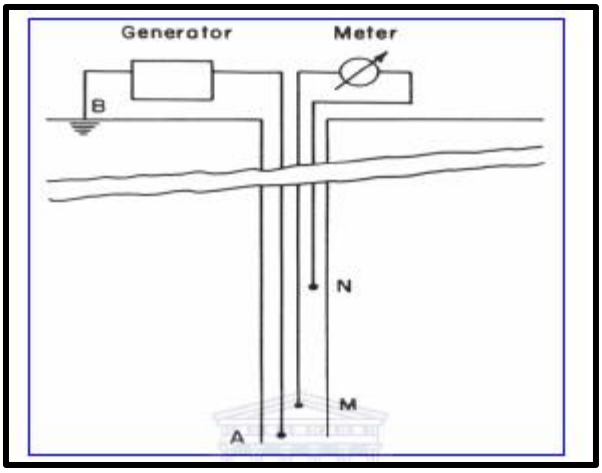

Figure 2. 9: Showing Resistivity tools, normal device with electrode A, M, N (modified from Schlumberger 1989).

2. 6. 3. Sonic logs:

A sonic log measures interval transit time (t) of a compressional sound wave in feet per second and hence, a reciprocal of the compressional wave velocity. The sonic log device consists of one or more transmitters and two or more receivers. The time for the acoustic energy to travel a distance through the formation equals to the distance spanned by the two receivers is the desired measurement and the unit expressed as microseconds per foot. The interval travel time can be integrated to give the total travel time over the logged interval.

Borehole compensated sonic log consists of two transmitters located above and below the receiver, which are pulsed alternately to produce an improved log. Errors due to sonde tilt or change in the hole size are minimized by averaging the measurements. Quantitatively, sonic log used to evaluate porosity in liquid filled holes, also aids in seismic interpretation which used to denote the interval velocities and velocity profile and could be calibrated with seismic section. Sonic logs are used in the following area such as:

- Determine porosity of reservoir rock.
- Improve correlation and interpretation of seismic records.
- Identify zones with abnormally high pressures.
- Assist in identifying lithology.
- Estimate secondary pore space.

- Indicate mechanical integrity of reservoir rocks and formations that surround them (in conjunction with density data).
- Estimate rock permeability.

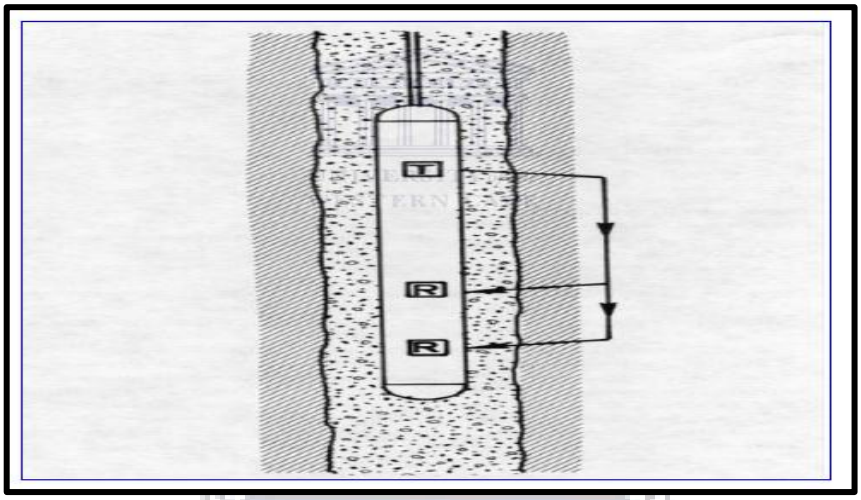

Figure 2. 10: Showing Sonic logging tool with Receiver (R) and Transmitter (T) (Modified from http://www.spwla.org/library_info/glossary)

In addition, sonic log is reflected as a porosity log in sedimentary rocks and which can produce a sonic based sandstone or limestone porosity log to compare with those generated from neutron and density log, no calibration required as is it strictly fixed with perfect spaced geometry. Sonic log shows raw transit times in micro seconds per foot (us/f). It has common interval transit times fall between 40 and 140ms. The slowness of sonic in porosity shows a bit differentiate from the density and neutron tools. It has effect only in primary porosity and does not realize fracture or vugs. The Wyllie Time Average equation for sonic porosity is given below

$\emptyset = \Delta t_{log} - \Delta t_{ma} / \Delta t_f - \Delta t_{ma}$ ……equation 2.24

Where: Ø is the sonic porosity.

Δt_{log} is the formation interval interest of the sonic log reading.

Δt_{ma} is the matrix travel time.

Δt_f is the mud fluid travel time.

Also, Raymer Gardner Hunt has an equation for converting slowness to porosity, this equation tend to explain some anomalies detected in the field. The Raymer Gardner Hunt equation is given below.

$\emptyset = C * \Delta t_{log} - \Delta t_{ma} / \Delta t_{log}$……equation2.25

Where: C' is the compaction constant generally taken as 0.67. The table 2.4 shows some of the sonic travel time of rocks.

Table 2.3: Showing the sonic travel time of rocks (Rider, 1996).

Mineral	**Matrix travel time (∆tmax) ms**
Sandstone	51 - 55
Limestone	47.6 – 53
Dolomite	38.5 – 45
Anhydrite	50
Salt	67 – 90
Shale	62.5 - 167

2. 6 . 4. Neutron log:

Neutron log is types of the wireline log used for logging borehole, which was commercially established in 1941 by Well Surveys international (WSI) after the event introductory of gamma ray log. The neutron log mainly responds to the quantity of hydrogen ion concentration in a formation, hydrogen contained in oil, natural gas and water, thereby used to evaluate the zone of porosity in a formation. If there is large zone of hydrogen concentration ion surrounding the well bore, majority of the neutron move slowed and apprehended nearly closed to the wellbore, this low count rate result are deduced as an indication of high porosity while, the zone surrounding the wellbore with a small concentration of hydrogen ion enhanced the farther travel away from the source before being captured and this resulted in high count rate and can be deduced as low porosity.

Neutron log are recorded in both open and cased holes, either with any other logs or separately which enable correlation between the open and cased hole logs mostly in conjunction with the magnetic casing collar locator (CCL) and the gamma ray log. Actually, neutron log can as well

be run in any types of borehole fluids such as oil, water, mud and gas, or air filled, this log is hardly differentiate between the porosity which filled with water and oil in process of field production logging, occasionally detect gas entirely, as a result of the tool responds which considerably affected by the gas presence within. However, chlorine log is the application particularly designed to distinguish between saline water (high chloride content) and oil saturation. In neutron log has the tendency measurement of induced radiation from the formations infiltrated by the borehole, the induced radiation produced from the formation by the bombardment with a neutron source presence in the logging tool.

The types of neutron log tools commonly used are single detector, dual detector and compensated neutron log.

The single detector neutron log tools: The neutrons are emitted from the radioactive source, and collide to lose energy by mean of billiard effect. It majorly depends on hydrogen concentration ion or index also detects epithermal neutrons, thermal neutron or combination and capture gamma ray therefore, processes the formations ability to reduce the passage of neutrons. As show in figure2.11a

The dual detector neutron log tools: Is a thermal phase neutron detection instrument with two detectors such as long spaced and short spaced detector which are used to minimize the borehole effects and has a vertical resolution of 2ft, which produced radial investigation of porosity, no (porosity -1ft), high porosity less. It can be used in both open and cased hole as well statistical in nature and logging speed of 20 – 30 fpm (feet per minute), probably run with other logs. on figure 2.12

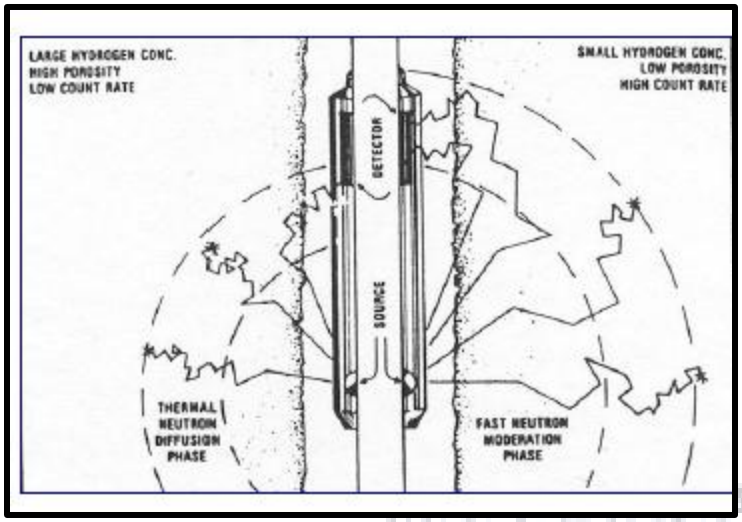

Figure 2.11: The single detector neutron tools in borehole environment

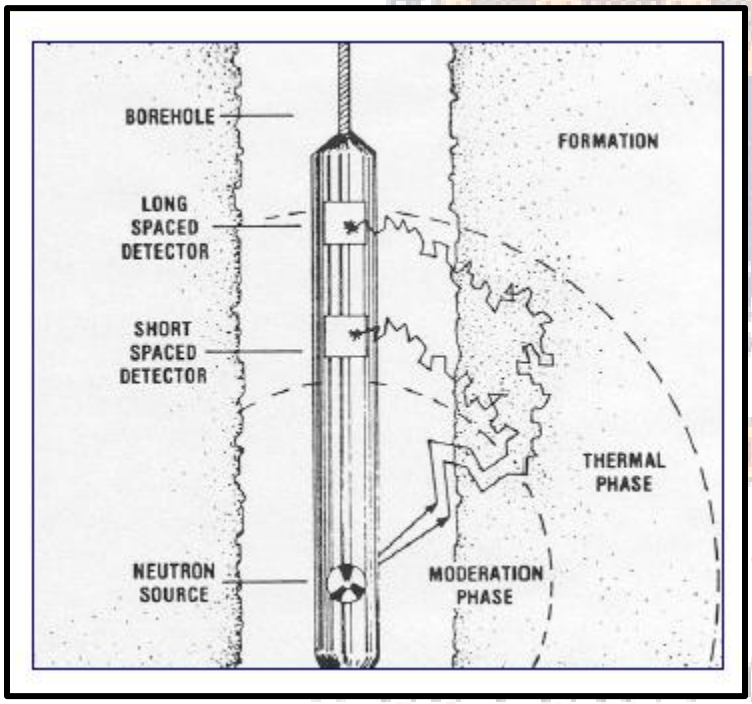

http://infohost.nmt.edu/~petro/faculty/Engler370/fmev-chap10-neutronlog.pdf

Figure 2. 12: The dual detection neutron logs in borehole environment

Compensated neutron log tool: Compensation neutron log tools are provided to measure the hydrogen index of down hole formations. The measurements are changed to porosity value which in combination with density too measurements that runs an indication of lithology and gas in the interested zone. Some of the compensated neutron tools provides both thermal and epithermal measurements. The thermal (slowed) measurements required a liquid filled

borehole while the epithermal (partly slowed) measurements can be made possible in air or gas filled boreholes.

This tool comprised of a radioactive source of either Cf or AmBe isotopes and set of two detectors. The emitting neutron source produces fast neutron that bombard the formation. The emitted neutrons are slowed (thermalized) by collision mostly with hydrogen nuclei in the formation. Parts of the slowed neutrons reoccurrence to the tools where they are counted by two He3 detectors, spread out at different distances from the source. The double yields supply compensation for rugose borehole settings.

Figure 2. 13 Showing Morden Compensated neutron log tool. Available at: http://www.ge-energy.com/products_and_services/products/wireline_systems/compensated neutron log.jsp Access on 15th/May/2013.

The application of neutron logs can be summarise as follow:

- Use to determine the porosity and lithology
- To delineate of porous formations
- To detect gas with other logs
- Estimation of shale contents with other logs.

2. 6. 5. Density log:

Density logs is a well logs that designed to measure the formation's bulk density i.e the entire density of rock includes solid matrix and the fluid enclosed. The logging tools consist of gamma ray (Cs_{137}) and shielded detectors from the source in other to records backscattered gamma rays from the formation depending on the electron density of the formation. The formation density is proportional to its bulk density. However, the source and the detector are usually mounted on a skid that pressed against the borehole wall. In addition, compensated density logging tool with the secondary detector are responds more to the mud cake together with the small borehole irregularities, the second detector used to correct the primary detector measurements. Density log is basically applied to uncased holes.

Quantitatively, the density log used to calculated porosity and indirectly, hydrocarbon density as well as acoustic impedance. Qualitatively used as lithology indicator, to identify certain minerals and assess source rock organic matter contents also help to identify overpressure and fracture porosity.

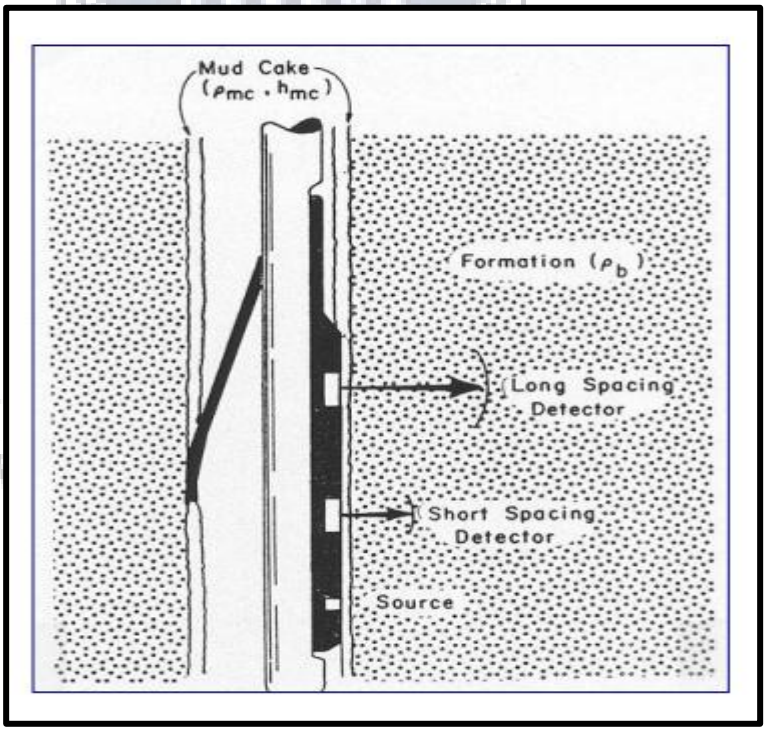

Figure 2.14: Showing compensated density tools (From Schlumberger, 1989, modified from Wahl, et al 1964).

In addition, porosity is calculated from density log based on the relationship below, the bulk density, (ρb) from the density log is measured as the sum of the fluid density (ρf) times its relative volume,(∅), plus the density of the matrix (ρ_{ma}) multiply by its relative volume i.e $1-\theta$ or $\theta = \rho_{ma} - \rho b / \rho_{ma} - \rho f$ ……equation……2.26

Some of the common densities of sedimentary rocks and fluids are presented in table 2.5 below.

Table 2.4: Showing the density of some sedimentary rocks by Myers, Gary D.,(2007).

Material	**Density(gm/cc)**	**Fluid**	**Density(gm/cc)**
Quartz	2.65	Fresh water	1.00
Calcite	2.71	Salt water	1.15
Dolomite	2.87	Oil	0.85
Anhydrite	2.96		

2. 7. Direct Hydrocarbon Indicator (DHI):

Direct Hydrocarbon Indicator is based on the observation of the acoustic characteristic of a gas-related reflector. Anstey (1977) defined Direct Hydrocarbon Indicator (DHI) as the method that based on recognition of specific acoustic characteristic that necessary for seismic signal in order to be associated to hydrocarbon presence. Such seismic characteristic include ''bright spot presence,'' dim spot'' and ''flat spot presence'' which are all post-stack amplitude analysis techniques and bright spot is the most classic direct hydrocarbon indicator which is caused by an increase in amplitude on seismic data. However, Direct Hydrocarbon Indicator can be simply defined as any feature or measurements on seismic data that gives evidence for presence of hydrocarbons accumulation in sediments and is normally used in reducing the risk associated with drilling a dry exploration well.

The application of seismic amplitude as hydrocarbon indicators was first used in 1970's when it was discovered that bright spot amplitude anomalies could be associated with hydrocarbon traps. However, the method of analysing seismic data quantitatively proposed by Hammond (1974), fundamentally changed the mode of searching for oil and gas worldwide. This process brought about the key increased of interest in the physical properties of rocks and the understanding of amplitude changes with the difference types of rocks and pore fluids (Gardner et al., 1974). The seismic amplitude reflect primarily a contrast in elastic properties between individual layers, having information about the lithology, porosity, pore-fluid types and saturation as well as pore pressure facts which cannot be obtained from the conventional seismic interpretation.

CHAPTER THREE

3.0: Geological Background of Pletmos Basin:

3. 1: Introduction

The Pletmos basin lies beneath the Indian Ocean Offshore from the Southern Coast of South Africa between Mossel Bay and Cape St.Francis. The basin covers about 10,000 km2 and filled with Postrift Cretaceous rock. It bounded on the north-east by the St.Francis Arch and on the South by the Infanta Embayment. The fault northern boundary of the Pletmos Basin closely follows the present Shoreline, and the Southern boundary is approximately at the 200m isobaths, south of which is the deep Southern Outeniqua Basin. Extending to the South ward is the Agulhas-Falkland fracture zone.

The Pletmos basin comprises the Plettenberg, northeastern, northern, southern and southeastern sub-basin. The sub-basins are mostly grabens, bounded all or in part by the Plettenberg, superior and pletmos faults. Although the fault systems were initiated during rift onset, they continue to impose significant structural control on the basin complex during most of it postrift Cretaceous history.

The lithostratigraphy and chronostratigraphy of the Pletmos sub-basin are similar to those of the Bredasdorp sub-basin have been described by Brown et al., 1995. The northeastern and southwestern flanks of the Pletmos basin, the St. Francis arch and Infanta arch, are enlongated basement highs (Figure 3.0). Basement in the Pletmos basin comprises slates and quartzites of the Ordovician to Devonian Cape Supergroup (Roux, 1997). Three tectonstratigraphic packages reflecting varying rates of subsidence and sediment supply constitute the synrift sequence in the Pletmos basin (Bate and Malan., 1992).

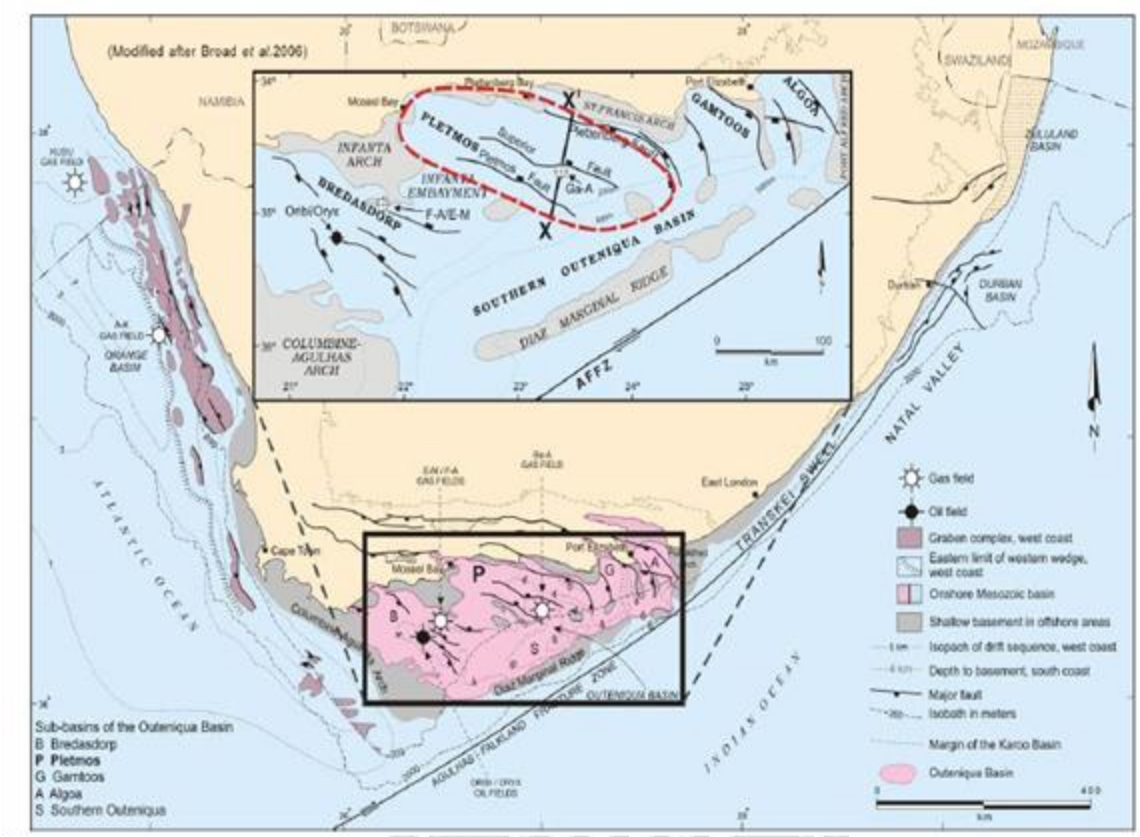

Figure 3.1 Location map of the Pletmos sub-basin.

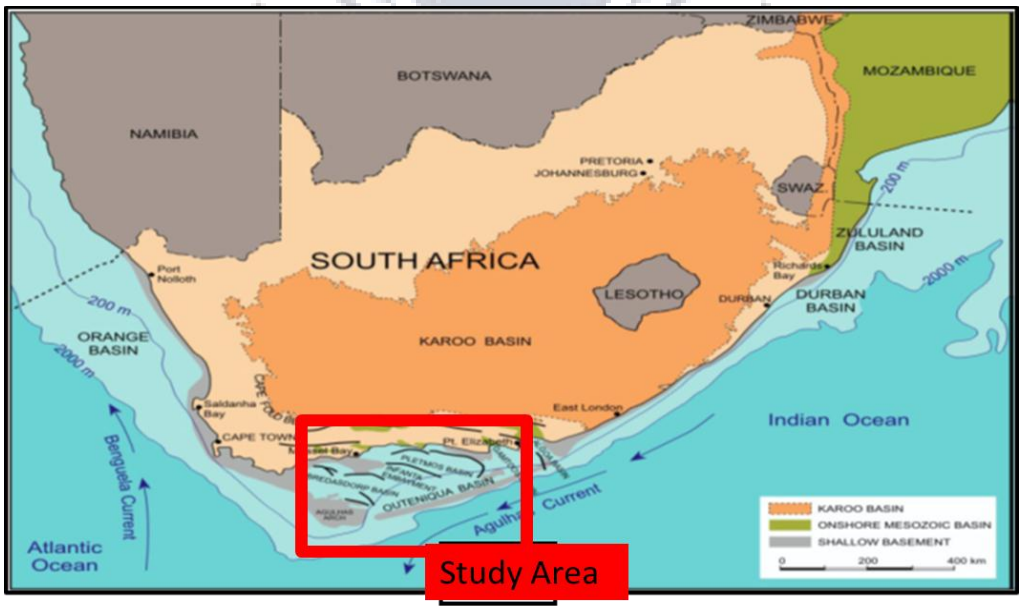

Figure 3. 2: Western, eastern and southern offshore zones of South Africa (Petroleum Agency SA brochure 2003).

3. 2: Tectonic settings of Pletmos Basin

Rifting in the Plemos Basin area began during the middle – late Jurassic. The result dextral transitional stress exerted north of the Agulhas –Falkland fracture zone. The initiated normal faulting along the northwest – southeast striking Plettenberg, superior and Pletmos fault system. Normal faulting and synrift deposition continue until early Valanginaian at ~126 Ma when most of the extensional faulting ceased, terminating synrift deposition and initiating postrift tectonics erosion and deposition. The widespread uplift north of the Aulhas-falkland zone enhanced the subaerial erosion of the second-order drift onset uncomformity, designated 1At1 of early Valanginian age 126 Ma. The subsequent deposition of the postrift supercycle 1At1 – 5 At1 126 – 117.5 Ma was localized in the plettenberg subbasin where fault subsidence continue to be the dominant tectonic control on the sedimentation. An event of transpressional uplift ~ 117.5 Ma enhances basement anticline produce clockwise rotation of the former rift fault system and terminated the first post rift surpercycle by the erosion of the second-order unconformity 6At1 117.5 Ma. A second postrft comprising sequence 6At1 to 12At1 117.5 - 112 Ma was generated by initiaaly rapid subsidence followed by diminished subsidence rates, perhaps caused by renewed transpressional stress between 117.5 Ma and 112 Ma. Transpressional stress may have locked the Pletmos subbasin and essentially reduced subsidence for about 4M.Y 116 – 112 Ma. Figure 3.6: Plate tectonic reconstruction illustrating the likely pre-break-up configuration of Late Jurassic to Early rift basins within southwest Gondwana.

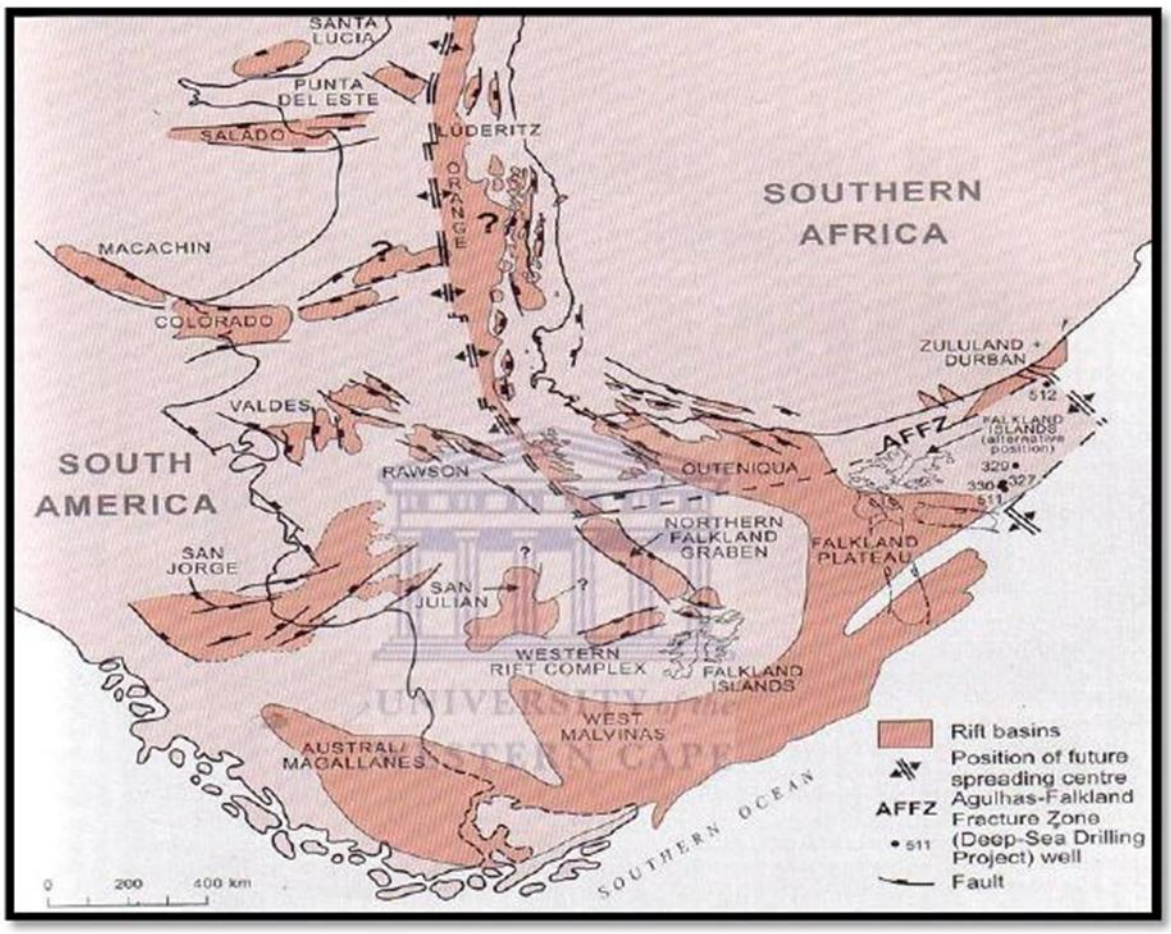

Figure 3.3: Plate tectonic reconstruction illustrating the likely pre-break-up configuration of Late Jurassic to Early rift basins within southwest Gondwana. An alternative inverted northeast position of the Falkland Islands illustrates the possibility that the Falklands microplate may have undergone clockwise rotation of 180o during continental separation (After Jungslager, 1999a).

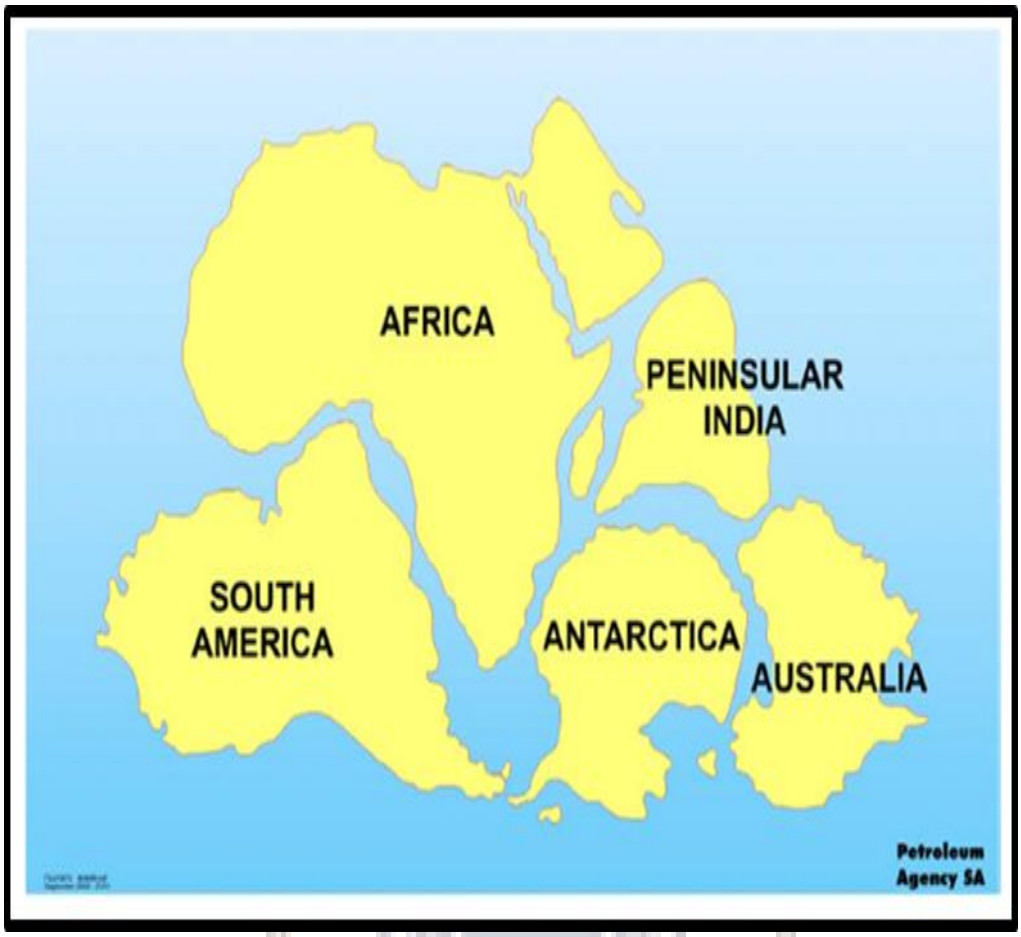

Figure 3.4: The rift phase in the Late Jurassic-Lower Valanginian showing the breakup of Africa, Madagascar and Antarctica (modified from Broad, 2004).

3. 4 Structural Development of the Pletmos Basin.

The Pletmos basin which is one of the subbasin of Outeniqua Basin consists of a series of en-echelon sub-basins each of which comprises a complex of rift half-graben overlain by variable thicknesses of drift sediments. The deepwater extensions of these merge into the Southern Outeniqua basin (Visser, 1998).

The syn-rift gas accumulations are trapped in tilted fault-block structures formed, or accentuated, during the second rifting phase in the Valanginian. These structures depend on the presence of mudstones overlying the rift-drift unconformity for their seal. The traps for the post-rift oil, gas and condensate accumulations are primarily stratigraphic, depending on depositional enclosure of the sandstone bodies within the thick mudstone succession, and modified by structural elements (IHS, 2010).

In the southern Cape, the elongate asymmetric anticlines and synclines of the Cape Fold Belt trend approximately E-W between about 20 and 24°E, before swinging sharply SE in the vicinity of Port Elizabeth Dingle et al., (1983). According to them, the major anticlines are typically bounded on their southern sides by large, southward throwing normal faults, and it is within the resultant, asymmetric, northward-tilting half grabens that the onshore mid-Jurassic to Lower Cretaceous taphrogenic basins developed. Although individual faults are not usually continuous for more than about 200km, two major fault lines controlled the location of the Worcester-Mossel Bay, and Oudtshoorn-Gamtoos series of outliers. Both fracture zones can be traced under the Agulhas Bank (as the Plettenberg and Gamtoos faults, respectively), where they form the northern boundaries of two major offshore sub basins: Pletmos and Gamtoos. Dingle et al., (1983) go on to say that in addition to these two main series of outliers, other basins occur in the Knysna-Plettenberg area and north of Algoa Bay, the former being partially fault-bounded on their southern sides, and rest on top of the main basement high which separates the Oudtshoorn-Gamtoos and Worcester-Pletmos basin lineaments. This high feature continues under the Agulhas Bank as the St Francis Arch. In the Algoa, Oudtshoorn-Gamtoos, and Worcester-Pletmos lineaments, the basins are strongly asymmetric, and sedimentation was

controlled by differential subsidence across major boundary faults, so that maximum thicknesses invariably lie adjacent to these main fractures (Dingle et al., 1983).

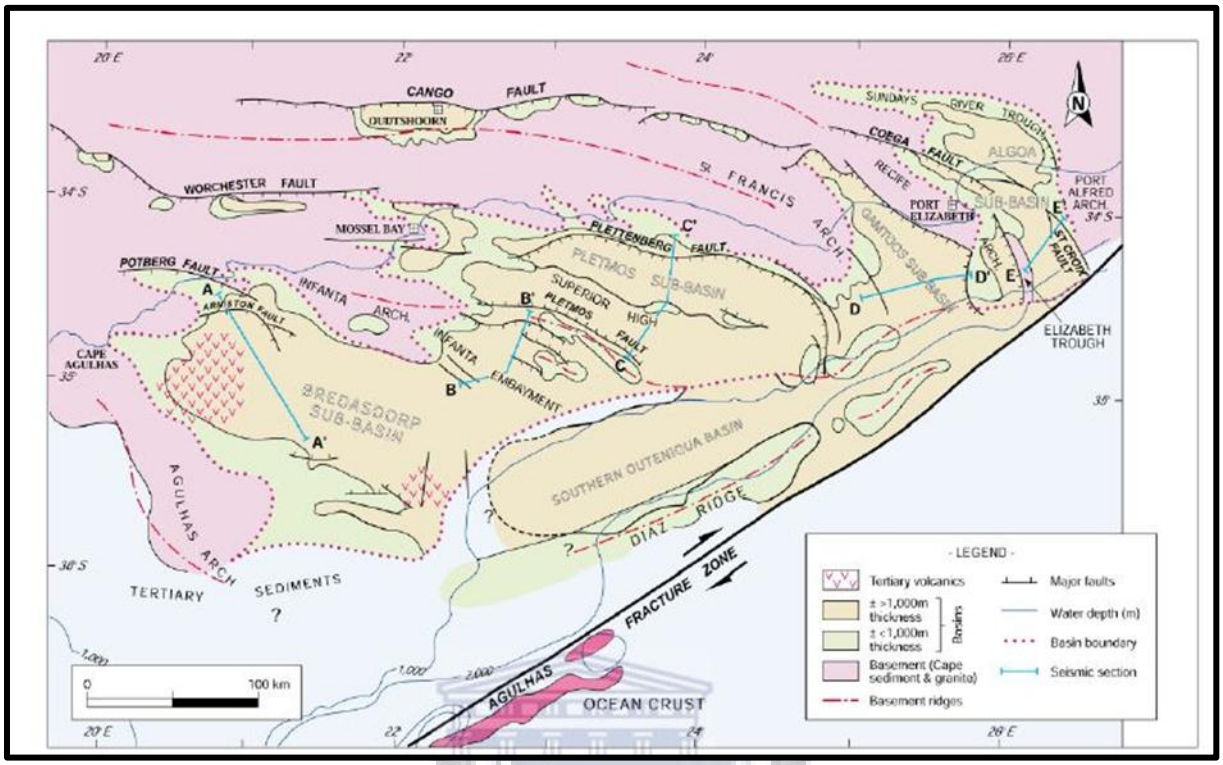

Figure 3.5: Major faults in the Pletmos Basin (Modified after Letullier, 1992 and McMillan et al., 1997.

3. 5: Sequence Stratigraphic and Chronostratigraphic Framework of Pletmos Basin.

The sequence stratigraphy and chronostratigraphy of Pletmos Basin were developed by Soekor geoscientist who interpreted more than 7000km of two dimensional seismic data and wireline log, microfossil, geochemical and petrographic information from twenty-eight boreholes. The boundaries of postrift Cretaceous sequence, system tracts and lowstand depositional system between the drift onset unconformity at ~126 Ma and the top of the lower Campanian at 77.5Ma were correlated throughout the entired seismic data set and tied to all of the wells in the basin.

In Pletmos Basin, the sequence are mostly type 1, some of the unconformities which shows intensive tectonically enhanced erosion are coincident second and third-order sequence boundaries. Others type 1 unconformities are coincident boundaries of both third-and-four-order sequence.

There are twenty-one fundamental third-order sequence (Seq) and twelve composite third-order sequence (Cseq) comprising sixty-four-order sequence in the basin. All of the sequence composite five postrift second-order surpersequence in the figure 3.8. The fundamental third-order sequence such as 6At1 117.5 – 116 Ma are composed of parasequence sets, which make up the component system tracts. Composite third other-order sequence such as 7At1 and 8At1 116 – 115Ma contain system tracts composed of fourth-order simple sequence sets.

In the Pletmos Basin of some of the composite sequence comprise extensive well developed system tracts that are seismically resolvable such as fourth-order sequence set 7At1 to 12At1 116 – 112 Ma. The fourth-order sequence typically show well defined seismically resolvable low stand system tracts. The sixty-seven postrift Cretaceous depositional sequence identified and analyzed from the Pletmos Basin are component of six supersequence bounded by seven tectonically enhanced highly erosional second-other type 1 unconformities such as 1At1 126 Ma, 6At1 117.5 Ma, 13At1 112 Ma, 14At1 103 Ma, 15At1 93 Ma, 17At1 80 Ma and the b21 At1 68 Ma.

The Supersequence 1At1 to 5At1 126 – 117.5 Ma is generally characterized by component third-order aggradation to progradation sequence sets. The super sequence 6At1 – 12At1 117.5

– 112 Ma in contrast, is characterized by alternating obique progradational and sigmoidal aggradational stacking patterns. The sequence sets are composed of third-order composite sequence and their component fourth-order seqeuence. The figure 3.8: showing Sequence chronostratigraphic framework of the Pletmos Basin (PASA, 2003).

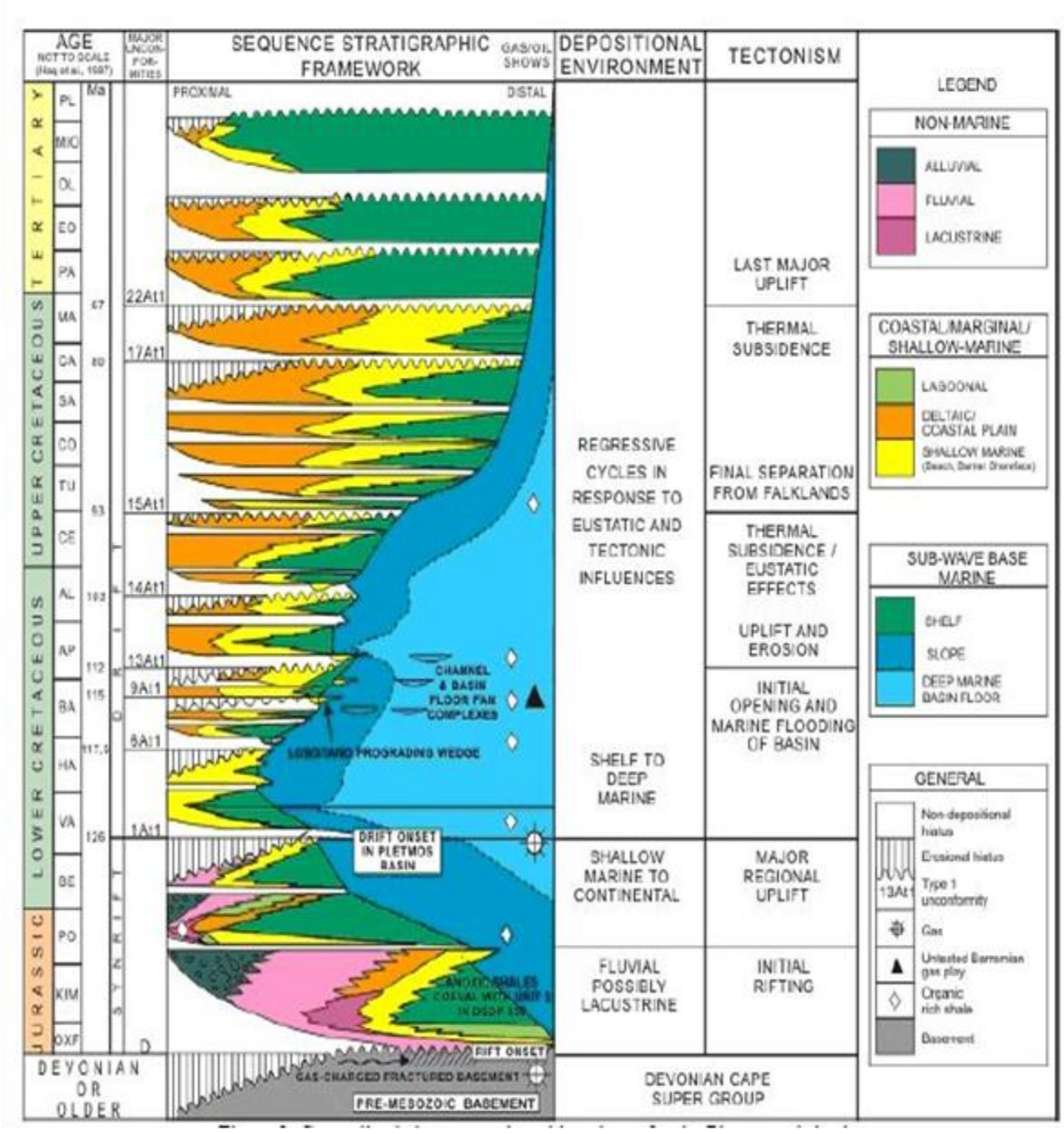

Figure 3.6: Sequence chronostratigraphic framework of the Bredasdorp Basin (PASA, 2003)

3.6: Geology History of Pletmos Basin.

3. 6.1 Basin Evolution:

Northwest-southeast trending half-grabens developed during the initial breakup of Gondwana in the Middle to Late Jurassic. Further rifting took place in the Valanginian, as South America separated from Africa. Tectonic activity persisted until the Aptian, especially in the eastern sub-basins, so long as transcurrent movement continued between the Falkland Plateau and the southern margin of Africa along the Agulhas-Falkland Fracture Zone (IHS, 2010).

According IHS 2010 report, the syn-rift grabens are infilled with continental clastic sediments and red beds, becoming lagoonal to shallow marine at the top of the syn-rift succession. A Late Valanginian unconformity marks the onset of drifting.

3.6.2 Rifting (Synrift Phase) (Portlandian – Valanginian)

Initiation of rifting and formation of the Mesozoic half grabens in the southern offshore began in the Middle Jurassic and is related to the separation of East and West Gondwana Dingle et al., (1983). The resultant extensional stresses reactivated the earlier compression related, pre-Cape and Cape lineaments to form the major basin-bounding normal faults such as the St Croix, Port Elizabeth, Gamtoos and Plettenberg Faults, where negative inversion (collapse) along these boundary faults created several Mesozoic depocentres namely the Sundays River, Uitenhage and Port Elizabeth Troughs and the Gamtoos and Pletmos basins (Bate and Malan, 1992). The arcuate shape of the basin boundary faults is likely to be inherited by the Cape Fold Belt tectonic grain as noted by De Swart and McLachlan, (1982).

According to Bate and Malan, (1992), the synrift succession (Horizon D to 1At1) can be divided into several tectonostratigraphic sequences recognisable in the study area:

1- A basal divergent wedge inferred to be Portlandian (above Kimmeridgian and below Berriasian) and older onlapping into crystalline basement and Cape Supergroup rocks.

2- A sequence with a high frequency/high amplitude seismic character displaying moderate to weak divergence of seismic reflectors dated Berriasian to Valanginian.

3- A Valanginian slope wedge with the rate of divergence increasing in thickness towards the fault far exceeding that of the previous packages.

These sequences suggest a multi-phase motion history of the boundary faults where a rapid initial propagation and subsequent creation of depocentres outstripped sediment supply leading to the formation of a highly divergent wedge onlapping basement. It can be inferred that the basal wedge consists of coarse and fine continental sediments typical of the initial stages of synrift sedimentation Lowell, (1990).

The slightly diverging second sequence is more conformable and considerably thicker than the adjacent packages. The continuity of a seismic character across the half grabens and the more conformable nature of the reflectors point to decelerated tectonic subsidence allowing the sediment supply to keep pace with fault-controlled subsidence. Slow and protracted rifting occurred over a wide zone forming sedimentary packages typical of an outershelf to inner slope environment Bate and Malan, (1992).

Early graben fill consists of Synrift I sediments, which have been dated Kimmeridgian, but may be as old as Oxfordian in the deep, undrilled areas. Where intersected, Synrift sediments comprise thick aggradational fluvial sediments in the north and marginal marine sandstones in the south Broad et al., (2006). They go on to state that later synrift I interval (Potlandian to Valanginian) comprise fluvial, shallow-marine and shelf deposits, which were sourced from the south-western and north-western margins of the basin and that the overlying horizon 1At1 unconformity has previously been referred to as the drift-onset unconformity but by analogy with the Bredasdorp sub-basin, it must also mark the onset of transform movement on the AFFZ and the onset of the second phase of rifting (Synrift II).

Synrift sedimentation continued until the Late Valanginian, when a further pulse of tectonism influenced the southern offshore basins. This second phase of tectonism was again extensional but of less intense nature that the earlier rifting stage forming Horizon D 38 Sequence stratigraphic characterisation of petroleum reservoirs in block 11b/12b of the Southern Outeniqua Basin.

Bate and Malan, (1992). This phase of extensional tectonics occurred as separation between South America and Africa was initiated Norton and Sclater, (1979); Dingle et al., (1983). Movement of South America away from Africa along a transform system, the Agulhas Falkland Fracture Zone situated off the southern edge of the African continental plate, was accompanied by the creation of oceanic crust in the Proto-Atlantic at 135 m.y. Martin et al., (1982).

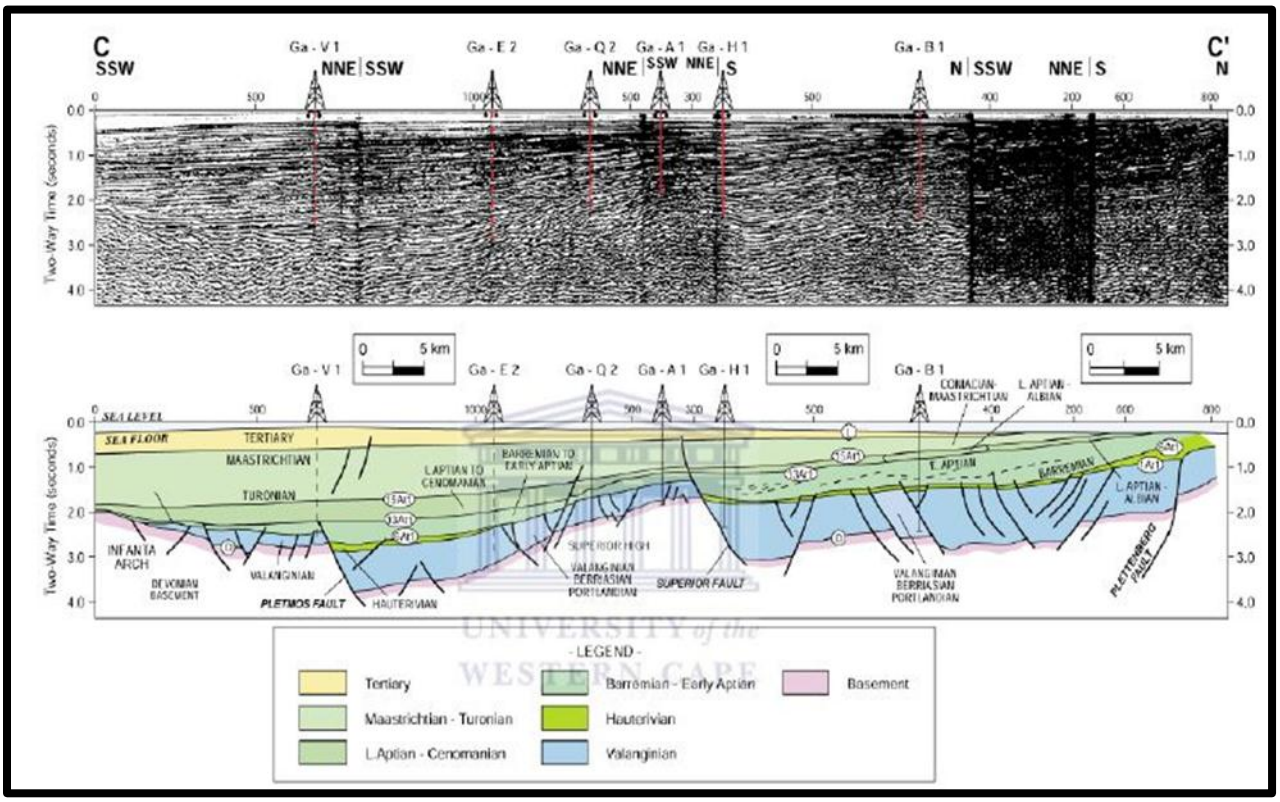

Figure 3.7 showing Seismic/interpreted geologic profile across the Pletmos Basin, showing tectonostratigraphis units (Modified after McMillan et al., 1997).

In the Algoa, Gamtoos and Pletmos Basins, 1At1 appears to be a non-erosive or only locally erosive unconformity with limited erosion of fault block crests and subsequent redeposition adjacent to the fault scarps. Thus 1At1 represents a slightly modified rifted landscape which has subsequently become buried by the thermal subsidence succession. It also represents the boundary between two different tectonostratigraphic styles Bate and Malan, (1992).

These sediments were sourced directly off the flanks of the basin and down the axis of the grabens in a south-easterly direction Roux, (1997).

Major subsidence of the Outeniqua Basin after the transform-onset unconformity (1At1) led to deep-marine, poorly oxygenated conditions within the Pletmos and other sub-basins. Sequences 1A to A, which constitute syn-rift II deposition, comprise aggradational deep-marine claystones and thin turbidites and contain organic-rich shales which are significant petroleum source rocks Broad et al.,(2006).

According to Roux, 1997, the normal faults associated with rifting are parallel to the compressional tectonic grain of the Permo-Triassic Cape fold belt. The St. Francis and Infanta arches are bounded by major normal faults between which the Pletmos basin depocenter is developed.

The early rift fill consists of thick Kimmeridgian age sediments that filled a number of south-easterly trending grabens during horizon D (top basement) to horizon O times in figure 3.9 Some of these early depocentres, like the Plettenberg graben and the Southern Outeniqua basin are expected to contain Kimmeridgian oil-prone shales, similar Sequence stratigraphic characterisation of petroleum reservoirs in block 11b/12b of the Southern Outeniqua Basin. Roux, (1997).

He further explains that early fill is overlain by thick aggradational fluvial sediments in the northern Pletmos basin and marginal sandstones in the southern Pletmos basin. The late synrift interval from horizons O to 1At1 comprises fluvial, shallow marine, and shelf deposits of Portlandian to Valanginian age. The sandstone content of the entire synrift succession increases towards the Southern Outeniqua basin in a south-westerly direction away from the sand-starved Plettenberg graben.

3.6.3: Petroleum Systems

From IHS Basin Monitor Report, 2010 there is essentially only one petroleum system in the Outeniqua Basin, comprising Aptian (sequence 13A) source rocks and predominantly Early Cretaceous reservoirs. Maturation may have occurred first in Cretaceous times, but the periods of generation believed to have charged the observed accumulations took place in Early (60 Ma) and Late (5 Ma) Tertiary. Considerably larger volumes of hydrocarbons have probably been generated than remain in the basin today. Retention is lower risk in the west than in the east, where tectonic control persisted through latest and major faults as they penetrate higher up into the succession.

3.6.3.1: Reservoir Rock: The reservoirs for the Mossel Bay area gas fields in the northern Bredasdrop Sub-basin are Valanginian shallow marine sandstones underlying the rift-drift unconformity.

These are typically well sorted and have significant secondary porosity (IHS, 2010).

They go further to affirm that the other major reservoirs are deepwater mass flow sandstones in channels and fans within the mudstone-dominated sequences that overlie the rift-drift unconformity; the most important of these sequences for reservoir development is the 14A sequence of Albian age. Fractured basement forms a secondary, minor, reservoir in a single discovery.

3.6.3.2: Source Rocks: Deepwater conditions with a tendency to anoxia were established repeatedly through the Lower Cretaceous succession, overlying each of a number of basin-wide unconformities. Organic-rich mudstones were deposited in each of these episodes, forming potential source rocks. The Aptian 13A sequence contains the most significant of these, and much of it is in the oil-generating window at the present time. Older source rocks are more sequence stratigraphic characterisation of petroleum reservoirs in block 11b/12b of the Southern Outeniqua Basin, deeply buried and are over mature. Younger source rocks could be mature in the deeper water areas of the basin, including the undrilled Southern Outeniqua Sub-basin (IHS, 2010).

3.6.3.3: Seals: Early post-rift deepwater mudstones directly overlying the rift-drift unconformity provide seals for the Valanginian syn-rift reservoirs. The post-rift deepwater sandstone reservoirs are sealed and enclosed by the deepwater mudstones into which they were deposited (IHS, 2010).

CHAPTER FOUR

4. 0: MATERIALS AND ANALYTICAL METHODS:

This chapter portrays the techniques utilized for this study. Figure 4.1 show the flow chart of the different methods that was utilized within the course of this study. The well logs and the seismic data were provided by the Petroleum Agency, SA. The software utilized for this study is Interactive Petrophysics IP and the Kingdom suites SMT.

- The data sets include: Well completion report.
- Well survey data including checkshot data and well top.
- Digitized wireline log data (LAS format).
- Seismic survey data in SGY format and 2D seismic lines.
- Engineering well completion records.
- Conceptual map of the block.

The procedure starts with the review of preceding studies and literature search in similar oil and gas fields needed to give data on the basin geometry, tectonic history, sediment source, the digenetic history, structural characteristics and the flow unit 'i.e. to know the basic geology and the detail of the hydrocarbon exploration within the offshore environments of the South Africa region. The discussion of the pore pressure prediction techniques includes the principal of determination, the fracture gradient and effective stress also the estimation using compaction trend curve as a result of local difference in the relation between the porosity and vertical effective stress. The contribution of this mechanism apart from the disequilibrium compaction, unloading processes, tectonic stresses and chemical compaction which believe to have caused overpressure zone in reservoir to observed overpressure are necessary to improve pressure prediction in high pressure region, and analytical program are used in this study. The effective stress, fracture gradient and the overburden gradient of some interested depth intervals, pore pressure, fracture pressures are carrying out. This is supported with the utilized of wire line logs to select depth of interest for analyze reason The direct hydrocarbon indicator (DHI) was determined by the amplitude and reflectivity strength through the horizon picking from the seismic based on well tops by means of using post stack surface seismic amplitude

extraction to validate it association with hydrocarbon trap. The geology architecture of bright spot, flat spot and the dim spot study would create a geologic model which will be used to enhance the characterization of amplitude anomalies changed with the rock type. The data gathering segment has rundown of all the data gathered from petroleum Agency SA, which is utilized as a part of this thesis. They are loaded into the software to display the log curves reference to Kelly bushing (RKB).

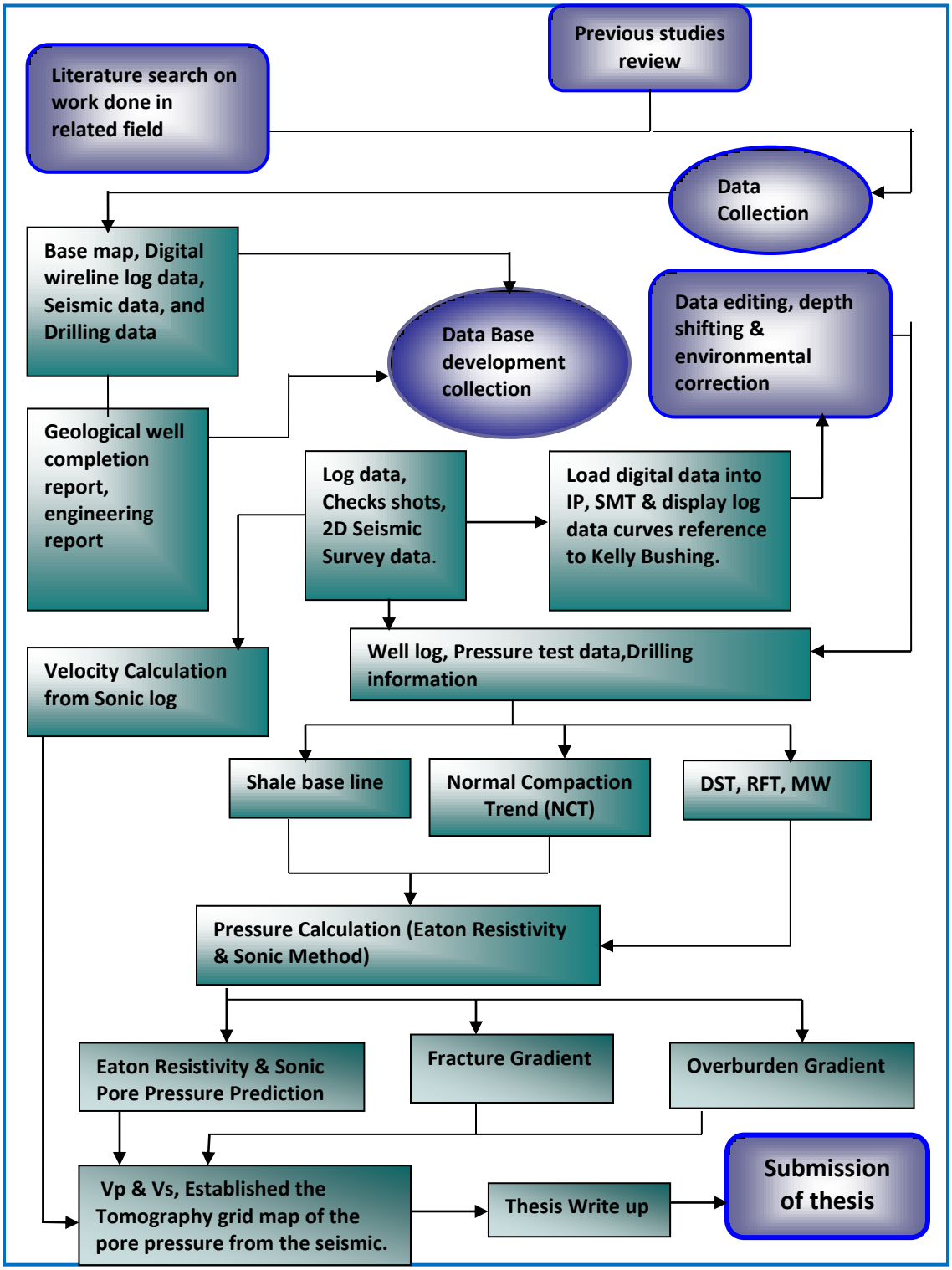

Part 1, Figure 4.1 a: Methodology flow chart for Pore pressure prediction from wireline log and Seismic data.

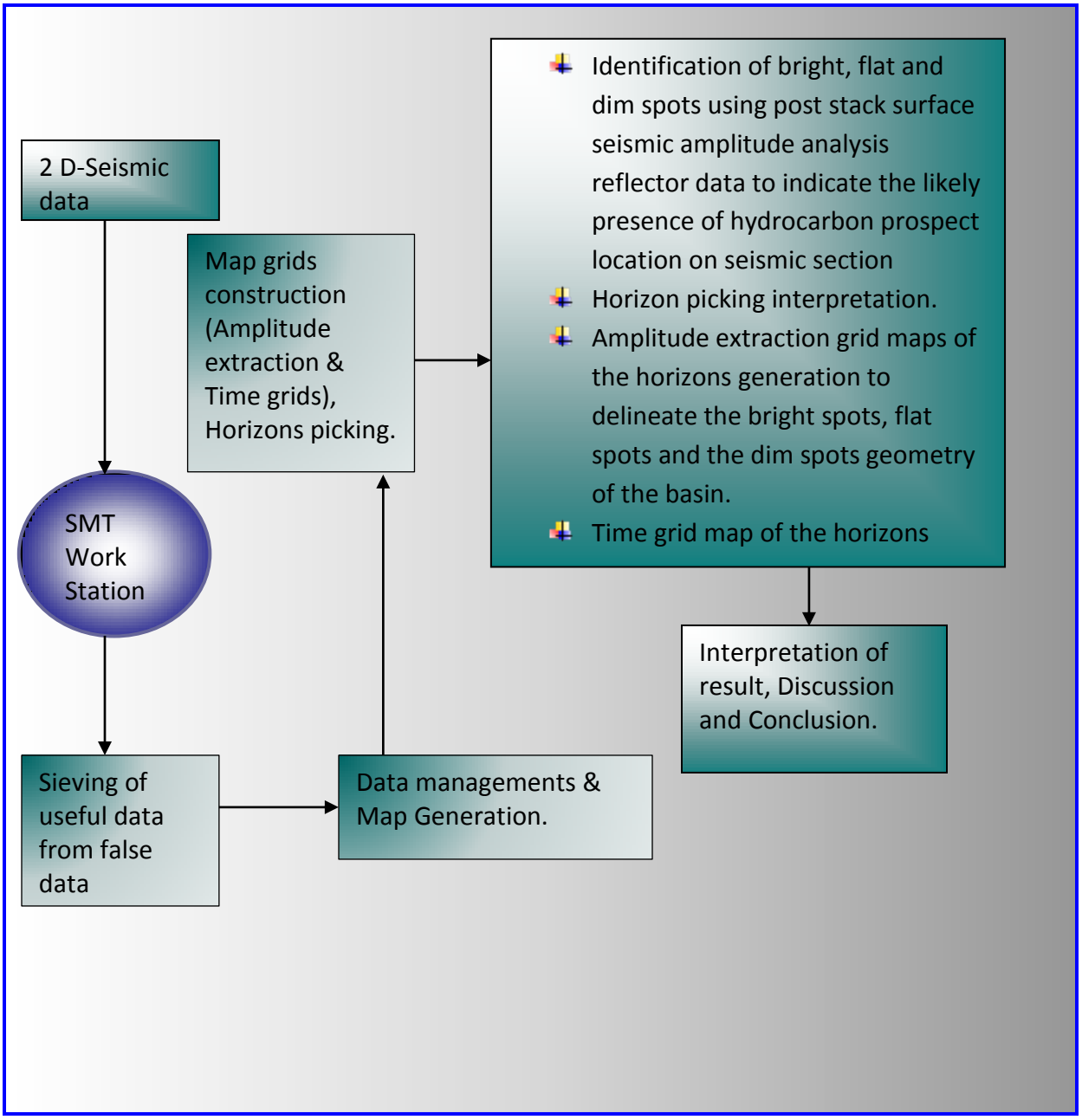

Figure 4.1b: Methodology flow chart for DHI (Direct Hydrocarbon Indicator).

4. 1: Wireline log loading:

The wireline loading and display of the log curves were carried out using Interactive Petrophysics (IP) and Kingdom Suite (SMT). The data were conventional in LAS format and loaded into the Interactive Petrophysics workstation where depth shifting was carried out according to the core description and required environmental corrections was also carried out. However, this data were also loaded into the SMT (kingdom suite) in LAS format as for the logs and the Seismic was also loaded in SEG-Y format. The SMT's (Kingdom Suite) were used to carry out various interpretations, modeling and analysis of the digitized data. Adequate quality controls such as splicing and editing of the log curves were performed in order to aid the identification of the reservoir zones using the suitable well logs. SMT's (Kingdom suite) was selected to model the likely hydrocarbon prospect within the Seismic horizons, data base was created within the SMT's plainly delineating the different information and data required to complete this project. Moreover, the geological, petrophysical and geological data were imported to the SMT's data based workstation which enhanced the possibility to generate and visualize the imported data in 2D. Nevertheless, in this project Eaton's resistivity method with depth normal compaction trendline and Sonic travel time velocity log curves will be used to determine the overpressure and normal pressured zone to aids in predicting the pore pressure condition of the selected interval zone.

4.2.0 Description of Eaton's resistivity method with depth-dependent normal compaction trendline :

The Eaton's method is an empirical method used to estimate pore pressure from the sonic, resistivity and the density log which have been calibrated to measure pore pressure from the RFT (Repeat Formation Test) and DST (Drill Stem Test). This logs data can give clique indication of pressure condition of the overpressure and normal pressure zone. The Eaton methods such as resistivity plots and sonic log plots are one of the extensively used quantitative methods, this method put on a regionally defined exponent to a an empirical formula. Eaton uses equation 4.1 for the calculation of pore pressure gradients through resistivity as follows:

$PP = OBG - (OBG - PP_N)(R_O/R_N)^X$……equation 4.1

Where : 'PP' is the Pore Pressure gradient (ppg), 'OBG' is the Overburden gradients (ppg), '$PP_{N'}$ regarded as the Normal Pore pressure gradient (ppg), 'Ro' is the Observed resistivity (ohms-m), '$R_{N'}$ is the Normal Resistivity (ohms-m) and 'x' is the Eaton exponent which is 1.2.

In Eaton's equation above is it very problematic to determine the shale resistivity state of the hydrostatic pore pressure, the best way out is to determine normal compaction trenline for the pore pressure prediction, since the 'Rn' which is normal resistivity is a function of burial depth. However, due to the relationship of restrained resistivity and burial depth in normal pressure formation, this equation of the normal compaction trend of resistivity can be used such as follow: $\ln R_n = \ln R_o + bZ$ .....equation 4.2

Where: 'Rn' is the shale resistivity in the normal compaction states, 'R_0' is the shale resistivity in a mudline, 'b' is the constant while 'Z' is the depth of the mud line below. By substituting the equation 4.1 into equation 4.2 Eaton resistivity equations can be written as following:

$P_{pg} = OBG - (OBG - P_{ng})(R/R_o e^{bz})^n$ .....equation 4.3

Where 'R' is the shale resistivity measured at depth 'Z', Ro is the normal compaction shale resistivity in the mudline and 'b' is the logarithmic resistivity normal compaction line slope.

4.2.1 Description of Eaton's sonic velocity method with depth-dependent normal compaction trendline :

Eaton (1975) presented an empirical equation used for pore pressure gradient prediction from sonic compressional transit time (Δt_n) based on :

$P_{pg} = OBG - (OBG - P_{ng})(\Delta t_n/\Delta t)^3$.....equation 4.4

Where Δt_n is the sonic transit time or the slowness in shale at normal pressure.

Sayers et al. (2002) worked on Slonick (1936) relationship as follow:

$V = V_0 + Kz$.....equation 4.5

Where V is the seismic velocity at the depth Z and V_0 is the ground surface velocity, k is a constant, as a normally pressure velocity for pore pressure prediction. He recognized a normal compaction trend for shale acoustic travel time with depth with an exponential relationship to an averaged acoustic travel time from 17 normally pressured wells (van Ruth et al., 2004): as follow: $\Delta t_n = 225 + 391e^{-0.00103Z}$ .....equation 4.6

Where Δt_n is the acoustic transit time from the normal compaction trend at the depth of investigation (μs/m), and Z the depth in meters. However, (Tingay et al., 2009) also used the similar relationship as follow: $\Delta t_n = 176.5 + 461.5e^{-0.0007Z}$ ……..equation 4.7 in some petroleum basin such as Brunei, thereafter generated the following relationship of the normal compaction trend of the transit time as follow:

$\Delta t_n = \Delta t_m + (\Delta t_{ml} - \Delta t_m)e^{-cZ}$…….equation 4.8

Where Δt_m is the compressional transit time in the shale matrix with zero porosity, Δt_{ml} is the transit time mudline, and 'c' is constant.

By substituting equation 4.7 into equation 4.8, the Eaton 'sonic modification can be expressed as follow:

$P_{pg} – OBG – (OBG – P_{ng}) (\Delta t_m + (\Delta t_{ml} - \Delta t_m) e^{-cz}/\Delta t$…….equation 4.9.

According to Matthew (2004), discovered that the majority of the uncertainty associated with pore pressure prediction is related with the correct choice of normal compaction trend (NCT), citing some example of resistivity log. The normal compaction trend (NCT) is used to predict pore pressure according to divergence of the petrophysical measurements from the normal compaction trend, offered an optimum fitted linear trend at which compaction occur. Therefore the prediction of pore pressure from the seismic data was aided by mean of using velocity transit time data from the sonic logs. Hence, the normal compaction trend (NCT) constructed for this study are mainly from the resistivity logs and velocity logs from sonic data.

4. 3. 0. Some Petrophysical calculation procedures:

The procedures approach used in determining the petrophysical result is as follows:

4.3.0.1 Volume of shale (vsh): The volume of shale was calculated to derive appropriate values of overburden gradient. The total shale volumes (Vsh) were computed from the gamma ray log with the aid of this equation:

Vsh = GRlog – GRmin/GRmax – GRmin……..equation 4.10

Where GRmin correspond to the minimum values in the sandy formation area and GRmax indicate the maximum values of the shale formation area.

4.3.0.3 Porosity: The porosity of the selected reservoir formation was calculated from the recorded porosity logs. Density (RHOB) and neutron (NPHI) are the logs used for this research work. Porosity from density log ($\emptyset_D$) is given as: $\rho_{ma} - \rho_{log} / \rho_{ma} - \rho_f$ ……equation 4.11

4.3.0.4 Overburden gradients: The overburden gradient was estimated by calculating from bulk density volume of clay from the gamma ray log relatively to the Kelly height and water depth to determine the rate of compressibility of the selected wells i.e. the effective stress, because porous rocks are subjected to both internal and external stresses when buried, the internal stresses occur from the fluid pore pressure with typical gradient of 0.433psi while the external stresses created from the weight of the overburden with typical value 1.00psi/ft. These combination of the external and internal stress resulted in corresponding strain or rock deformation in the reservoir. The external stress tend to compact the rock and reduce the pore pressure volume while the internal stress resist the pore volume, the difference between this are regarded as effective stress as expressed (Terzaghi, 1943) in the equation below:

∂eff = ∂s – $P\rho$……equation 4.12

Where ∂eff is the effective stress, ∂s is the total overburden pressure and $P\rho$ is the pore pressure.

4.3.0.5 Compressional and Shear wave velocity: The Compressional and Shear wave velocity (Vp and Vs) in m/s were not given and was generated from the Sonic log DT (us/f) by using the equation below as fellow:

Vp (m/s) = 10^6(0.3048) /DT (us/f) ……equation 4.13

Also, the Shear wave velocity Vs (m/s) was estimated from the from Vp (m/s) using (Greenberg-Castagna 1992), equation, empirical relationship for Shale as the well corresponding to Shale based on the gamma ray log, the equation is expressed below:

Vs (m/s) = 0.76969 Vp – 0.86735……equation 4.14

Note; Vp and Vs must be measured in km/s in this equation for appropriate use and converted to m/s.

4. 3. 0.6 Density Estimation: The density was calculated for the wells to determine the level of the porosity and formation fluid volume. The density was estimated by using sonic velocity (DTs), Gardner method using this equation as follow:

Rho = a*Vp ^ b……equation 4.15

Where Rho is the density, a & b are constant value of (0.23 & 0.25).

Also Lindseth method was also used for the density estimation to determining the transit travel time compressional velocity (DTc) based on the equation below as follow:

Rho = (Vp – 3460)/ 0.308 * Vp) ……..equation 4.16

Where Rho is the density, Vp is the compressional velocity.

4.3.0.7 Temperature Estimation: The actual temperature needed for this study is the temperature obtained from the wireline formation test (WFT), since no well formation such as RFT, DST test was performed for these wells. However, static formation temperature from well log an empirical method of temperature recorded for individual logging runs was used to estimate formational temperature. The considered average geothermal gradient for the wells was 3.52 degree Celsius per 100m. Therefore, the temperature estimated for the selected wells are calculated in degree Fahrenheit (^{0}F), the temperature –depth relationship for the wells are calculated based on this relationship below as follow in a linear function:

TD = TS + αD……equation 4.17

Based on the fact that earth contains some molten core where heat is generated thereby it is consistent to accept that temperature should increase with depth.

Thus, (TD) is the reservoir temperature at any depth; (TS) is regarded as the average surface temperature; (α) is the temperature gradient (degree/ft) and (D) is the depth in ft.

4. 4. 0. Seismic section: The seismic data was loaded in Kingdom suite Technology software's (SMT) in SEG-Y format, and the well was also loaded able to displaced on seismic relatively to it Latitude and Longitude coordinates (X & Y) as well as the checskshot correction data. However, the checkshot is the borehole seismic data survey design to measure the seismic travel time from the surface to a given depth. The sonic log was calculated with the available of checkshot data. The wells tops were also loaded to infer each of the lithology boundaries. Horizon picking

come into play by mean of the amplitude reflection from the seismic and no fault were marked. However, to produce the map by using the Kingdomsuite, first is to create grid options and two types of grids for the horizons such as amplitude extraction grids map and time grid map were created. The gridding parameters within the kingdom suite were adjusted manually to control some false anomalies that may arise with the amplitude extraction grids known as sieving process.

4. 4. 1. Mapping the horizons:

Horizons were created in a Kingdom Suite interpretation module called 2d- 3d Pak, where the horizon management dialog box was opened and a new horizon name was created and a colour was selected for the horizon of interest. Horizon picking followed, which was done manually by clicking the event that matches the base of the sand body which had to be interpreted. The event could be a peak (positive) or a trough (negative). The base of a sand body was chosen to observe how the depositional environment changes through time with the muddy plain.

Once the horizon has been mapped it will show on the base map from the Kingdom main menu, the horizons picking toolbar was selected to change from one horizon interpretation to another. Quality control of the horizons picking was considered where the tracking failed to pick due to poor signal-to-noise ratio.

4. 4. 2. Amplitude Exctraction:

The amplitude extraction map grid was created in the Kingdom Suite from the existing mapped horizons by means of basic Math calculator from the tools where the parameters box was opened to select the smooth function mean and the input surface name horizon were choosing and amplitude extraction grid and time were computed and view from the base map Kingdom suite main menu.

4. 4. 3. The grid Tomography Extraction Map:

The grid tomography extraction map was generated from the seismic in the Kingdom Suite where the consistent set of refecting horizons was picked to create the interval velocity volume in depth by means of basic Math calculator from the tools where the parameters box was opened to select the smooth function mean and the input surface name horizons were

choosing to extract and compted, view from the base map Kingdom suite main menu. In order to delineate the pore pressure attribute of the wells.

4. 5. 0. The limitation of the study:

I. The seismic data used for this study is 2D-seismic, its quality and resolution are not sufficient, very poor and is old datas thereby some geologic model structures could not be identified.

II. In addition, the qualities of the seismics data could not be loaded on Petrel software due to its mode of aquiring and processing. As a result, the geologic model structure are impossible to visualise, as Petrel software would have been the prefered choice workstation than Kingdom suite technology (SMT).

III. No pressure data such as repeat formation test (RFT), drill stem test (DST), leak off test (LOT) and porosity data was performed for the selected wells (GA-W1, GA-N1 and GA-AA1) during the drilling operation. Thus, the formation pressures situation of the reservoir wells was ascertained based on well data reports.

IV. However, the study was mainly done with the available data provided for arriving at proper prediction of the pore pressure with the value of mudweights obtained from the pore pressure gradient and fracture gradients. These values was considered to minimized the lost and risk that associated with drilling rigs such as blow out.

4. 5.1. nterpretations: the interpretation stage involves placing together all the information and the observations from the different wells in a unified and meaningful approach. For this study, data interpretation comprises, first of all, predicting the pore pressure condition of the selected wells and identifying the presence of the overpressured and normal pressured zones of the intervals depths of interest as well possible contributory mechanisms. This was possible by evaluating the compaction trendline (NCT) from the resistivity log and the sonic log as well as generating pressure vs depth plot with the of Eaton's equivalent depth method. Identification of bright spot, flat spot and dim spot as well as thick sand deposits through horizon picking. Creation of amplitude extraction grid maps and time grid maps of the picked horizons was used as bases of the direct hydrocarbon indicators (DHIs) to delineate the likely presence of hydrocarbon location on seismic section.

CHAPTER FIVE

5.0 The Petrophysical wire line logs and Pore Pressure Results: Interpetation and Discussion.

Accurate prediction of pore pressure is the major component of exploration risk analysis and the knowledge of formation pore pressure for any overpressure reservoir is very important in the evaluation of oil and gas fields. Detecting abnormal pressured zones has become an integral part of the prospect evaluation and well planning, because negligence in accurate prediction of pore pressure prior to drilling or during well development may result to formation damage. The study of the pressure prediction from the selected drilled wildcat wells GA-N1, GA-W1, & GA-AA1 of Early Cretaceous (Hauterivian to Early Aptian 112 - 117.5 Ma.).In the Pletmos, Basin offers an opportunity to interpret the subsurface pressure conditions, to calibrate mechanical logs with interpreted lithology as well as to use the data in enhancing field development during drilling.

This chapter presents the results of the geophysical logs and the pore pressure prediction interpretation of the three wells GA-N1, GA-W1, and GA-AA1 respectively from the resistivity and sonic logs using Eaton's equivalent depth method as applied by Zhang (2011).

The geophysical well log interpretation of well GA-W1. The reservoir depth intervals of interest range from 1866.79 m to 1887.93 m, this zone was selected based on its reservoir capability attributes from of the studied neutron log, and resistivity and gamma-ray logs readings. The lithology interpretation from the gamma ray clearly indicated a good seal potential above and below the indicated depths. One of the criteria of a good reservoir is that it must have a good seal (shale rock) acting to form of four way closure which will resist further migration of hydrocarbon from the reservoir. The shale serves as a good seal due to its very fine- grained texture of limited pore spaces with high capillary force to retard fluid flow. Based on the gamma-ray, neutron and resistivity log readings, the interval of interest sub-divided into sections (A-D) which clearly differentiate the reservoir sandstone formation from the shale formation. This has been done in order to ascertain the pore pressure condition of well GA-W1. The well log suite of well GA-W1 is shown below in the figure 5.1. The first track on the log suite

shows the gamma-ray log, second track indicates the depth interval in meters. This is followed by other relevant logs such as resistivity log, (track three) caliper and bit sizes, (track four) density log, (track five) neutron log, and (track six)corrected density log and the sonic log which were all utilized. The (track seven) in the log suite indicates temperature, (track eight) compressional and (track nine) shear wave log track.

5.0.1 Petrophysical wireline logs interpretations of well GA-W1.

The gamma-ray log suite in (Figure 5.1) of well GA-W1 mainly evidence of an interbedded series of sandstones and shales. The deflection of the gamma-ray towards high values scale is an indication of shale while deflection to the lower values on the scale is indicating a sandy. The interval of interest sub-divided into four sections A-D (Figure 5.1) .The baseline which is the line use to demarcate between the shale formation and sand formation along the gamma ray log. The low and high gamma ray log values within the selected interval are 28.89 API and 118.31 API respectively, which are interpreted as sand and shale formations respectively. Section A' ranges from 1866.71 m to 1875.40 m, which clearly indicates the reservoir sand formation with the combination of neutron and resistivity logs. Section B' ranges from 1875.25 m to 1878.50 m and shows shale formation. Section C' ranges from 1878.50 m to 1881.32 m also indicating reservoir sand formation. Finally, section D' falls between 1881. 32 m to 1887.95 m and this indicates a reservoir quality sand formation. The irregular gamma-ray log signature shows the significant variation of the sand grain size as a cylindrical pattern coarsening upward suggests that the sand bodies might have been deposited due to vertical accretion progradation (Braide, 2012 which allow the sand bar to overlay the initial bar of shale and silt. This indicates the pattern of the deposit but does not identify the sedimentary facies or environment.

The induction deep log resistivity (ILD) and micro spherical focus log (MSFL) Figure 5.1 track three are used to measure the formation resistivity in the borehole containing oil and fresh water based drilling mud. The microspherical focus log (MSFL) has a good vertical resolution and a capability of investigating shallow depths, detecting small mudcake effects in the borehole wall as well as it is able to measure only the invaded zone and identify thin bed. The

induction deep log resistivity (ILD) is used due to its capability of measuring deeper into the borehole.

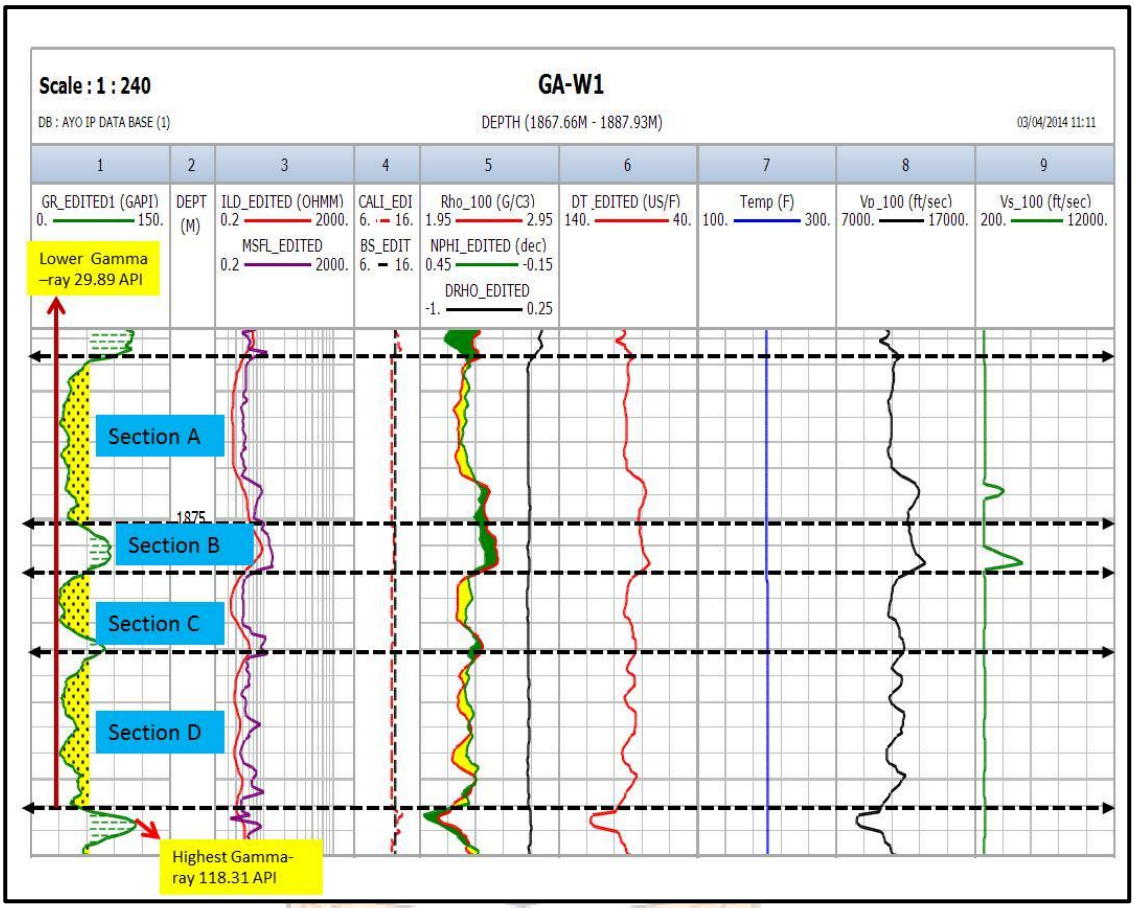

Figure 5.1: The Well logs suites for Well GA-W1.

The resistivity values within the selected interval depth vary. The interval depths of the reservoirs sections A, C, and D, with depths 1866.71 m to 1875.40 m, 1878.50 m to 1881.32 m and 1881. 32 m to 1887.95 m respectively have lower resistivity values ranging between 0.663 (ohm/m ILD) and 1.39 (ohm/m MSFL) which suggests that the reservoirs interval formations are porous and have been invaded by fresh water mud, which enhanced the overpressure formation of these interval as a result of under-compaction of the zones. The interval depth section B, 1875.25 m to 1878.50 m is a shale formation with resistivity values ranging from 2.45 (ohm/m ILD) to 4. 76 (ohm/m MSFL). This suggests that the reservoir intervals of this formation are compacted thereby invaded with less fresh water which resulted in the development of a normal pressure zone (Rider. 2002).

Track 4 the calipers log and the bit-size which are used to determining the variation of diameter borehole with depth, size and shape of the hole. The bit-size is the reference line use to determining the increase or decrease of the borehole diameter which enhance easy penetration during the drilling of the borehole. The interval depth reservoirs sections A, C and D, depth 1866.71 m to 1875.40 m, 1878.50 m to 1881.32 m and 1881. 32 m to 1887.95 m have diameters of their borehole reading from the caliper log as 10.1" (inch) and the bit-size reading is 12.2" (inch). Based on these values of caliper and bit-size readings, shows caliper reading is less than bit-size reading, it indicates the occurrence of tight spot during the drilling. This may cause the stucking of the bits during the pulling out process from the well. The tight spot may have occurred as a result of abundant clay mineral such as smectite, because smectite is a swelling clay mineral which normally absorbs water from the drilling mud. Therefore, could enhance the pressure formation of the zone. In addition, reservoir depth section B, 1875.25 m to 1878.50 m have the same reading of Caliper log as 12.2" (inch) and the bit-size as 12.2'' (inch). This suggests the possibility of gauge condition within this zone during the drilling of the borehole GA-W1. Gauge holes are commonly targeted by drillers and always indicate good drilling condition (Rider. 2002).

Track 5 on figure 5.1 is the log suite s of the density log, corrected density log and neutron log which are used to develop a petrophysical model. They are porosity logs and shallow reading device. The density log and neutron log are used to measure the bulk density of the formation in order to derive the total porosity of the well GA-W1. Also, use to detect gas bearing reservoir interval sections A, B, C & D, 1866.71 m to 1875.40 m, 1875.25 m to 1878.50 m, 1878.50 m to 1881.32 m and 1881. 32 m to 1887.95 m respectively. The crossover of density and neutron logs at any depth within the reservoir, is an indication of a hydrocarbon bearing zone (Rider. 2002). The density, corrected density and neutron logs reading values in the intervals sections A, B, C and D, ranges between (RHOB 2.211 g/cm^3), (NPHI 0.257 dec) and corrected density log (-0.019 g/cm^3). Normal pressure zones of compacted formation usually have an increasing density trend with depth where there is a uniform lithology. An overpressure zone indicates a

lower density value with depth as a result of porosity increases and higher fluid contents in the formation. Well GA-W1 within the reservoir interval sections A, C and D, have a lower density, corrected density and neutron logs reading values of (RHOB 2.211 g/cm^3), (NPHI 0.257 dec) and corrected density log (-0.019 g/cm^3) respectively. This shows that the formation is porous, not well compacted which resulted in the development of an overpressure formation as a result of high fluid content. The fluid is suggested to be brine, apparently because of the lower resistivity values between 0.663 (ohm/m ILD) and 1.39 (ohm/m MSFL). The observation above is in contrast to interval depth 1875.25 m to 1878.50 m, of section B, which is a compacted shale formation that has been invaded with less fresh water as indicated by the resistivity reading ranging from 2.45 (ohm/m ILD) to 4. 76 (ohm/m MSFL) and resulting in the development normal pressure zone.

Track 6, on figure 5.1 is also the sonic log (DT) which is used to identify the travel time in the formation borehole dependent on lithology and porosity of the reservoir. The sonic log (DT) in the reservoir interval sections A, B, C & D of the well GA-W1 indicate the transit time of (92 µs/f) and (79 µs/f) along the sand and shale formation. The transit time was slower in the shale region, this indicates that there is little gas or hydrocarbon may be encountered within this reservoir interval at depth 1875.25 m to 1878.50 m of section B' which is the normal pressure zone of the well.

Track 7 is the temperature log suite an important parameter used in detecting fluid movement and analysis of fluid pressure in a formation thereby enhanced sharp detection of an overpressure zone. In sub-surface, temperature is a function of depth i.e. temperature increases with depth, the rate at which is occurring is known as geothermal gradient.

The interval sections A, C and D, 1866.71 m to 1875.40 m, 1878.50 m to 1881.32 m and 1881. 32 m to 1887.95 m respectively of well GA-W1. An overpressure zone was detected as a result of invaded overpressure fluid from the mud-weight. This enhanced the temperature of these formation to increase from 200^{0}F (93.3^{0}C) to 219^{0}F to (104^{0}C). This indicates overpressure formation, because high temperature and geothermal gradient is one of the signs of

overpressured formation. The interval depth 1875.25 m to 1878.50 m in section B' which is the normal pressure zone shows decrease in temperature from 219^0F (104^0C) to 154^0F (68^0C) due to the increase in compaction of the formation, hence lowering porosity of the zone.

Tracks 8 and 9 are the compressional wave velocity (Vp) and shear wave (Vs) respectively used in well GA-W1 to delineate the abnormal pressure zone and the normal pressure zone within the interval sections A, B, C, and D, (1866.71 m to 1875.40 m, 1875.25 m to 1878.50 m, 1878.50 m to 1881.32 m and 1881. 32 m to 1887.95 m) respectively. In these intervals, an overpressure zone and normal pressure zone were experienced during the drilling. Overpressure was observed along the sections A, C and D, while normal pressure was observed at section B. In the interval sections A, C and D, the compressional wave velocity (Vp) reading varies across these depths ranges from 7,970 (ft/sec), 9,940 (ft/sec) to 10,704 (ft/sec).

This suggests that compressional wave velocity Vp (ft/sec) is lower in an overpressure formation as a result of high fluid content from the mud weight which ensued in compaction disequilibrium. This is a dominant mechanism of overpressure formation in deep water. The compressional wave velocity Vp (ft/sec) of interval section B, which is a normal pressure zone have high reading value of 24,350 (ft/sec). Therefore, indicates that compressional wave velocity (Vp) is higher in normal pressure zone as a result of the compaction of the formation which has no empty pores which can enhanced the invaded fluids or water contents from the mud weight. The shear wave velocity (Vs) within the intervals in the overpressure zone and normal pressure zone in sections A, B, C and D, indicates low reading values ranges from 1,047 (ft/sec), 1,011 (ft/sec) and 2,800 (ft/sec). This evidence that shear wave velocity (Vs) has lower effectiveness and stiffness (low gradient) in the sand reservoir when the overburden stress of the formation increased.

5. 0. 2 Well GA-W1 pore Pressure Prediction Results, Interpetation and Discussion from well log using Resistivity log

5.0.2.1: RESISTIVITY, SONIC MODEL AND NORMAL COMPACTION TREND (NCT) FOR WELL GA-W1 (1864.70 m -1888.50 m) DEPTH.

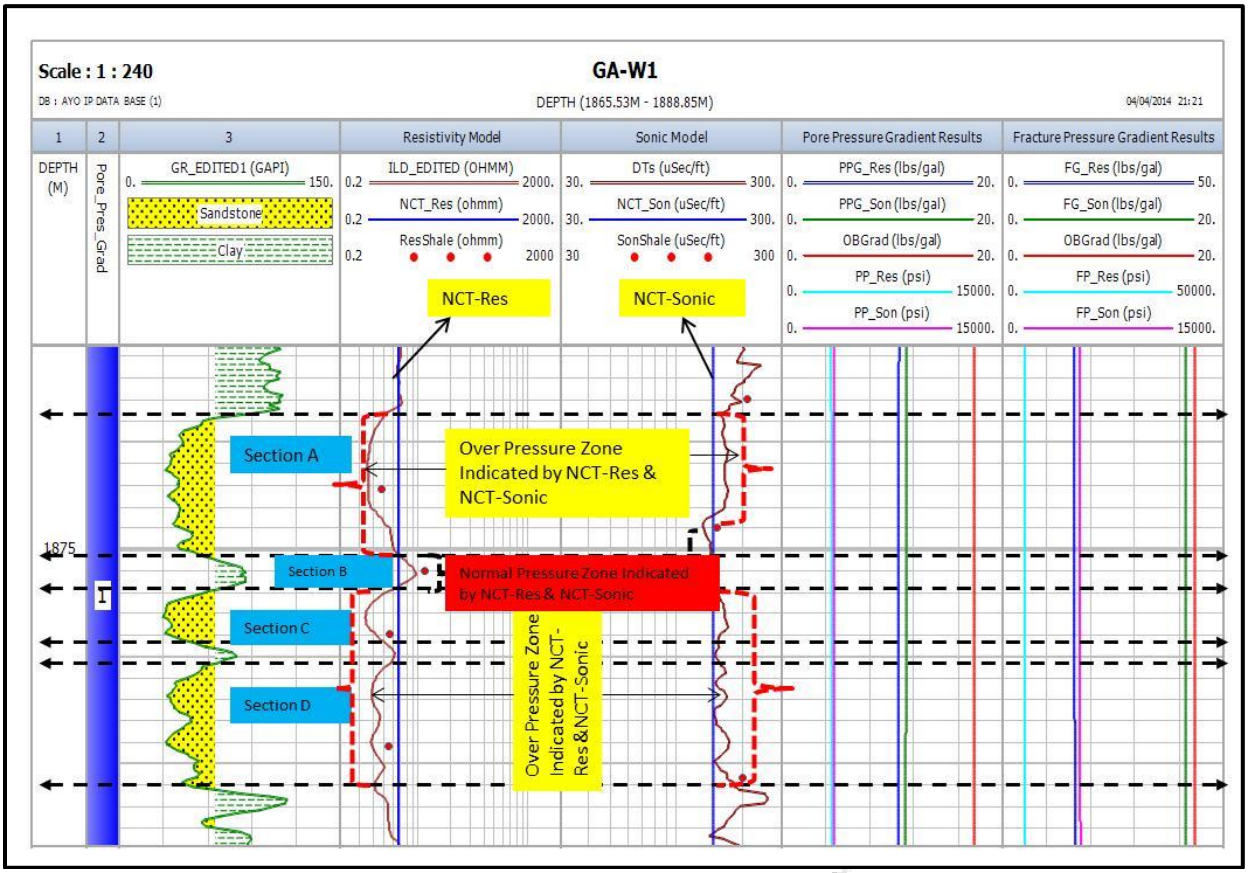

Figure 5.2 the resistivity and sonic transit time velocity model of Eaton's equivalent depth dependence method with NCT (Normal compaction trendline) to estimate pore pressure from Well logs and seismic data for well GA-W1.

The selected interval depth for well GA-W1 ranges from 1868.7 m to 1888.85 m. This interval is sub-divided into reservoir sections A, B, C and D, at depths 1868.73 m – 1875.40 m, 1875.40 m – 1876.7 m, 1876.7 m -1880.3 m and 1880.3 m – 1887.3 m respectively as shown in track 3 of figure 5. 2. The overpressure zone and normal pressure zone were encountered within the selected intervals depth.

The volume of the clay gamma ray (VCLGR) was used in order to indicate the lithologies as well as to calculate the accurate value of the overburden gradient. The normal compaction trendline (NCT) is coupled with shale resistivity logs as shown in track 4 of figure 5.2. The shale resistivity logs decrease from the established normal compaction trendline (NCT) which are designed to detect the abnormal pressure zones (overpressure zone) and normal pressure zone as well as predicting the pore pressure condition of the well GA-W1 as applied by Zhang (2011).

The induction deep log (ILD) resistivity was used in order to obtain the accurate formation pore pressure for the pore pressure calculation, because pore pressure in the formation near the wellbore is affected by drilling-induced stresses (Zhang and Roegiers, 2005). The decrease of the shale-resistivity behind the established normal-compaction trend line (NCT) from resistivity logs indicates the overpressure zones. Also, the deviations of the shale-resistivity logs from the established normal compaction line towards the high values scale indicate the normal pressure zone which may be attributed to the presence of different lithologies of shale and sandstone interbeds. This procedure was applicable to all wells.

The well GA-W1 indicates an overpressure zone which was found in sections A, C and D, with depths ranges of 1868.73 m – 1875.40 m in A, 1876.7 m -1880.3 m in C and 1880.3 m – 1887.3 m in D, due to the presence of the source rock (shale) in the intervals' formations. Section B, indicates the normal pressure zone at depth 1875.40 m – 1876.7 m. Generally, an under-compacted formation which can be regarded as an overpressure zone in a reservoir has a lower resistivity than the compacted formation (Zhang and Roegiers, 2005). Thus, intervals contain more fluids in their pores spaces which will enhance increase in pore pressure. The sections A, C and D, of well GA-W1 have a low shale-resistivity value of 0.622 ohm/m which can be interpreted as interval depths filled with brine water. Section B, which is the normal pressure zone, displays a high value of shale-resistivity at 4.65 ohm/m, which can be interpreted as the interval depth filled with hydrocarbon fluid.

The normal compaction trendline (NCT) corresponding value of 2.33 ohm/m indicates the optimum fitted linear trend of the measured overpressure and normal pressure formation

between the hydrostatically pressured and geopressured formations and thus constitutes a transition zone.

In addition, the well GA-W1 is a deep well. The sea water column has been taken as stand-in overburden for the well which implies that the overburden gradient is dependent on the magnitude of the water column. The overburden column for well GA-W1 within the depth interval sections A, B C and D is 17.5 lbs/gal (2.09 g/cm^3). This shows that the overburden gradient is low which is an indication that the well GA-W1 penetrated through a lower water column; this low water column also enhanced the filling of the pore spaces with brine fluid which may have caused the overpressure encountered within certain depths of the formation.

The pore pressure gradient (PPG-res) calculated for well GA-W1 is 10.6 lbs./gal (1.27 g/cm^3), a value similar to the pore pressure gradient (PPG) value of 1.24 g/cm^3 obtained from the well report. This justifies using resistivity wireline log to accurately estimate pore pressure gradients using Eaton's depth dependent method.

Generally, pore pressure gradient (PPG) is quite important and required before penetrating through a selected formation and can be used to determine the amount of mud weight (mud density) required for wellbore stability. Fracture gradients must be known before setting and cementing the casing of wells and care must be taken to ensure that the mud weight is not higher than the fracture gradient in order to avoid formation fracturing of the well which could result in mud losses or loss of circulation (Zhang, 2011).

The fracture pressure-resistivity (FP-res) of well GA-W1 within the interval depth sections A, B C and D,(which can also be regarded as a formation fracture pressure gradient in (g/cm^3) is the amount of the fracturing pressure required to fracture a formation in order to allow the mud loss from the wellbore into the induced fracture zone. The fracture pressure-resistivity (FP-res) of well GA-W1 is 5,267 psi or 12.15 g/cm^3.

The fracture gradient is the maximum mud weight required in drilling a well, and is 16.5 lbs./gal (1.98 g/cm^3) for well GA-W1. This is therefore the maximum mud weight required to fracture the formation of well GA-W1. Hence, the formation fracture pressure gradient of well GA-W1 is

12.15 g/cm^3, and has a low mud weight of 1.27 g/cm^3 and the predicted maximum mud weight of 1.98 g/cm^3 as it is well below the fracture pressure gradient. This is an indication that well GA-W1 was stabilized, and that neither mud loss nor lost circulation occurred during drilling.

The effective stress of a well formation is conventionally defined as the subtraction of pore pressure from the overburden stress. Thus, increase in pore pressure (i.e. overpressure) causes reduction in the effective stress. The overburden stress is 17.5 Ibs/gal (2.09 g/cm^3) and the pore pressure is 3,406 psi average (equivalent to 7.85 g/cm^3) of the well formation GA-W1. Therefore the effective stress of the well formation is -5.76 g/cm^3 (i.e. 2.09 g/cm^3 – 7.85 g/cm^3); this suggests that there was an increase in the overpressure in the well formation of well GA-W1 leading to a negative effective stress. Thus, the cause of the reduction of the effective stress and the predicted pore pressure encountered, is the pressure acting on the fluids in the pore spaces of the formations ranging from 3,401 psi, 3,405 psi, 3,407 psi to 3,412 psi for interval depth reservoir sections A, B, C and D respectively. As a result of the overpressure zone which was experienced in well GA-W1 within the interval depth, a casing is required in order to prevent the overlying formation from collapsing.

5. 0. 3 Well GA-W1 Pore Pressure Prediction Results, Interpetation and Discussion from Seismic using sonic log

Slotnick (1936), recognized that compressional velocity (Vp) is a function of depth i.e. the velocity increases with depth in subsurface formations and that the pore pressure prediction using seismic data is mainly depending on the interval velocity. Using seismic data, pore pressure can be predicted down to the bottom of the seismic volume. The overpressure zone of well GA-W1 and the pore pressure calculation with correct amount of mud-weight were determined from the seismic data by using Eaton's sonic method with depth-dependent normal compaction trendline (NCT), as applied by Zhang (2011) and indicated in track 5 of figure 5. 2.

Using sonic log was used to delineate the overpressure zone and normal pressure zone in a well formation works as a reverse case of the resistivity log method. The normal compaction trendline (NCT) is coupled with sonic shale logs as derived from the sonic logs (DT) as shown in track 5 of figure5. 2. The deviation of both the sonic shale logs and the sonic logs (DT) across the established normal compaction trendline (NCT) towards the high values side of the scale is an indication of an overpressure zone while the deviation of the sonic shale logs and the sonic logs (DT) across the established normal compaction trendline (NCT) toward the lower values scale indicates a normal pressure zone. These pore pressure predictions are more precise than the resistivity log independent method (Zhang 2011). This is applicable to all the wells using this method.

The overpressures zones are also encountered along the sections A, C and D, using this method. The reservoir interval depths range from 868.73 m – 1875.40 m, 1876.7 m -1880.3 m and 1880.3 m – 1887.3 m respectively. The overpressure zones were determined by means of the established normal compaction trendline (NCT) coupled with the sonic shale logs scale. The curve deviates towards the high values scale with corresponding high values of the normal compaction trendline (NCT) at 147µsec/ft. Because of it being an overpressure zone, an increase in interval transit time results because of higher porosity and lower density in the

formation. The predicted pore pressures of 3,618 psi, 3,621 psi 3,627 psi increase gradually with increase in depth as drilling continues.

Section B is the normal pressure zone at depth 1875.40 m – 1876.7 m. The sonic shale logs scale curve deviates towards the lower values of the scale with the corresponding transit time of normal compaction trendline (NCT) at 147µsec/ft. This is the result of a decrease in the porosity, and an increase in the density in a normal pressure zone, besides showing increases in predicted pore pressure up to 3,623 psi.

The calculated overburden gradient for well GA-W1 using Eaton's sonic model is 17.5 (lbs/gal) (2.09 g/cm^3), which is low and shows that the well GA-W1 passes through a lower water column. This agrees with our findings on the pressure gradient and links the pressure of the matrix with the pressure in the pores of the well.

The pore pressure gradient from the sonic log (PPG-Sonic) was calculated to determine the amount of mud weight required for the stability of the well GA-W1 to avoid rapid influx of reservoir fluid or so called kicks. The pore pressure gradient (PPG-Sonic) of the well GA-W1 within the interval sections A, B, C and D (depths 1868.73 m – 1875.40 m, 1875.40 m – 1876.7 m, 1876.7 m -1880.3 m and 1880.3 m – 1887.3 m respectively) is 11.3 lbs/gal (1.35 g/cm^3) which is higher than the pore pressure gradient of PPG-Resistivity from the well logs which is 10.6 lbs/gal (1.27 g/cm^3). This indicates how the pore pressure gradient varies with different lithologies as a result of the presence of the shale observed within the interval depths causing higher porosity with less permeability.

The fracture gradients (FG-sonic) is 16.6 lbs/gal by calculation is (1.98 g/cm^3) which also indicates the maximum mud weight required to fracture the formation of well GA-W1 and the fracture pressure (FP-sonic) is 5,336 psi by calculation equivalent to 12.3 g/cm^3 mud-density for the overpressure zones A, C and D, at depth 1868.73 m – 1875.40 m, 1876.7 m - 1880.3 m and 1880.3 m – 1887.3 m respectively.

The fracture pressure (FP-sonic) of normal pressure zone B, is 5,318 psi by calculation equivalent to (12.2g/cm^3) mud-density at depths 1875.40 m – 1876.7 m required to fracture

the well GA-W1 formation. The fracture gradient of 16.6 lbs/gal (1.98 g/cm^3) which serves as maximum mud-weight does not exceed the fracture pressure of equivalent mud-density 12.2g/cm^3. This shows that there is stability of well GA-W1 during the drilling, and neither mud loss nor loss of circulation was observed during the drilling.

The increase in overpressure causes reduction in the effective stress as outlined above. The overburden stress is 17.5 Ibs/gal (2.09 g/cm^3) and the pore pressure is 3,622 psi (equivalent to 8.35 g/cm^3) for well GA-W1. Therefore the effective stress of the well formation is -6.26 g/cm^3 (i.e. 2.09 g/cm^3 – 8.35 g/cm^3) which suggests that there was an increase in the overpressure of the well formation GA-W1, thereby causing the reduction of the effective stress.

The predicted pore pressure (PP-sonic) which is the pressure acting on the fluids in the pore space of the formations of the interval reservoir depth sections A, B, C and D, ranges between 3,621 psi and 3,623 psi to be encountered during the drilling for both the overpressure zone and the normal pressure zone (section B). Figures 5.3 and 5.4 show the fracture pressure and pressure gradient depth curves of well GA-W1.

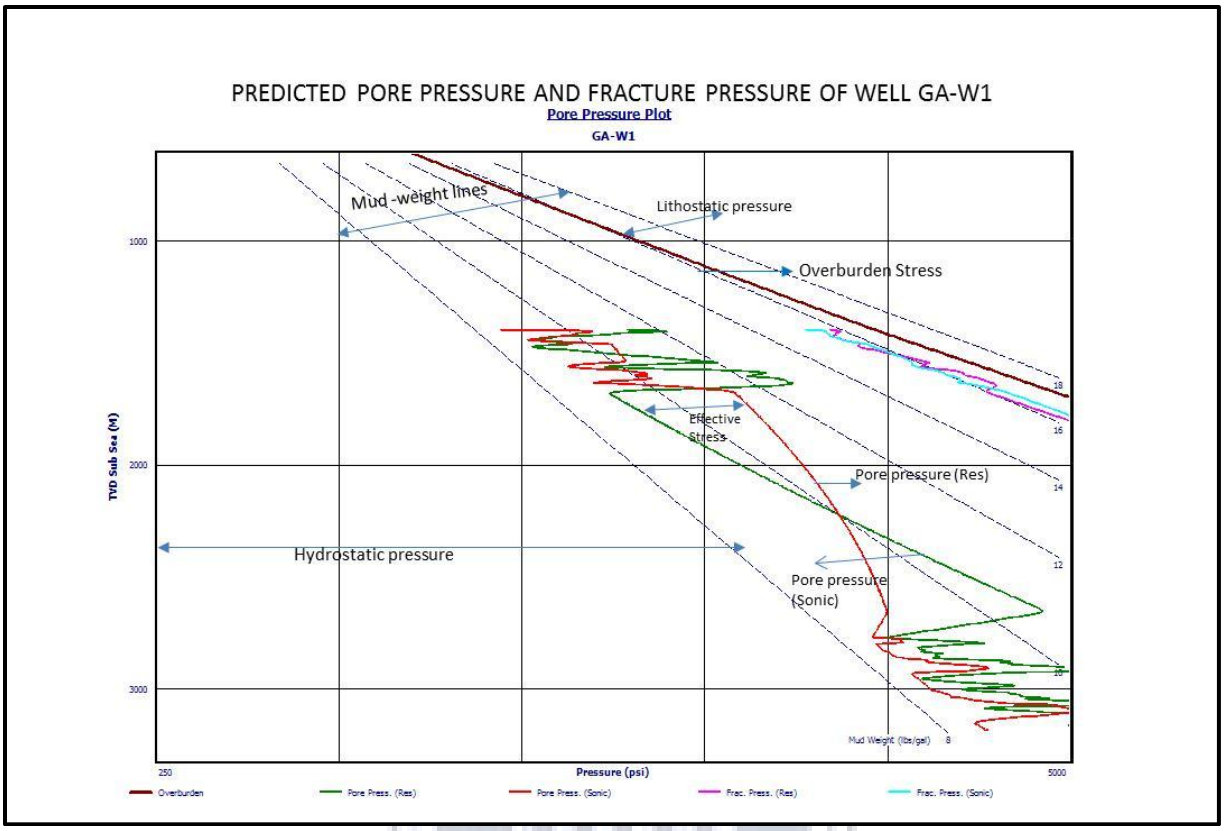

Overburden, ***Pore pressure (Res),*** ***Pore pressure (Sonic),***

Fracture pressure (Res), ***Fracture pressure (Sonic).***

Figure 5.3: The predicted pore pressure and fracture pressure for well GA-W1.

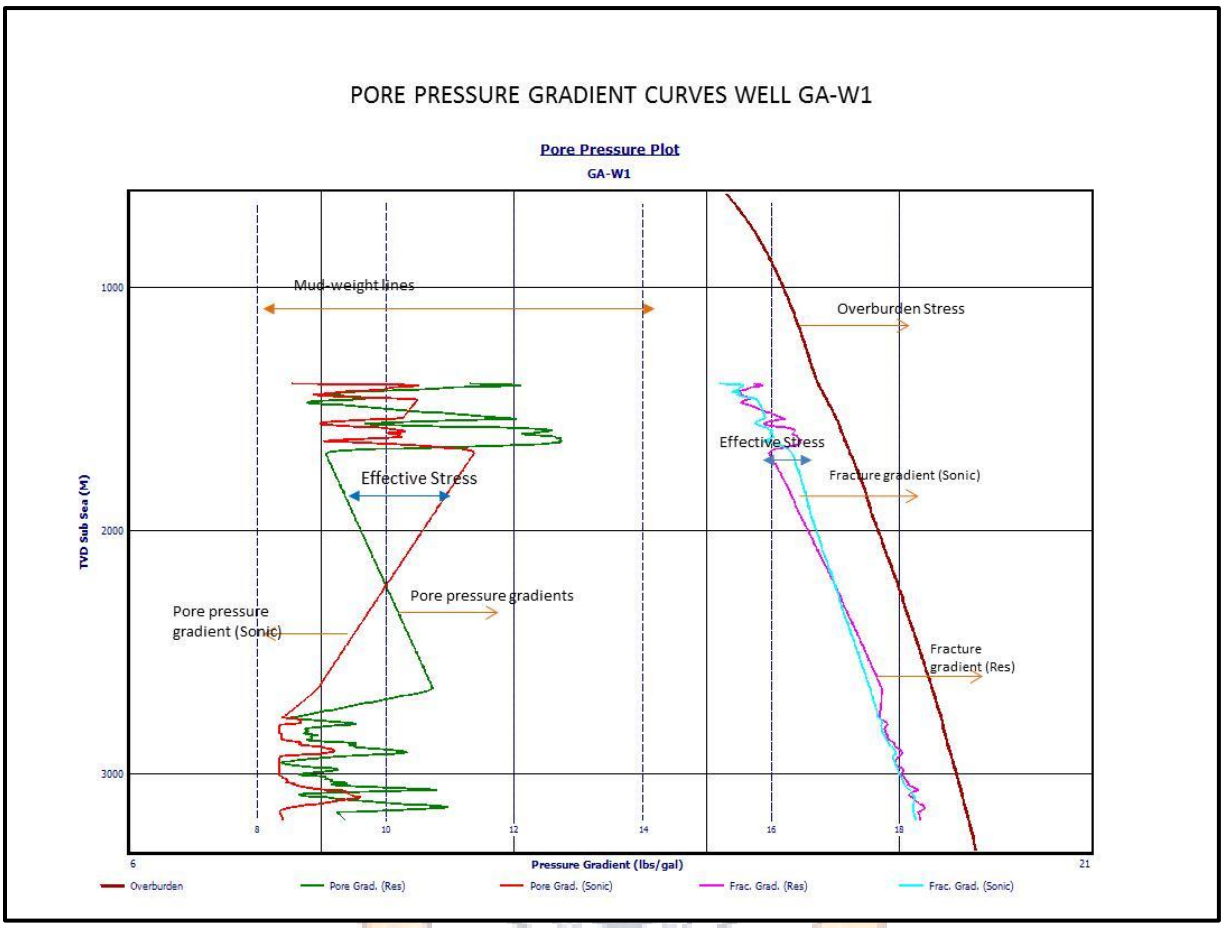

Overburden, ***Pore Grad (Res),*** ***Pore Grad (sonic)***

Fracture Grad (Res), ***Fracture Grad (Sonic)***.

Figure 5.4: The pore pressure gradients and fracture gradients of well GA-W1

5. 1. 0 Petrophysical wireline logs interpretations of well GA-N1.

WELL GA-N1 LOG SUITE (2876.7m – 2912.36 m) DEPTH

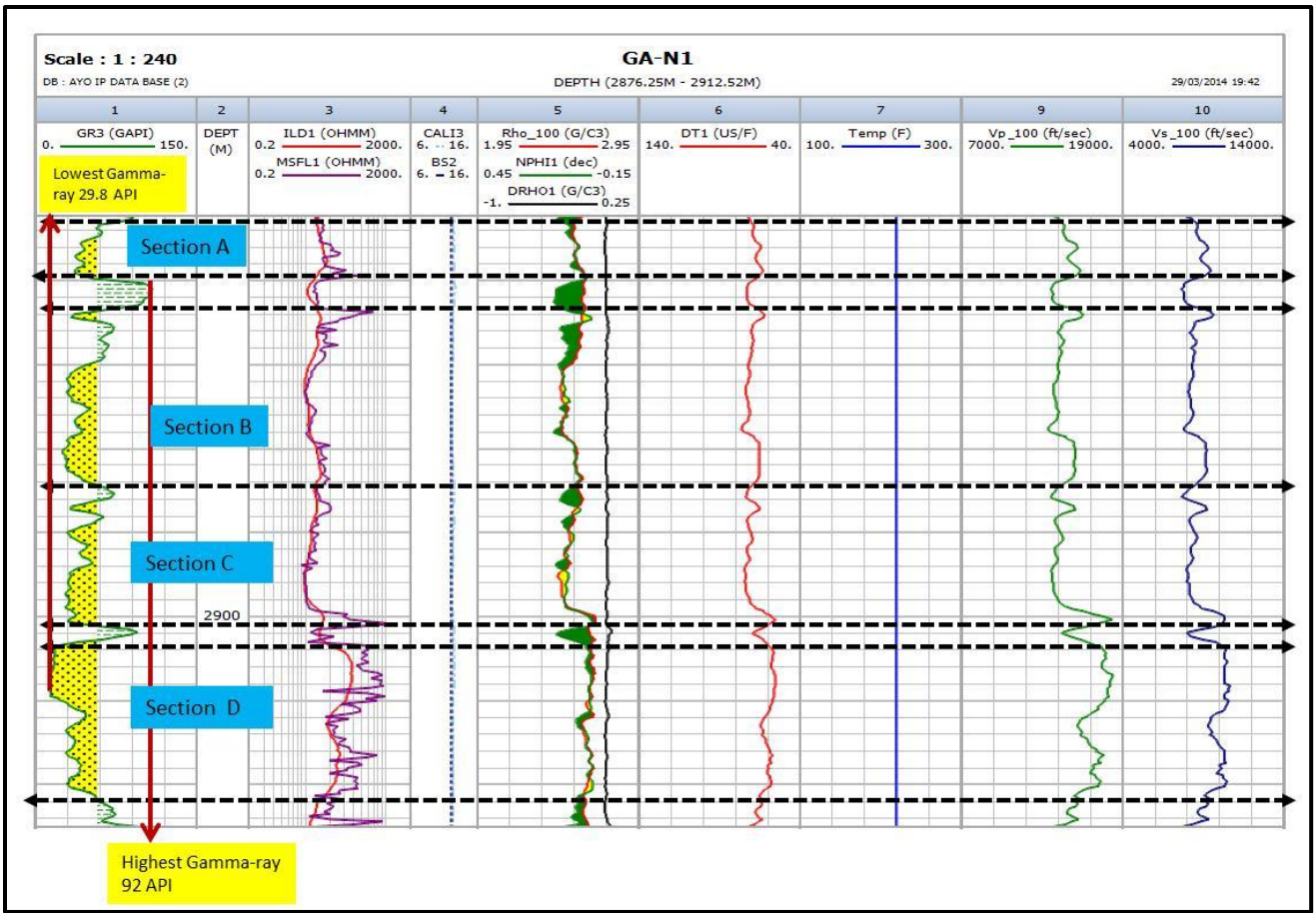

Figure 5. 5 The Well logs suites for Well GA-N1.

Track 1 well GA-N1, the gamma-ray logs which was used to identify the lithology of the well corresponding to shale and the sand formation based on its deflection across the base line. This was developed in order to identify the reservoir sand formation with the supports of neutron and resistivity logs. The highest and the lowest gamma-ray logs values are 92 API and 29.8 API which represent shale and sand respectively. This enables the delineation of reservoir zones of well GA-N1, as well as used to determine the depositional environments of the well formation. The reservoir intervals sections of well GA-N1 ranges between 2876.70 m – 2912. 36 m and sub-divided into four sections A, B, C, and D with depth interval ranges between 2876.70 m - 2880.10 m, 2880.10 m – 2881.7 m, 2892.2 m- 2900.6 m 2900.6 m – 2912.36 m respectively.

The interval section A, (2876.70 m – 2880.10 m) is a shale formation and the reservoir interval depth sections of B, C, and D, (2880.10 m – 2881.7 m, 2892.2 m- 2900.6 m 2900.6 m – 2912.36 m) respectively sand prone formation.

Track 2 and 3 indicate the depth and the resistivity log respectively. The induction deep log (ILD) and the micro spherical focus log (MSFL) are the resistivity logs used in well GA-N1. Their objectives are to measure the formation resistivity in the borehole containing oil and fresh water based drilling mud. Interval section A, B, C and D show higher resistivity reading ranges from 18.32 ohm/m to 24.94 ohm/m for ILD and MSFL respectively. This suggests that the reservoir formation of these interval depths are compacted thereby less invaded with fresh water and little amount of hydrocarbon may have been encountered during drilling. In addition, within the same interval section no overpressured zones were encountered due to the compacted formation thereby resulted in normal pressure zone.

Track 4 indicates the caliper log and the bit size log suite which are used to determine the variation of the borehole diameter with depth, size and shape of the hole. The bit-size serves as reference line used to determne the increase or decrease of the borehole diameter during drilling. In the interval sections A, B, C and D, the caliper reading was 12.5” (inch) and the bit-size reading was also 12.5” (inch). This suggests that there was free movement of bits during the drilling and the borehole at these depths are in gauge condition (Rider, 2002) always indicating good drilling condition in well GA-N1. This was made possible as a result of compacted formation of the well GA-N1, which experienced normal pressure within the reservoir interval depths.

Track 5 comprises of the density, corrected density and neutron logs suite. These are used for petrophysical modeling purposes. They are porosity logs and shallow reading device. The density logs and neutron logs are used to measure the bulk density of the formation in order to derive the total porosity within a reservoir interval. They are also used to detect gas or hydrocarbon bearing formation at the point of their good crossover at any depth in permeable

zones within the reservoir section. In the reservoir interval sections A, B C and D, of well GA-N1, the density log, corrected density and neutron logs reading were 2.602 g/cm^3(RHOB), 0.126 dec(NPHI) and corrected density logs 0.012 g/cm^3 (DRHO). This indicates high reading values parameters which can be interpreted as an indication of a compacted formation in well GA-N1. This resulted in normal pressure zone which can as well be observed from the high resistivity reading ranges of 18.34 ohm/m and 24.94 ohm/m for ILD and MSFL respectively. Also Within the interval depths 2880.10 m – 2881.7 m and 2892.2 m- 2900.6 m sections B and C, little amount of hydrocarbon may have been encountered due to permeable zones encountered at these depths.

Track 6 is the sonic logs (DT) suite which was used to identify the travel time in the formation borehole. Its reading is normally based on lithology and the porosity of the reservoir. The sonic logs (DT) within the reservoir interval sections A, B, C & D, of well GA-N1 indicates high transit times ranging from 82 µs/f to 68 µs/f. This suggests that the reservoir formations of the well are more compacted and less porous thereby resulted in normal pressured zones. There is also possibility of hydrocarbon presence during the drilling of well GA-N1.

Track 7 indicates the temperature log of well GA-N1. This serves as a parameter used in detecting fluid movement and the analysis of fluid pressure in a formation, therefore enhancing sharp detection of an overpressure zone formation along the interval depth section of well GA-N1. The reservoir intervals sections A, B C and D, a temperature reading of 147^{0}F (64^{0}C), across these depths. This value is lower compared to the temperature of the overpressured formation of well GA-W1 with values ranging from (200^{0}F (93.3^{0}C) to 219^{0}F (104^{0}C). The formations in well GA-N1 are compacted less porous and less invaded by brine water thereby resulted to normal pressured zones.

Track 9 and 10 of the log suite of well GA-N1 shows the compressional wave velocity (Vp,ft/sec) and the shear wave velocity (Vs,ft/sec) used to detect the abnormal and normal pressure zone of the formation within the interval sections A, B, C, and D, (depths 2876.70 m -2880.10 m, 2880.10 m – 2881.7 m, 2892.2 m- 2900.6 m 2900.6 m – 2912.36 m) respectively. The compressional wave velocity (Vp, ft/sec) shows high readings being 15,446 (ft/sec), 17,119(ft/sec), 21,058(ft/sec) and 24,241 (ft/sec) in interval section A, B,C and D respectively. The velocity increases as a result of the pore pressure of the formation which reduces the compressibility of the pore fluid.

This suggests that hydrocarbon may have been encountered within these interval sections of well GA-N1. Also normal pressure zone formation may as well have been experienced due to the higher values of compressional-wave velocity (Vp, ft/sec) during the drilling. The shear wave velocity (Vs) within the interval depth selection indicates low reading values ranges between of 1,047 (ft/sec) and 1,002 (ft/sec). This might be an indication of lower effectiveness and stiffness (low gradient) of reservoir rock due to the increase in overburden stress of the formation.

5. 1. 2 Well GA-N1 pore pressure prediction results, interpetation and discussion from well log using resistivity log.

5. 1. 2. 1 RESISTIVITY, SONIC MODEL AND NORMAL COMPACTION TREND (NCT) OF WELL GA-N1 (2876.7 m – 2912.36 m) DEPTH.

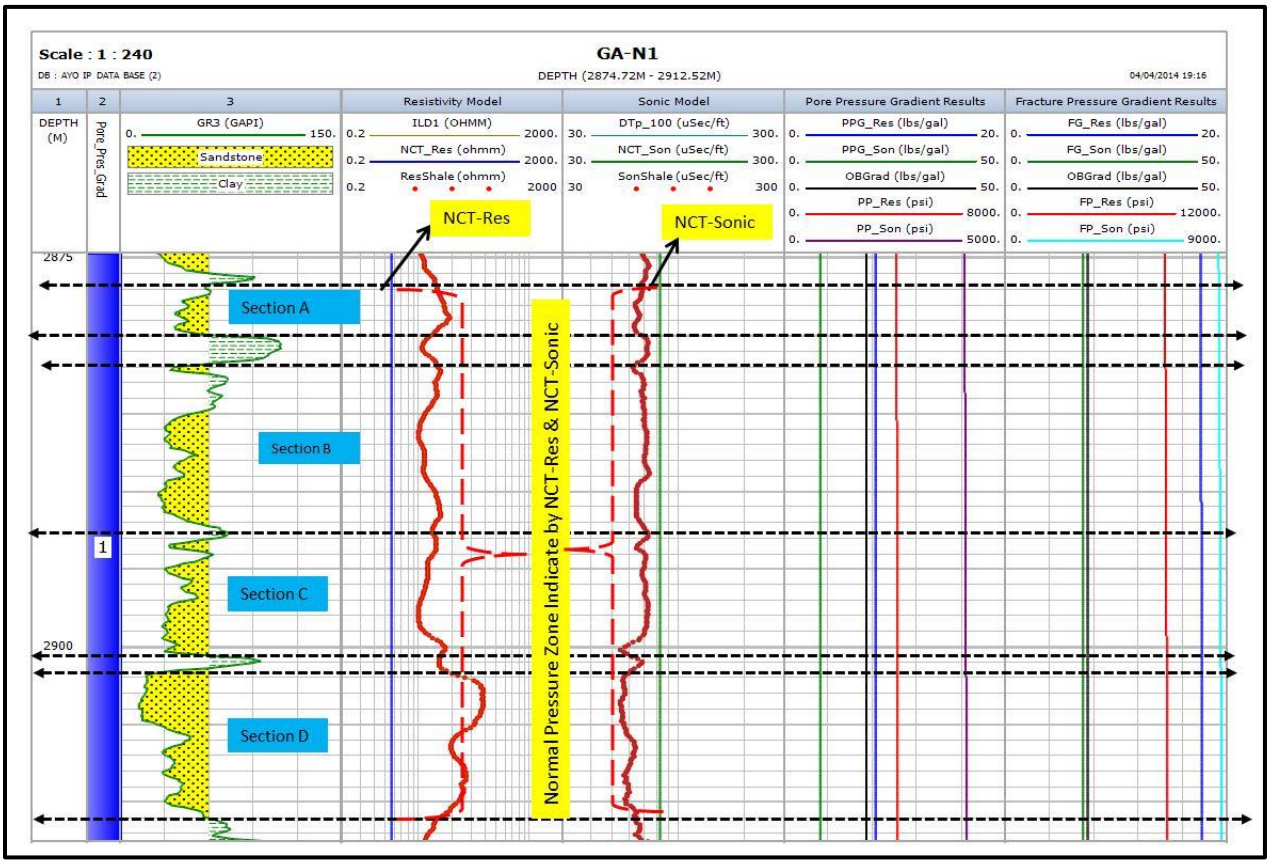

Figure 5.6: The resistivity logs and sonic transit time velocity model of Eaton's equivalent depth dependence method with NCT (Normal compaction trendline) to estimating pore pressure from Well logs and seismic data for Well GA-N1.

The resistivity and sonic transit time model with normal compaction trend line (NCT) was used to detect the overpressured zone and normal pressured zone as well as predicting the pore pressure of the drilled well GA-N1 within the selected interval depths 2876.7 m - 2912.36 m, applied by Zhang (2011). The interval depth of interest was sub-divided into four reservoirs sections A, B, C and D (depths 2876.70 m -2880.10 m, 2880.10 m – 2881.7 m, 2892.2 m - 2900.6 m and 2900.6 m – 2912.36 m) respectively, as shown in track 3 of the figure 5.6

The normal compaction trend resistivity (NCT-Res) which was used to distinguish the normal pressure zone from the overpressure zone of well GA-N1 has a 1.67 ohm/m value which clearly indicates that well GA-N1 possesses normal pressures formations within the interval depths sections. The corresponding values of shale-resistivity logs range from 15.07ohm/m, 25.2ohm/m, and 58.9 ohm/m to 72.5 ohm/m respectively across the interval depth sections A, B, C and D. These high readings imply that the fluids in the well formations are likely to contain hydrocarbons.

Thus, the overburden gradient of the well GA-N1 within the interval sections A, B, C, and D at depths 2876.70 m -2880.10 m, 2880.10 m – 2881.7 m, 2892.2 m- 2900.6 m 2900.6 m – 2912.36 m respectively is 18.6 lbs/gal or 2.23 g/cm^3. This means that well GA-N1 has a moderate overburden gradient (OBGrad) and that the well was penetrated under a higher water column, and thus an increased overburden pressure.

The amount of mud weight to be used to reduce the kick or loss of circulation on well GA-N1 can be determined from the corresponding value of the pore pressure gradients by means of converting to g/cm^3 from Ibs/gal; so the IP reading of PPG-res of 8.34 lbs/gal is calculated to be 0.99 g/cm^3. This mud weight value obtained from the pore pressure gradient resistivity (PPG-res) must be less than the fracture gradients to avoid the Kick or loss of circulation and to stabilize well GA-N1 during drilling and to ensure that the fracture gradients are intact before setting and cementing the well casing in order to avoid formation fracture of the well GA-N1 which could result in loss of circulation or mud losses.

The fracture pressure resistivity (FP-res) of well GA-N1 within the reservoir interval sections A, B, C, and D at respective depths of 2876.70 m -2880.10 m, 2880.10 m – 2881.7 m, 2892.2 m-2900.6 m and 2900.6 m – 2912.36 m ranges from 8,717 psi to 8,743 psi or an FFG of 20.11 g/cm3 to 20.17 g/cm^3. The fracture pressure resistivity (FP-res) of the well GA-N1 is also known as the formation fracture pressure gradient in (g/cm^3) and is the amount of the fracture pressure needed to fracture the well formation of GA-N1 for the mud loss to induce the fracture zone from the wellbore.

The fracture gradient is the maximum mud weight required in drilling a well. Thus, the fracture gradient of well GA-N1 is 17.7 lbs/gal (2.12 g/cm^3) which is the maximum mud weight required

to fracture the formation during drilling. If the mud weight (0.99 g/cm^3), is higher than the formation fracture pressure gradient (FFG g/cm^3) fracture might occur which may result in lost circulation during drilling. The formation fracture pressure gradient of well GA-N1 is 8,717 psi which converts to 20.11 g/cm^3 , has a lower mud weight of 0.99 g/cm^3. The predicted maximum mud weight from fracture gradient (FG-Res) for well GA-N1 is 2.12 g/cm3 which is less than the fracture pressure formation. Therefore, well GA-N1 was well stabilized, no mud losses or loss circulation will occur during drilling.

The effective stress of the well GA-N1, the overburden stress is 18.6 Ibs/gal (2.23 g/cm3) and the pore pressure is 4,121 psi which is equivalent to 9.51 g/cm3 for the well. Therefore, the effective stress of the well formation is 2.23 g/cm3 – 9.51 g/cm3= -7.28 g/cm3. This implies that an overpressure zone may likely be encountered by further drilling of the reservoir interval sections A, B, C, and D at depths 2876.70 m -2880.10 m, 2880.10 m – 2881.7 m, 2892.2 m- 2900.6 m and 2900.6 m – 2912.36 m.

However the predicted pore pressure (PP-res) values which are the pressures acting on the fluids in the pore spaces of the formations are 4,098 psi, 4,110 psi, 4,120 psi and 4,133 psi calculated across the interval sections A, B, C and D depth 2876.70 m -2880.10 m, 2880.10 m – 2881.7 m, 2892.2 m- 2900.6 m and 2900.6 m – 2912.36 m respectively which implies that no overpressure zone was encountered within the reservoir interval depth sections of well GA-N1; therefore well GA-N1 has normal pressure formations.

5. 1. 3 Well GA-N1 Pore Pressure Prediction Results, Interpretation and Discussion from Seismic using Sonic log.

The overpressure zone and the pore pressure prediction calculation for well GA-N1 were determined from seismic data using Eaton's sonic method with depth-dependent normal compaction trendline (NCT) as applied by Zhang (2011) and as shown in track 5 of figure 5.6. In the reservoir interval sections A, B, C, and D at depths 2876.70 m -2880.10 m, 2880.10 m – 2881.7 m, 2892.2 m- 2900.6 m and 2900.6 m – 2912.36 m no overpressure zone was encountered i.e. a normal pressure zone was found, based on the sonic shale logs and sonic logs (DT) deviation as shown in track 5 of figure 5.6. The same procedure used in well GA-W1 was also adopted in well GA-N1.

Also, within the reservoir interval depth sections A, B, C, and D at depths mentioned above of well GA-N1, the corresponding value for the normal compaction trendline (NCT) is 82.8 µsec/ft. It is suggested that the interval transit time velocity increases in a normal pressure zone due to its compaction rate as a result of lower porosity. It is concluded based on the observed increase of the shale sonic log compared to the established normal compaction trendline (NCT) that normal pressure formations occurred in the well.

The overburden gradient (OBGrad) shows moderate values for well GA-N1 of 18.6 lbs/gal (2.23 g/cm^3) which is also the pressure gradient of the pressure matrix combined with the well pores. This implies that well GA-N1 penetrated through a deep overburden water column so that the overburden pressure will be higher. The same value of the pore pressure gradient (PPG-sonic) of 8.34 lbs/gal (0.99 g/cm^3) of the well obtained from both Eaton's wireline logs and Eaton's sonic log also suggests that well GA-N1 has compacted normal pressure formations at interval depths.

The fracture gradients (FG-sonic) value of 17.7 lbs/gal (2.12 g/cm^3) is the predicted maximum mud weight required in drilling well GA-N1. The fracture pressure (FP-sonic) of 8,743 psi and 8,717 psi within the reservoir interval sections A, B, C D, at depths 2876.70 m -2880.10 m,

2880.10 m – 2881.7 m, 2892.2 m- 2900.6 m and 2900.6 m – 2912.36 m respectively is the amount of pressure required to fracture the well bore of the formation with an equivalent value of 20.16 g/cm^3 as the mud-density. From the above it follows that the fracture gradient (FG-Sonic) 17.7 Ibs/gal by calculation (2.12 g/cm^3) must not exceed the fracture pressure formation (FP-Sonic) (20.16 g/cm^3) in order to avoid mud loss or lost circulation, and to avoid blow out hazard.

The fracture pressure value for well GA-N1 ranges from 8,743 psi to 8,717 psi which is an equivalent value of 20.16 g/cm^3 mud-weight. This suggests that the maximum mud-weight used of 17.7 Ibs/gal (2.12 g/cm^3) was less than the fracture pressure formation FP-Sonic of 20.16 g/cm3. Therefore well GA-N1 was stabilized and no mud loss or lost circulation occurred during the drilling period.

The effective stress, the overburden stress is 18.6 Ibs/gal (2.23 g/cm^3) and the pore pressure is 4,115 psi or 9.49 g/cm^3 for the well formation GA-N1. Hence, the effective stress of the well formation is 2.23 g/cm^3 – 9.49 g/cm^3 = -7.26 g/cm^3 . This implies that an overpressure zone will likely be experienced by further drilling of the interval reservoir sections A, B, C, and D at depths of 2876.70 m -2880.10 m, 2880.10 m – 2881.7 m, 2892.2 m- 2900.6 m and 2900.6 m – 2912.36 m in the well formation GA-N1, as deduced from the reduction of the effective stress.

The corresponding predicted pore pressure values of 4,098 psi, 4,110 psi, 4,120 psi and 4,133 psi calculated to be encountered throughout the interval sections A, B, C and D, at depths 2876.70 m -2880.10 m, 2880.10 m – 2881.7 m, 2892.2 m- 2900.6 m and 2900.6 m – 2912.36m during the drilling of the well indicate that no overpressure zone will be encountered. These findings confirm the results of the sonic log method.

Figure 5.7 and 5. 8 show the fracture pressure and pressure gradient depth curves of well GA-N1.

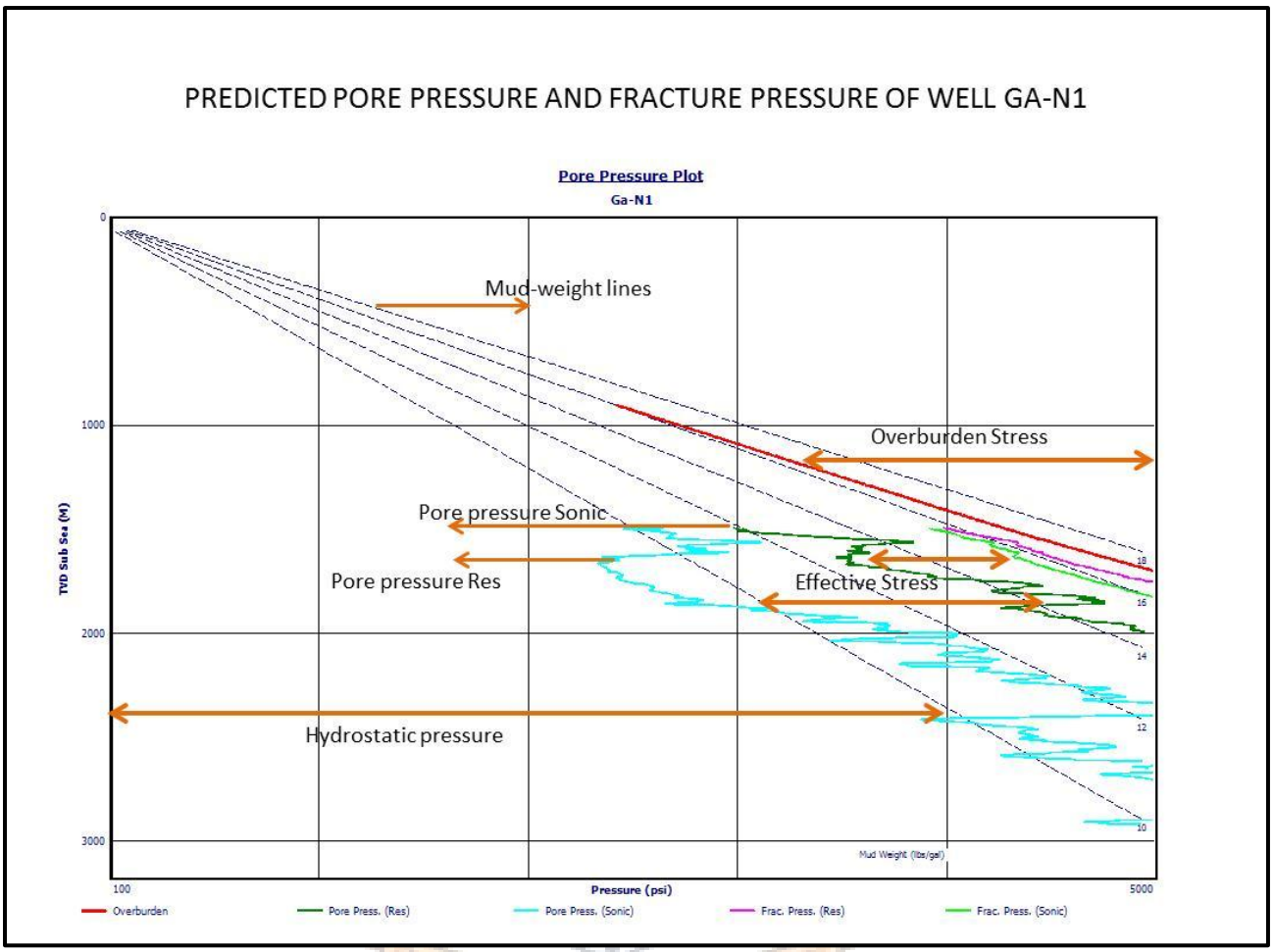

Overburden, ***Pore pressure (Res),*** ***Pore pressure (Sonic),***

Fracture pressure (Res), ***Fracture pressure (Sonic).***

Figure 5.7: Predicted pore pressure and fracture pressure for well GA-N1

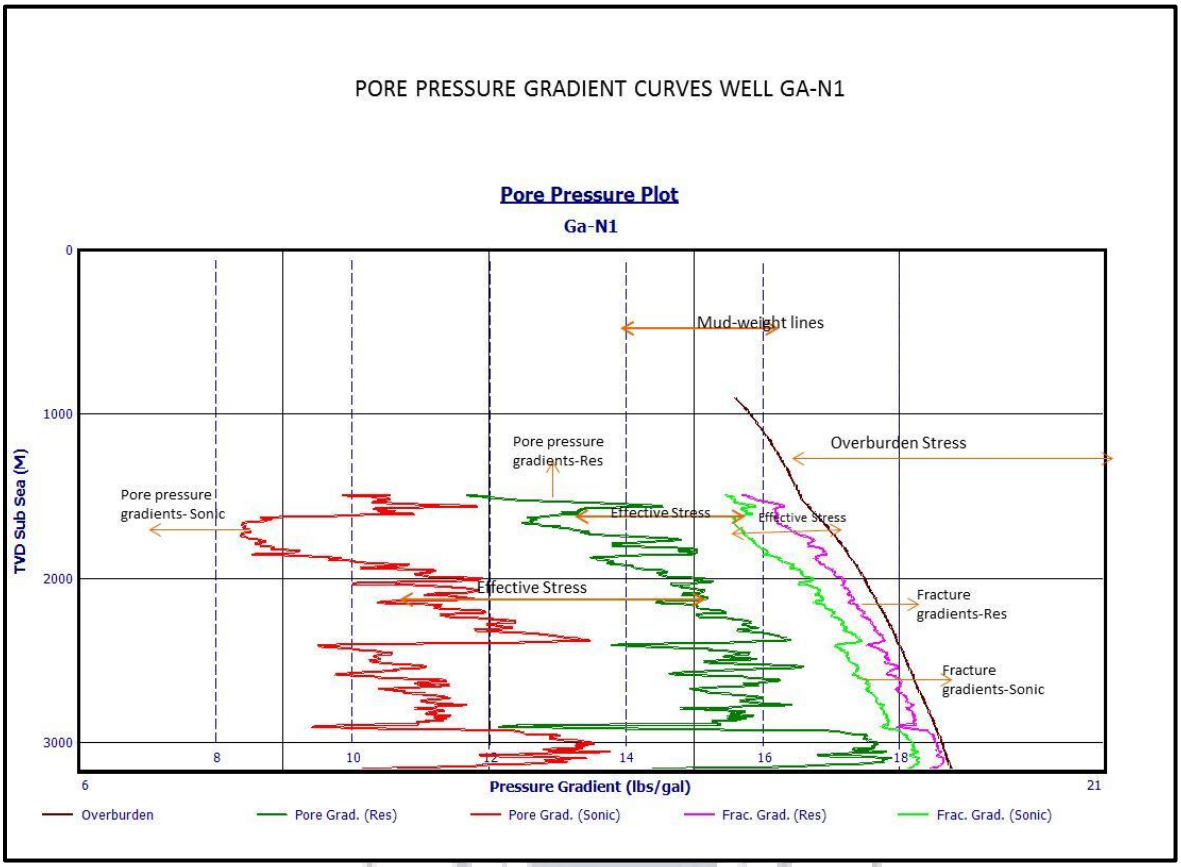

Overburden, Pore Grad. (Res), Pore pressure (Sonic), Frac. Grad (Res), Frac. Grad (Sonic).

Figure 5.8: Pressure gradient curves of well GA-N1.

5. 3. 0 Petrophysical wireline logs interpretations of well GA-AA1.

WELL GA-AA1 LOG SUITE (3533.55 m – 3548.94 m) DEPTH

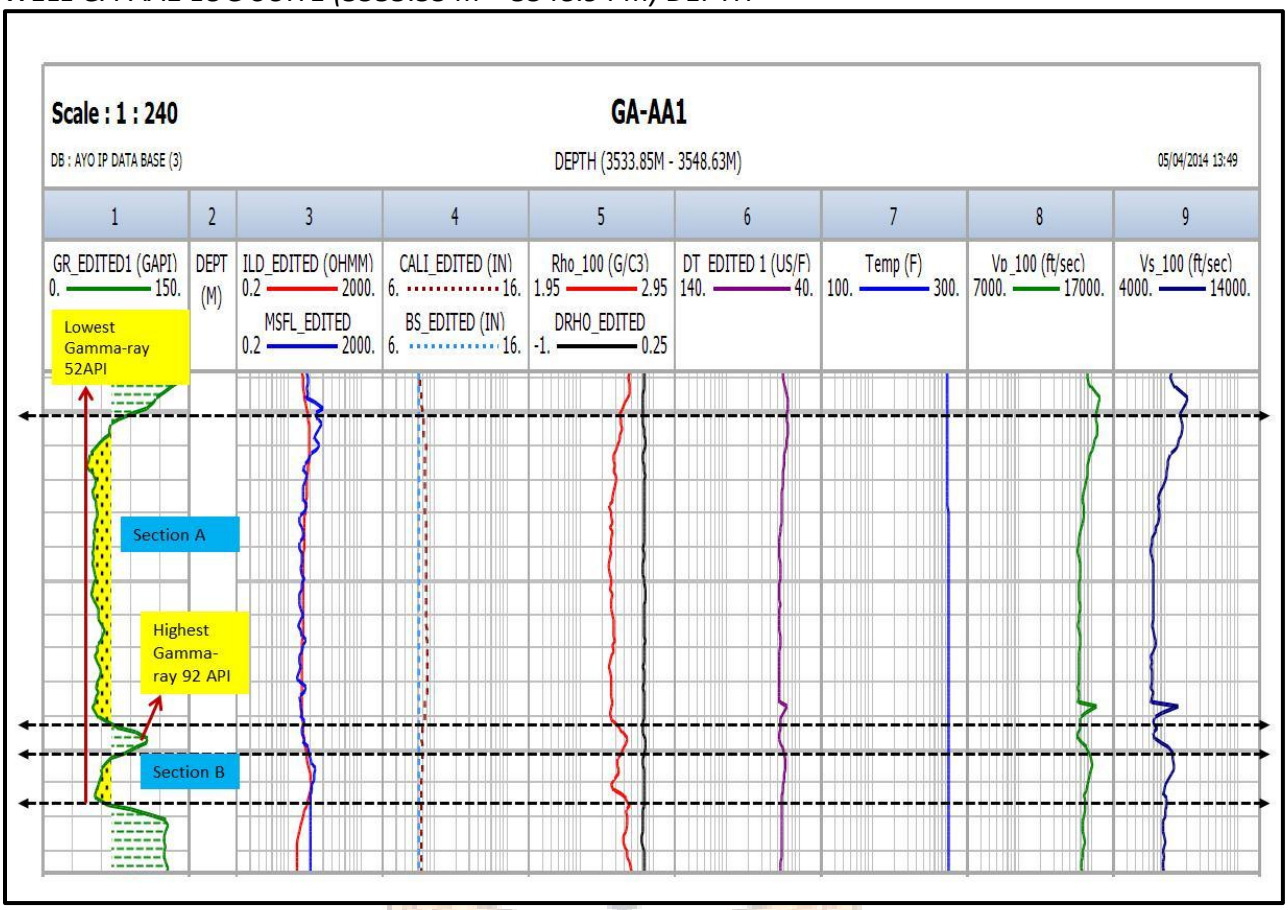

Figure 5.9: the Well logs suites for Well GA-AA1.

Track 1 on figure 5.9 of the log suite indicates the gamma-ray log to the lithology of the well GA-AA1 of sandstone and shale. The deflection of the gamma-ray towards high value scale shows shale formation while deflection to the lower value scales also indicating sandy formation such as 92 API and 52 API respectively. Based on the reservoir interval sections, the logs suite are sub-divided into two sections A and B with depth ranging from 3533.55 m to 3540. 43 m and 3540.43 m to 3548.94 m respectively. The intervals sections A and B clearly indicated reservoir sand formation from the base line. This interval sections was selected because of the low gamma ray values observed and with the combinations of neutron and resistivity logs. The well GA-AA1 has more shale formation than sand formation. The depositional environment of well GA-AA1 suggests to be submarine canyon fill and fluvial

environment due to the to the gamma-ray signature of cylindrical pattern type. The coarsening upward succession suggests that the sand bodies might due to progradation or vertical accretion which enhance sand bar to overlain the initial bar of shale and silt. Braide, 2012.

Track 2 and 3 logs suite indicates the depth values and resistivity logs, i.e. the induction deep log resistivity (ILD) and micro spherical focus log (MSFL). They are used to measure the formation resistivity in the borehole containing oil and fresh water based drilling mud. The induction deep log resistivity (ILD) has the capability of measuring deeper into the borehole while the microspherical focus logs (MSFL) and is a tools that focuses on current due to it ability of good vertical resolution and capable of investigating shallow depth, detecting small mudcake effect in borehole wall as well able to measure only the invaded zone. The interval sections A and B at depths 3533.55 m to 3548.94 m well GA-AA1. The induction deep log resistivity (ILD) and micro spherical focus log (MSFL) shows a higher reading values which varies from 18.5 ohmm to 21 ohmm and 16.8 ohmm to 23 ohmm. This suggests that the reservoir formation interval sections A and B are compacted formation and not a porous formation which could have resulted in overpressured formation.. Thus, exhibit a normal pressure formation which may be less invaded with fresh water as little amount of hydrocarbon may have been encountered during drilling.

Track 4 the logs suite shows the caliper log and the bit-size. In interval sections A and B of well GA-AA1, the caliper reading was 9.5" (inch) while the bit-size reading was also 9.5" (inch). This indicates that there was free penetration of bit during drilling of well GA-AA1 and the borehole at these depths is in gauge condition. Thus, good drilling condition was experienced for the well GA-AA1 due to its compacted formations, which also implies it has a normal pressure condition within the interval depth of selection.

Track 5 comprises of the density log and the corrected density log.

The interval sections A and B, of well GA-AA1, the density logs and the corrected density logs indicates high reading values of 2.62 g/cm^3 (RHOB) for density logs and 0.015 g/cm^3 (DRHO) This suggests that the formations of well GA-AA1 are compacted thereby exhibit normal pressure formation. No overpressure formation observed. The normal pressure formation usually indicates increase in resistivity and density with depths Rider, (2002), This can be confirms from the high resistivity reading ranging from 18.5 ohm/m to 21 ohm/m and 16.8 ohm/m to 23 ohm/m, (ILD &MSFL) respectively within interval sections A and B

Track 6 is the sonic logs (DT) suite which was used to identify the travel time in the formation borehole that normally depends on lithology and porosity of the reservoir. The sonic logs (DT) within the interval sections A and B of well GA-AA1 indicate high velocity transit time of 68 µs/f. Therefore, it indicates that the well formation is more compacted resulting in normal pressured zones, because velocity usually increases with depth in normal pressured formation (Rider, 2002). Thus, well GA-AA1 formation is a less porous zone which could result in lower pore pressure effect within formation.

Track 7 shows the temperature logs suite of well GA-AA1, which to detect fluid movement and to analyse fluid pressure in a formation. It allowing an accurate detection of an overpressured zone. The temperature reading of the interval sections A and B of well GA-AA1 is 274^{0}F (134^{0}C). This temperature is high due to the deeper depth of the reservoir as temperature normally increases with depth while porosity decreases with depth (Rider, 2002). The porosity decreases suggests that the interval depth sections A and B of well GA-AA1 are compacted which will result to normal pressure formation.

Track 8 and 9 of the logs suite of well GA-AA1 show the compressional wave velocity (Vp,ft/sec) and the shear wave velocity (Vs,ft/sec) used to detect the abnormal and normal pressure zone of the formation in interval depth sections of A and B. The compressional wave velocity (Vp,ft/sec) shows a high reading velocity of 24,699 ft/sec. The compressional wave velocity increases due to pore pressure of the formation which also caused less compressibility of the

pore fluid in the interval sections. As a result, hydrocarbon may be likely found within the intervals, based on the high value of the compressional wave velocity (Vp ft/sec). Normal pressure zones are also experienced within the interval depths due to the less pore pressure effect because an overpressure zone is usually associated with low velocity reading in sediment as the depth increases (Rider, 2002). The shear wave velocity (Vs) within the interval sections indicates low reading value ranges of 6,721 (ft/sec). This implies an effective stress increasing with depth as the overburden stress increased in the formation.

5. 3. 1 Well GA-AA1 Pore Pressure Prediction Results Interpetation and Discussion for well log using Resistivity log

5. 3. 2. 1 RESISTIVITY AND SONIC MODEL WITH NORMAL COMPACTION TREND (NCT) OF WELL GA-AA1 (3533.55 m – 3548.98 m) DEPTH.

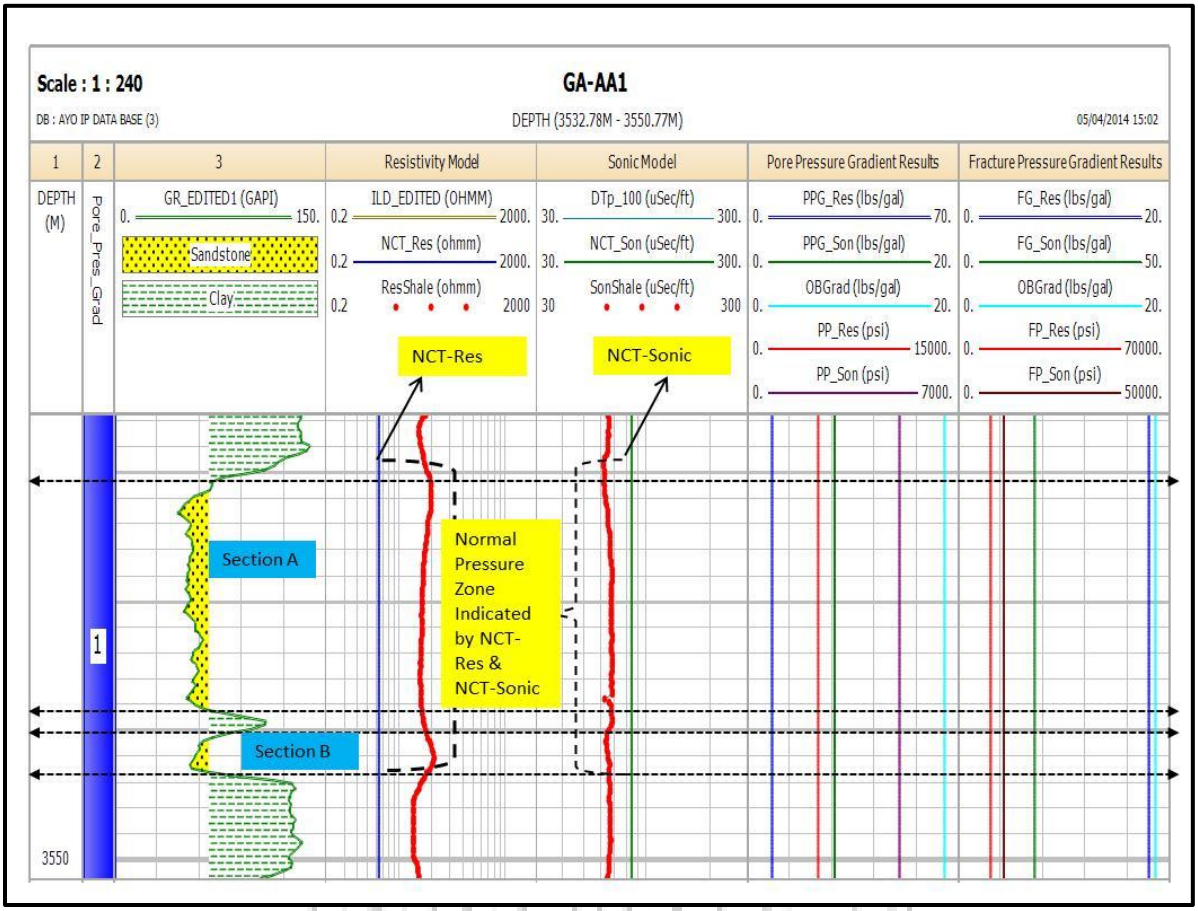

Figure 5.10: The resistivity and sonic transit time velocity model of Eaton's equivalent depth dependence method with NCT (Normal compaction trendline) to estimating pore pressure from Well logs and seismic data for Well GA-AA1.

The total depth interval selection for well GA-AA1 ranges from 3532.78 m to 3550.77 m, and was sub-divided into two reservoir sections A and B. The normal compaction trendline (NCT) coupled with the shale resistivity logs (ohm/m) and the sonic-shale logs (µsec/ft) are designed to detect the abnormal pressure zones (overpressure zone), normal pressure zones as well as predict the pore pressures of the well formation. The induction deep log (ILD) resistivity was

also used in order to obtain the accurate formation pore pressure of well GA-AA1. The procedure of these logs to determine the overpressure and normal pressure formation as well predicting the pore pressure of the wells has been explained in detail above for well GA-W1 and is applicable to all wells.

Therefore, the calculated overburden gradients (OBGrad) of well GA-AA1 within the total reservoir interval sections A and B at depths of 3532.78 m - 3550.77 m, is 18.7 lbs/gal or 2.24 g/cm^3. This value indicates moderate overburden gradient and implies that well GA-AA1 penetrated through a high water column which increased the overburden pressure; it shows less influence on the pressure regime in the reservoir intervals.

The fracture pressure (FP-res) can also be converted to the formation fracture pressure gradients in (g/cm^3) and is the amount of fracture pressure required to fracture the wellbore formation of well GA-AA1 for inducing of mud loss into the wellbore. Therefore, the fracture pressure (FP-res) of well GA-AA1 within the total interval sections A and B at a depth of 3532.78 m - 3550.77m respectively is 10,996 psi and when converted to fracture pressure gradient formation, is 25.36 g/cm^3.

In order to avoid formation fracture of well GA-AA1 which could lead to loss of circulation or mud loss, the mud weight of 0.99 g/cm^3 determined from the pore pressure gradient (PPG-res) of 8.34 lbs/gal must not be higher than the fracture gradient (FG-res).

The fracture gradient (FG-res). The fracture gradient of well GA-AA1 is 18.1 lbs/gal or 2.6 g/cm^3 and is the maximum mud weight required to fracture the wellbore formation of GA-AA1 during the drilling. If the maximum mud weight of 2.6 g/cm^3 were higher than the fracture pressure formation gradient (FFG), fracture might occur which would result in lost circulation or loss of drilling mud of well GA-AA1. But the formation fracture pressure gradient (FFG) of well GA-AA1 is 25.36 g/cm^3 and with a mud weight of 0.99 g/cm^3 and a predicted maximum mud weight of 2.6 g/cm^3 it is concluded that well GA-AA1 was well stabilized, explaining why no mud losses or loss of circulation did occur during drilling.

The effective stress. The overburden stress is 18.7 Ibs/gal (2.24 g/cm^3) and the pore pressure is 5,062 psi or 11.67 g/cm^3 in the well formation GA-AA1. Therefore, the effective stress of the well formation is 2.24 g/cm3 – 11.67 g/cm^3= -9.43 g/cm^3 i.e. an overpressure zone may likely be encountered when further drilling of the intervals A and B at depths 3532.78 m - 3550.77 m.

However the predicted pore pressure (PP-res) calculated with IP within the total interval depth sections A and B is 5,062 psi which is the pressure acting on the fluids in the pore spaces of the formations and indicates that no overpressure formation would be encountered within the reservoir interval of depth sections A and B.

5. 3. 2 Well GA-AA1 Pore Pressure Prediction Results, Interpretation and Discussion from the Seismic using Sonic log.

Eaton's sonic method with depth-dependent compaction trendline (NCT) was used to determine the overpressure zone and the pore pressure prediction calculation for well GA-AA1 from seismic data as shown in track 5 of figure 5.10. Within the total interval sections A and B, at depths 3532.78 m - 3550.77 m, no overpressure was encountered, thus these intervals were regarded as a normal pressure zone. The well GA-AA1 indicates the normal pressure formation as determined by the increase of the sonic shale logs compared to the established value of the normal compaction trendline (NCT) towards the lower values scale as shown in track 5 of figure 5.10.

The corresponding value of the compaction trendline (NCT) is 85.8 µsec/ft which suggests that the interval transit time of velocity increase with depth in a normal pressures zone is as a result of lower porosity in the formation due to its compaction.

Well GA-AA1 experienced a moderate overburden gradient (OBGrad) of 18.7 lbs/gal (2. 24 g/cm^3), which is the pressure gradient for the pressure of the matrix together with the reservoir's pores within the well GA-AA1. Since well GA-AA1 penetrated through a deep overburden water column, there will be increase in overburden pressure in the well formation.

The pore pressure gradient of PPG-sonic is 8.34 lbs/gal and is used to determine the mud-weight of 0.99 g/cm^3 required in drilling the well GA-AA1. It must not be higher than the fracture gradient in order to avoid fracturing the formation and to avoid loss of mud circulation in the wellbore. Also, the fracture gradient (FG-sonic) value of 18.1 lbs/gal (2.16 g/cm3) is the predicted maximum mud weight required during the drilling of the well and must not exceed the fracture pressure formation (FP-Sonic) in order to avoid mud loss or lost circulation and even to avoid blow out hazard.

The fracture pressure (FP-Sonic) 10,987 psi which is also known as the fracture pressure formation, is the amount of pressure required in fracturing a well formation, which is equivalent to 25.3g/cm^3 of mud-weight. It was observed that the IP obtained fracture gradient

(FG-sonic) value of 18.1 lbs/gal (2.16 g/cm^3) (which is the predicted maximum mud weight required during the drilling of GA-AA1) did not exceed the fracture pressure (FP-Sonic) formation equivalent mud-weight of 25.3 g/cm^3. This shows that well GA-AA1 was stabilized. This conclusion is supported by the recorded fact that no mud loss or lost circulation occurred during the drilling period.

To determine the effective stress of well GA-AA1, the overburden stress, which is 18.7 Ibs/gal (2.24 g/cm3) and the pore pressure which is 5,074 psi (equivalent to 11.70 g/cm^3) of the well formation GA-AA1 are subtracted from each other. Therefore, the effective stress of the well formation is 2.24 g/cm^3 – 11.70 g/cm^3 = -9.46 g/cm^3. As demonstrated above, an increase in overpressure causes reduction in the effective stress, it is suggested that an overpressure zone may likely be encountered during further drilling of the selected interval sections A and B at depths 3532.78 m - 3550.77 m.

The IP-derived pore pressure predicted value of 5,074 psi which is the pressure acting on the fluids in the pore spaces of the formations, will likely be encountered throughout the total interval sections of A and B at depths 3532.78 m - 3550.77 m. This conclusion was also supported by the fact that no overpressure condition was encountered within the reservoir interval.

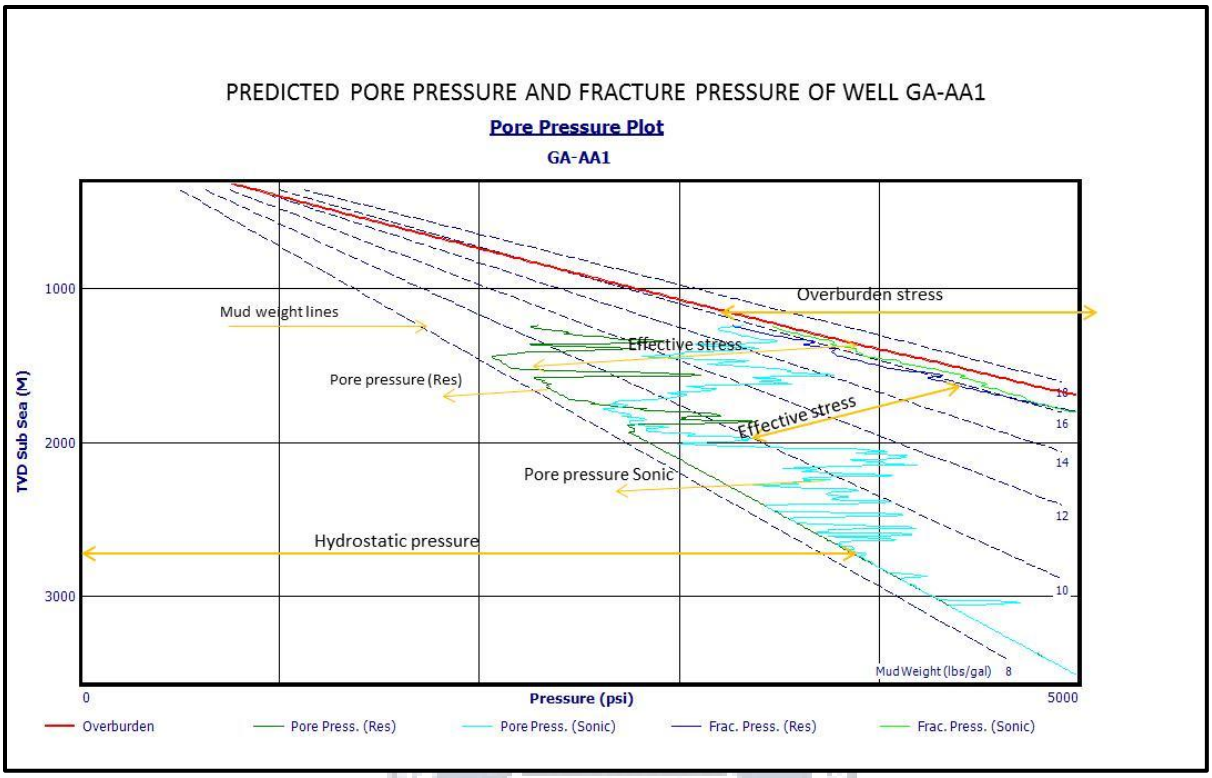

Figure 5.11: Pore pressure gradients and fracture gradients of well GA-AA1.

Overburden, **Pore pressure (Res),** **Pore pressure (Sonic)**
Fracture pressure (Res), ***Fracture pressure (sonic)***

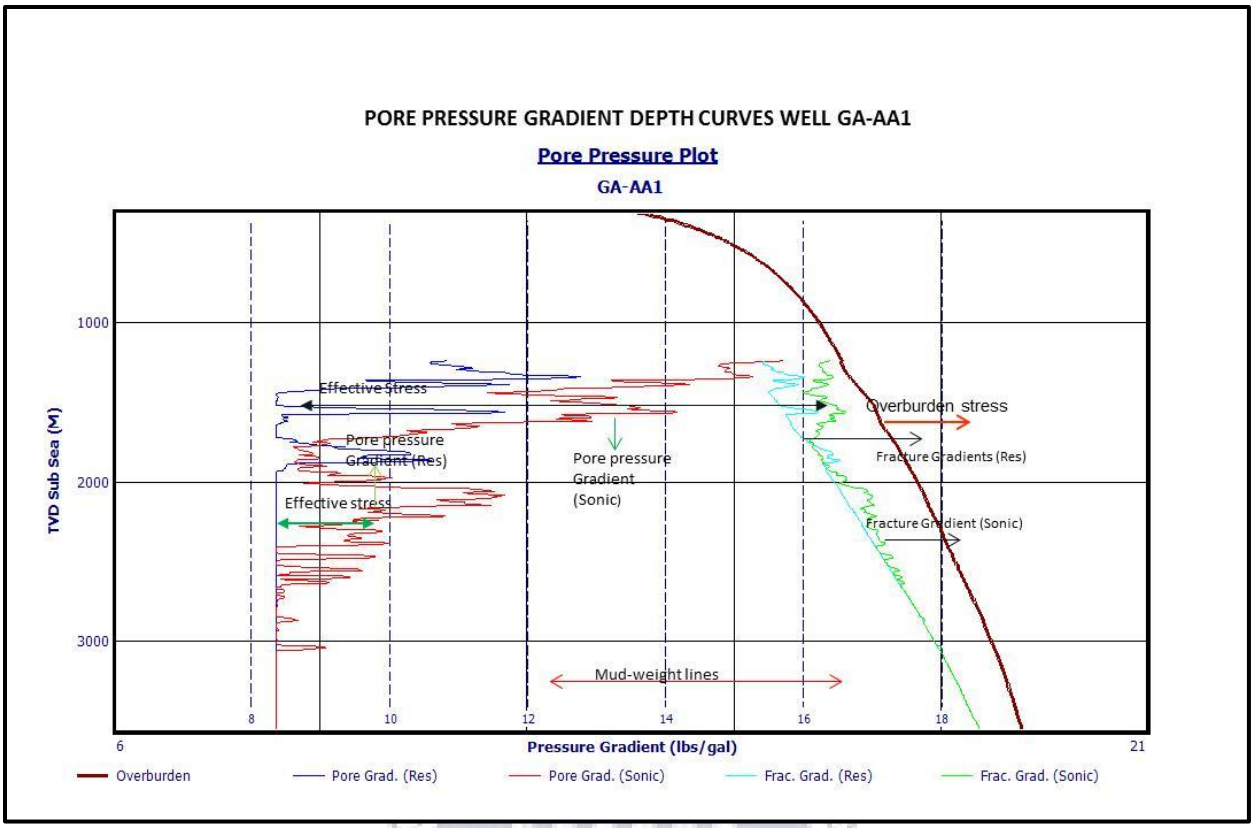

Figure 5. 12: Pressure gradient curves of well GA-AA1.

Overburden, Pore Grad (Res), Pore Grad (sonic)

Fracture Grad (Res), Fracture Grad (Sonic)

5.3.3 The Tomography Extraction Grid Map of the Pore Pressure from Seismic lines, 13AT1 – 1AT1 Horizons Reflection for the Wells GA-W1, GA-N1 and GA-AA1.

The tomography extraction grid map was generated from the seismic data for the wells to delineate the depth imaging of the pore pressure conditions of the overpressure formation and normal pressure formation of the wells. This was done by means of using the interval velocity volume depth grid. One of the signs of the presence of an overpressure formation is that it affects interval velocity, because the interval velocity usually decreases with depth in an overpressure formation as compared with the normal pressure formation which exhibits an increase in interval velocity with depth of a formation.

An overpressure formation was encountered in well GA-W1, which can be observed from the grid tomography extraction map of the seismic data as shown in Figure 5.13. This can be justified from the compressional wave interval velocity logs (Vp ft/sec) which also indicates the low velocity which ranges from 7,970 (ft/sec), 9,940 (ft/sec) to 10,704 (ft/sec) across the intervals' depths of sections. This is due to the high fluid content from the mud weight that resulted in compaction disequilibrium which is a dominant mechanism of overpressure formation in deep water.

In the wells GA-N1 and GA-AA1 normal pressure formations are observed indicated by a high interval velocity volume from the grid tomography extraction map, which is also noted from the compressional wave interval velocity logs (Vp ft/sec) which ranges between the 17,119 (ft/sec) to 24,699 (ft/sec) throughout the intervals' depths section of the respective wells. The velocity increases as a result of the pore pressure of the formation within the intervals which reduced the compressibility of the pore fluid.

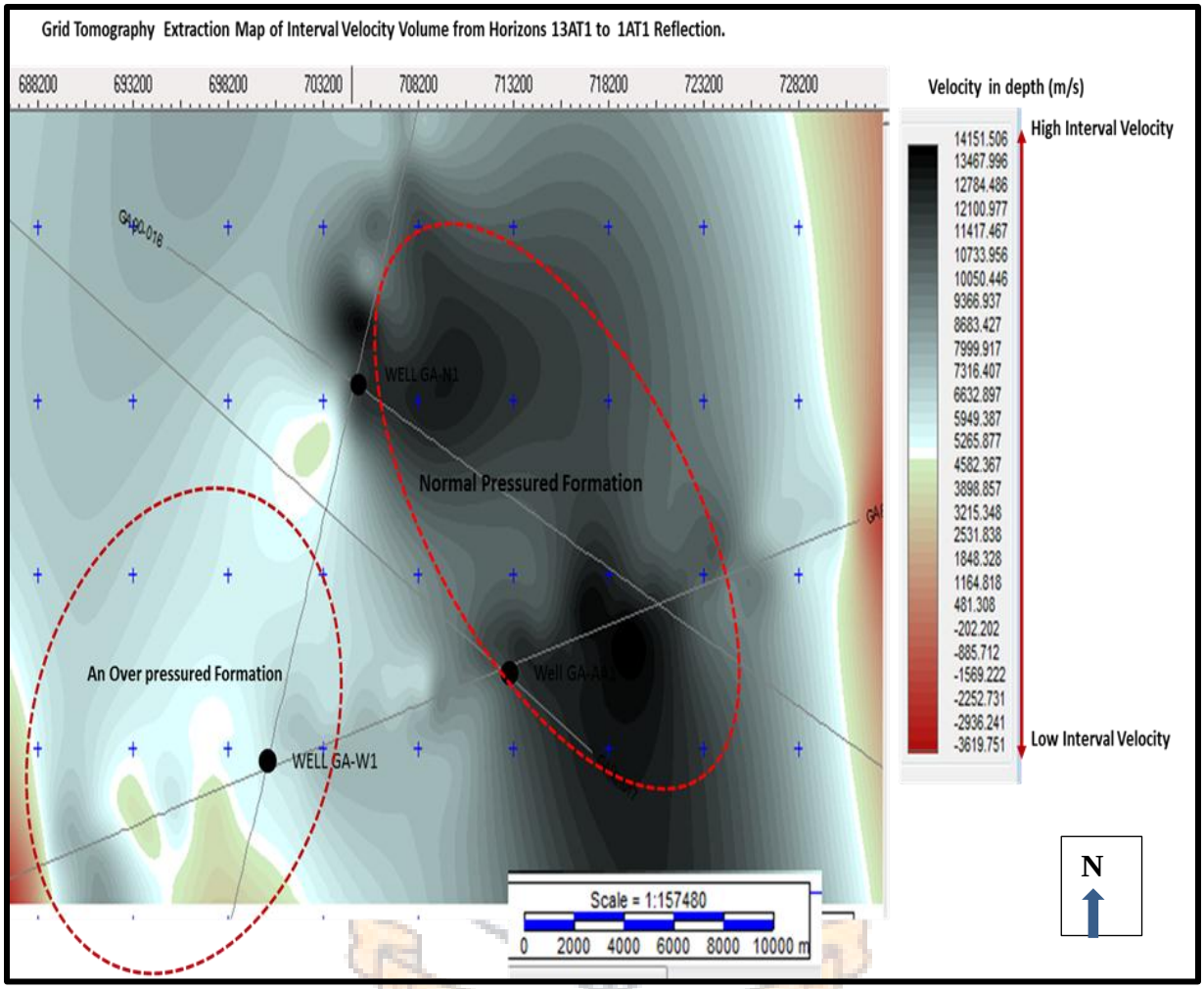

Figures 5.13 the tomography extraction grid map using interval velocity volume generated from the seismic horizons for pore pressure condition of the wells GA-W1, GA-N1 and GA-AA1.

CHAPTER SIX

6. 0: The Direct Hydrocarbon Indicator (DHI) Results Interpetation and Discussion.

This chapter presents the results of the direct hydrocarbon indicator (DHI) used to analyze the Hauterivian to Early Aptian (112 to 117.5 Ma) reservoir in wells GA-W1, GA-N1 and GA-AA1 in Southern Pletmos basin, Offshore South Africa. The direct hydrocarbon indicator (DHI) was obtained from the amplitude extraction, as well as the reflection strength which in turn was obtained by mapping the horizons' well tops of the wells on seismic section. The direct hydrocarbon indicator (DHI) is a measurement of indicates the presence or absence of hydrocarbon accumulation in sediments by means of some seismic attribute features such as bright spot, flat spot and dim spot. However, due to the limitation of seismic data for the selected wells, more emphasis would be laid on the bright spot, flat spot and dim spot on seismic by means of picking up horizon surfaces to extract the amplitude grid extraction and time grid to delineate the region of possible hydrocarbon accumulation on the seismic section. Bright spot is one of the top known direct hydrocarbon indicators on seismic data, it is a high amplitude anomaly by the strong decrease in acoustic impedance at the top of the reservoir charged with hydrocarbons. The bright spot effect weakens with depth, and appears much stronger with gas than with oil; therefore most of the bright spot examples are related to the shallow gas-charged reservoirs.

Furthermore, dim spot is a decrease in amplitude of reflection over a short distance, which occurs as a result of the contrast between the acoustic impedance of watered sand, shale (the embedding medium) and the reservoir giving way to a phase polarity change (a seismic peak on stack data changes to a seismic trough). Flat spot occurs mostly with decrease in amplitude and a phase inversion due to the impedance contrast at gas-Oil or Oil-water contacts in a relevant thick reservoir. If there is a relatively thin reservoir these two reflections can hardly be distinguished.

6. 0 .1 . Seismic Horizons Picking for Wells GA-W1, GA-N1 AND GA-AA1.

Picking seismic horizons is the process of tracking the laterally consistent seismic reflector in order to identify the geological structure, the stratigraphy, as well as to detect the hydrocarbon accumulations within the reservoir. Six horizons were picked for well GA-W1, GA-N1 and GA-AA1 respectively, based on their well tops. Within the extent of the horizon picked, the horizons are laterally extensive and continuous across the seismic section. In addition, two types of grid maps such as amplitude extraction grid map and time grid map were created in order to delineate the geometry of the basin and variation of the horizon. The time grid extraction map was an interpretation of the colours which join the areas of equal time to produce the time map which can be used to represent the depth variation across the horizons. While the amplitude extraction grid map represents the average amplitude value along the seismic horizons joined as a continuous surface to delineate the possible location of hydrocarbons accumulation on seismic sections. Figures 6.1 a-c indicate the horizon picking reflectors of the three wells based on their well-tops, which were used to produce the amplitude extraction grid maps and time grid maps.

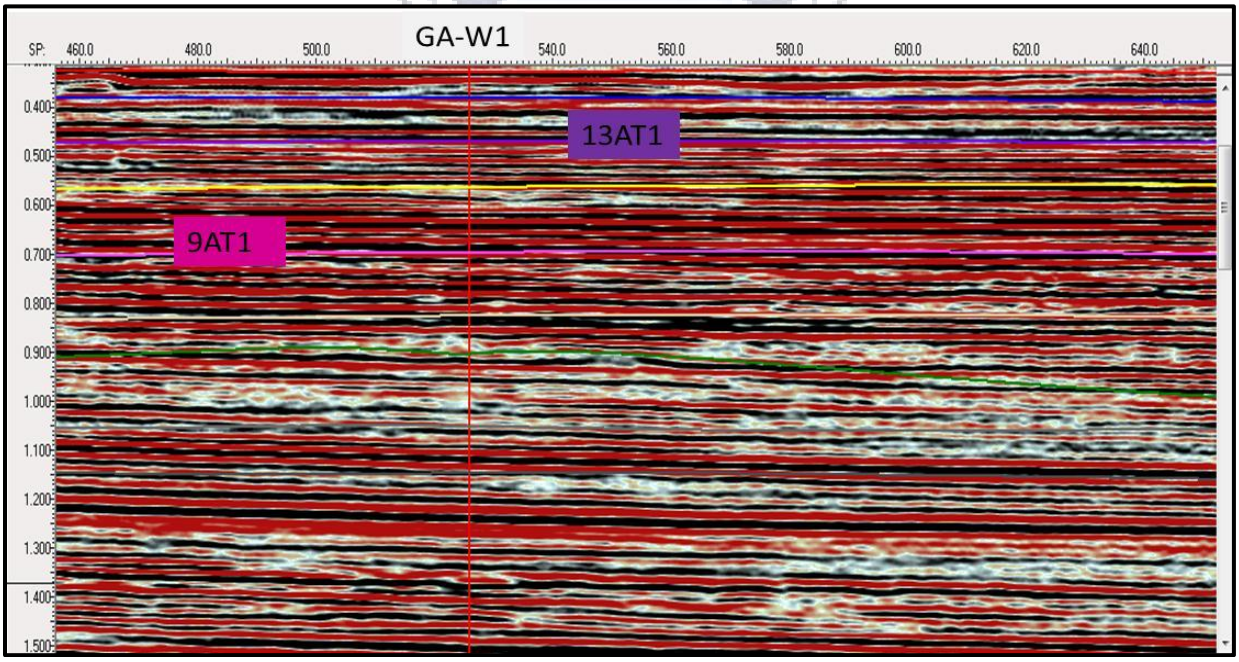

Figure 6.1 a : Seismic section horizons and the well tops of well GA-W1 across the seismic line GA78-016 and GA88-033 from a survey Offshore South Africa, Pletmos Basin as extracted during this project.

.

The interval depth selected for well GA-W1 is 1866.77 m – 1887.93 m, thus the well tops of 13AT1 and the 9AT1 depths are within the interval range used to produce the amplitude map and the time grid map for easy location of the bright spot, flat spot and dim spot as well as sand deposit across the mapped area to delineate hydrocarbon prospects in the well GA-W1 (Figure 6.a).

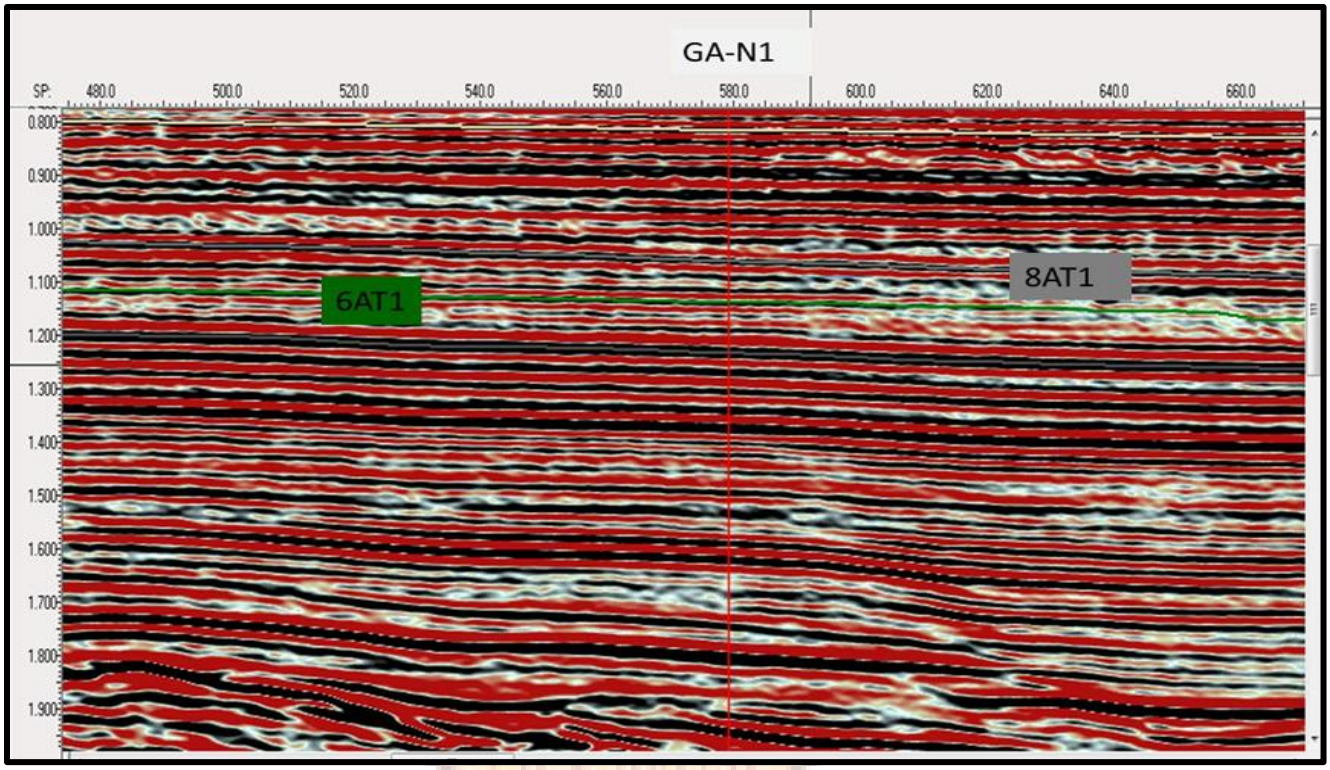

Figure 6.1 b: Seismic section horizons and the well tops of well GA-N1 across the seismic line GA78-016 and GA88-033 from a survey at Pletmos Basin Offshore South Africa, as extracted during this project.

In addition, the interval depth selected for well GA-N1 is 2876.7 m – 2912.36 m, thus the well-tops 6AT1 and 8AT1 are included within the interval range used to create the amplitude grid extraction map and the time grid map (Figure 6.1 b).

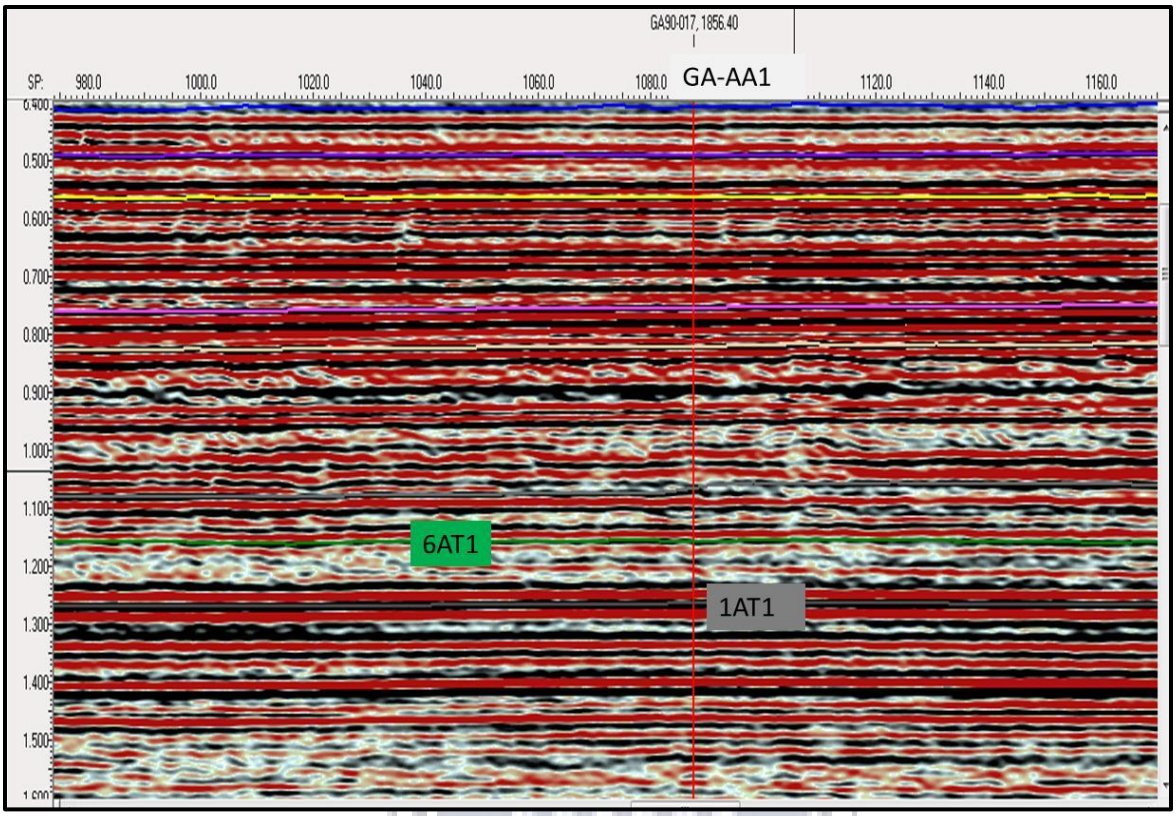

Figure 6.1 c: Showing the seismic section horizons and the well tops of well GA-AA1 across the seismic line GA90-017 from a survey at Pletmos Basin, Offshore South Africa as extracted during this project.

Like with the other wells, the interval depth selected for well GA-AA1 is 3532.78 m – 3550. 77m, and the well tops 6AT1 and 1AT1 depths are within this interval range (Figure 6.1c).

6.0.2 Amplitude Extraction Map Generation for the Horizons of Wells GA-W1, GA-N1 and GA-AA1:

The amplitude extraction grid map and the time grid map were generated from different horizons picked up from the wells based on their equivalent depth of the well top. It is possible to delineate the high amplitude surface with its corresponding time structure within the different horizons of the wells, to locate the possible region of the hydrocarbon prospects on the seismic section.

6. 0. 2. 1 Amplitude Extraction Depth Grid Map for Wells GA-W1, GA-N1 and GA-AA1:

The basic idea of using amplitude extraction for the analysis is based on the assumption that lithology, rock properties and fluid contents would affect seismic character. The amplitude extraction grid map and time grid map of well GA-W1 were generated from the picking horizon 13AT1 and 8AT1 corresponding to the selected interval depth 1868 .71 m – 1887.93 m. It was generated in a map pattern to locate the possible region of hydrocarbon accumulations in well GA-W1 on the seismic section. In addition, because of the closed proximity of the reflectors and the reservoir being relatively thins the peaks in the seismic line were picked at horizon 8AT1 as a result of its high value of positive amplitude reflection (black colour indicating sand deposit).

While the troughs picked from horizon 13AT1 because of its high negative amplitude reflectors (red colour indicating shale deposit), as shown in figure 6.2a. Likewise the amplitude extraction grid map was generated for wells GA-N1 and GA-AA1 from the horizons 8AT1 and 1AT1 which cut across the interval depths 2876.7 m – 2912.36m and 3533.77 – 3550.96 m of the wells respectively. Based on the amplitude reflector of the horizon 8AT1 and 1AT1, peaks in the seismic line were picked at horizon 8AT1 due to its high value of positive amplitude reflector (black colour) indicating sand deposits, while the troughs were picked from the horizon 1AT1 due to their high negative amplitude reflectors (red colour) that indicate shale deposits, as shown in figure 6.2b.

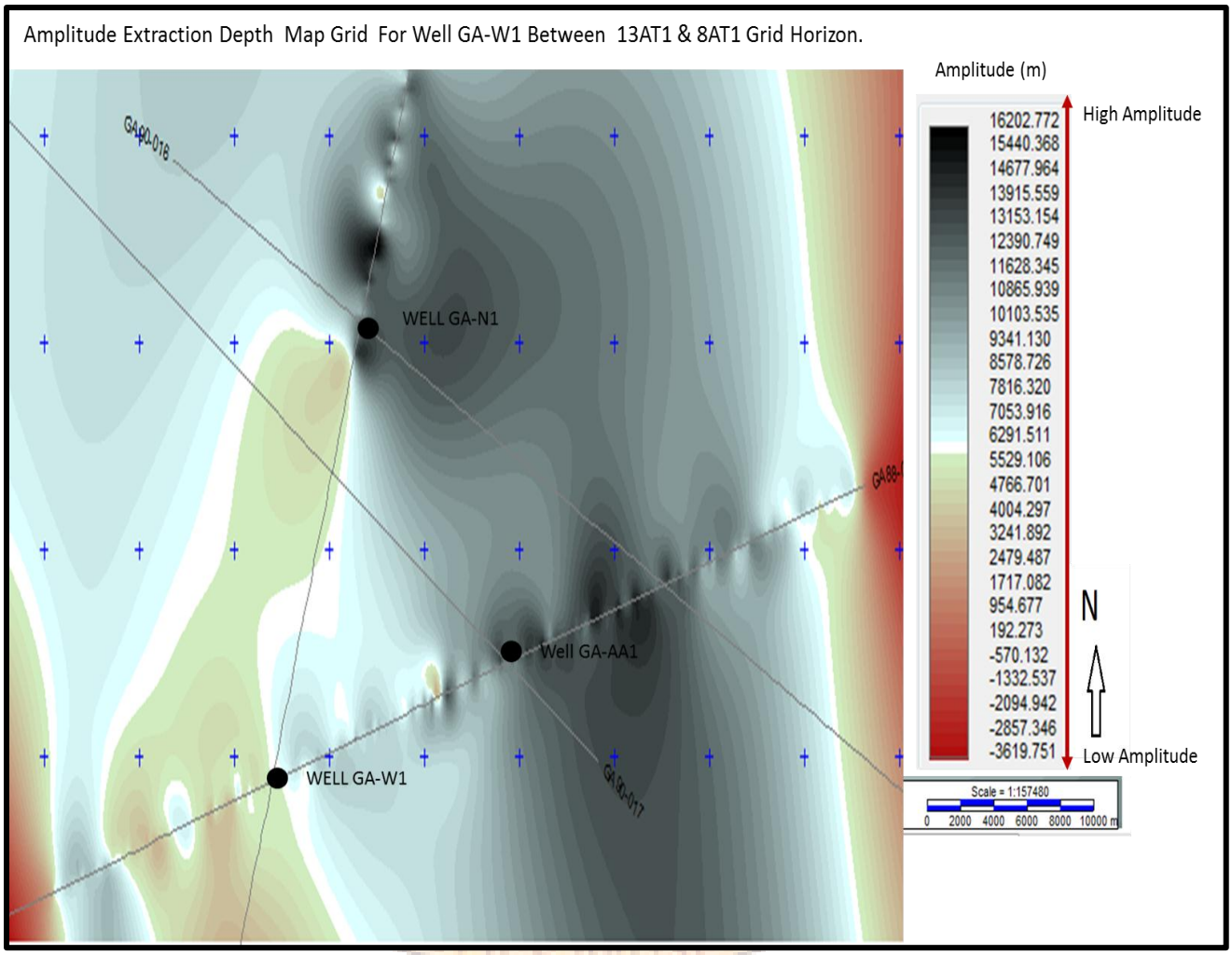

Figure 6.2 a: Amplitude extraction depth map grid of Well GA-W1 between 13AT1 & 8AT1 horizon generated from 2-D seismic line.

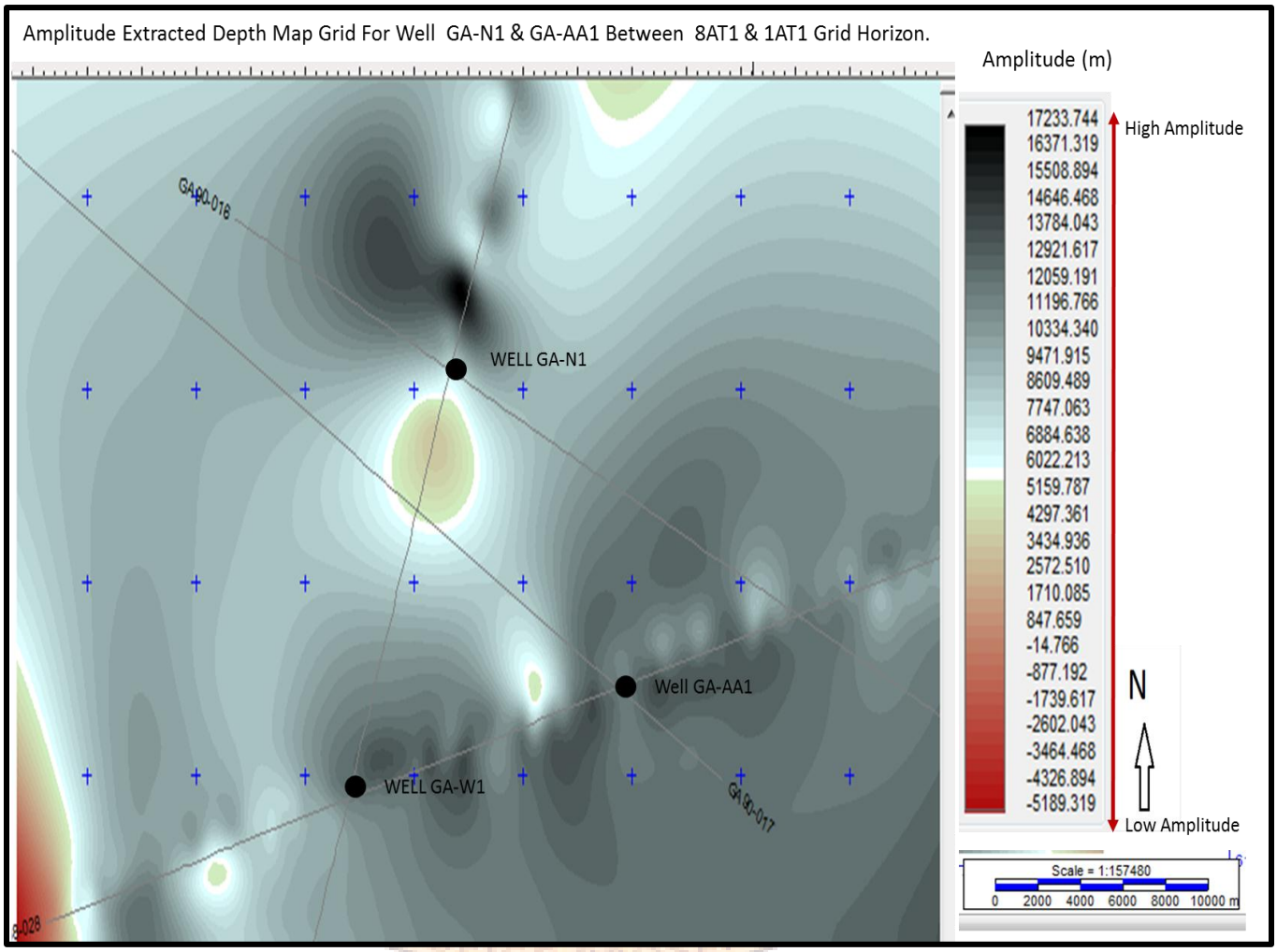

Figure 6.2 b: Amplitude extraction depth map grid of Well GA-W1 between 8AT1 & 1AT1 horizon generated from 2-D seismic line.

6. 0. 2. 2 Discussion on Amplitude Extraction Depth Grid Map for Wells GA-W1, GA-N1 and GA-AA1:

The amplitude extractions for the studied wells were used in this study to establish the lithology, rock properties and fluid content that could affect the seismic performance which can then be used to identify the region of the hydrocarbon prospect on seismic section.

The amplitude extraction zones of the map appear to be constrained to two major colour bands, namely the black colour which indicated the sand deposit of high amplitude values and the red colour which indicated as the shale deposit of low amplitude values. Toward the Northeast-Central and the Southeast-Central parts of the amplitude extraction grid map at 13AT1 and 8AT1 horizons for well GA-W1 (Figure 6.3), the high amplitude zones originate from the acoustic impedance contrast of the hydrocarbon saturated sand intercalated with shale. While along the North-Western and South-Eastern parts of the amplitude extraction grid map at 18AT1 and 1AT1 horizons for wells GA-N1 and GA-AA1, the high amplitude zones were also observed to originate from the acoustic impedance contrast of hydrocarbon saturated sand and intercalated shale. The high amplitude zones (black colour) of the extracted maps spread across the regions for the wells GA-N1 and GA-A1 are suggested to be high porosity trends and its exchange with low amplitude zone (shale, red colour) is interpreted from the lateral lithofacies. Besides, the concentration of the low amplitude zone (shale, red colour) was observed in the South-Central part of the amplitude extraction grid map at 13AT1 and 8AT1 horizons for well GA-W1 (Figure 6.3).

Along the South-Central and Northern part the intercalated low amplitude shale, (red colour) in the amplitude extraction grid map at 8AT1 and 1AT1 horizons for wells GA-N1 and GA-AA1 (Figure 6.4) was interpreted as thick clay bodies or shale.

Furthermore, the black zone (sand) which is the high amplitude region of the extracted map for the wells GA-W1, GA-N1 and GA-AA1 respectively is suggested as delineating the hydrocarbon bearing sand deposits where hydrocarbon accumulation is confirmed for the selected wells within their depth intervals selected on the seismic section. These zones may be observed as bright spots zones on the seismic section. The bright spots can be interpreted as localized anomalies on the amplitude extraction grid maps, but no bright spot, dim spot and flat spot was observed.

On seismic section within the selected intervals at wells GA-W1, GA-N1 and GA-AA1, high and low amplitude are related to bright spot and dim spot but the bright spots, flat spots and dim spots image could not be marked as a result of the underlying basalt flow basement of the Pletmos basin. The difficulty to image these by means of conventional 2D seismic profiling techniques is due to the highly reflective surface (producing strong surface reflector) and high-velocity of the basalt basement (White et al., 2008). The intensity of high velocity basalt flows favorably absorbs the high frequency in the incident wavelet, thereby demeaning the feasible resolution of any sub-basalt arrivals, and strong refraction caused by the large seismic velocity variation between the basalt and sediment, which may mislead the seismic image.

The high amplitude zones (sand, black colour) spread across the amplitude extraction grid map of 13AT1 and 8AT1 horizons for well GA-W1 (Figure 6.3) and horizon 8AT1 and 1AT1 for wells GA-N1 and GA-AA1 (Figure 6.4) respectively, are interpreted to be a thick hydrocarbon bearing sand deposit on the seismic section, occurring 0.76s – 0.80s on time grid map horizon (Figure 6.5). The low amplitude zone (shale, red-colour) of the amplitude extraction grid map of 13AT1 and 8AT1 horizons for well GA-W1 (Figure 6.3) and horizons 8AT1 and 1AT1 for wells GA-N1 and GA-AA1 (Figure 6.4) respectively, are interpreted to be pitfalls anomalies of dim spot associated with gas bearing sand on the seismic section. This can be caused by overpressurised sands or shale. We can now conclude that, the gas-filled sands have high impedance compared with the surrounding shale. In other words either the brine sand is relatively hard compared to the shale or the hydrocarbon –bearing sand is relatively softer than the brine sand, which was observed at 0.95s – 0.99s on time grid map horizon (Figure 6.5).

There was no flat spot (which is the seismic expression of a hydrocarbon - water contact) except pitfalls anomalies observed on both amplitude extraction grid maps of 13AT1 & 8AT1 horizons in well GA-W1 (Figure 6.3) and horizons 8AT1 & 1AT1 for wells GA-N1 and GA-AA1 (Figure 6.4). This may be interpreted to be a paleo-contact, caused by either diagenesis or residual hydrocarbons saturation. This was observed at 0.87s – 0.88s on the time grid map (Figure 6.5) in prospective zones where there is a large zone of the high amplitude zone reflection events. High amplitude may represent possible hydrocarbon accumulations, but not all bright spots are due to the presence of hydrocarbon, as they could also be the result of large acoustic impedance contrasts a change in lithology. Figure 6.3 and 6.4 illustrate the thick hydrocarbon-bearing sand of the amplitude extraction grid map from the horizons 13AT1 & 8AT1 in wells GA-W1 and horizons 8AT1 & 1AT1 for wells GA-N1 and GA-AA1 respectively.

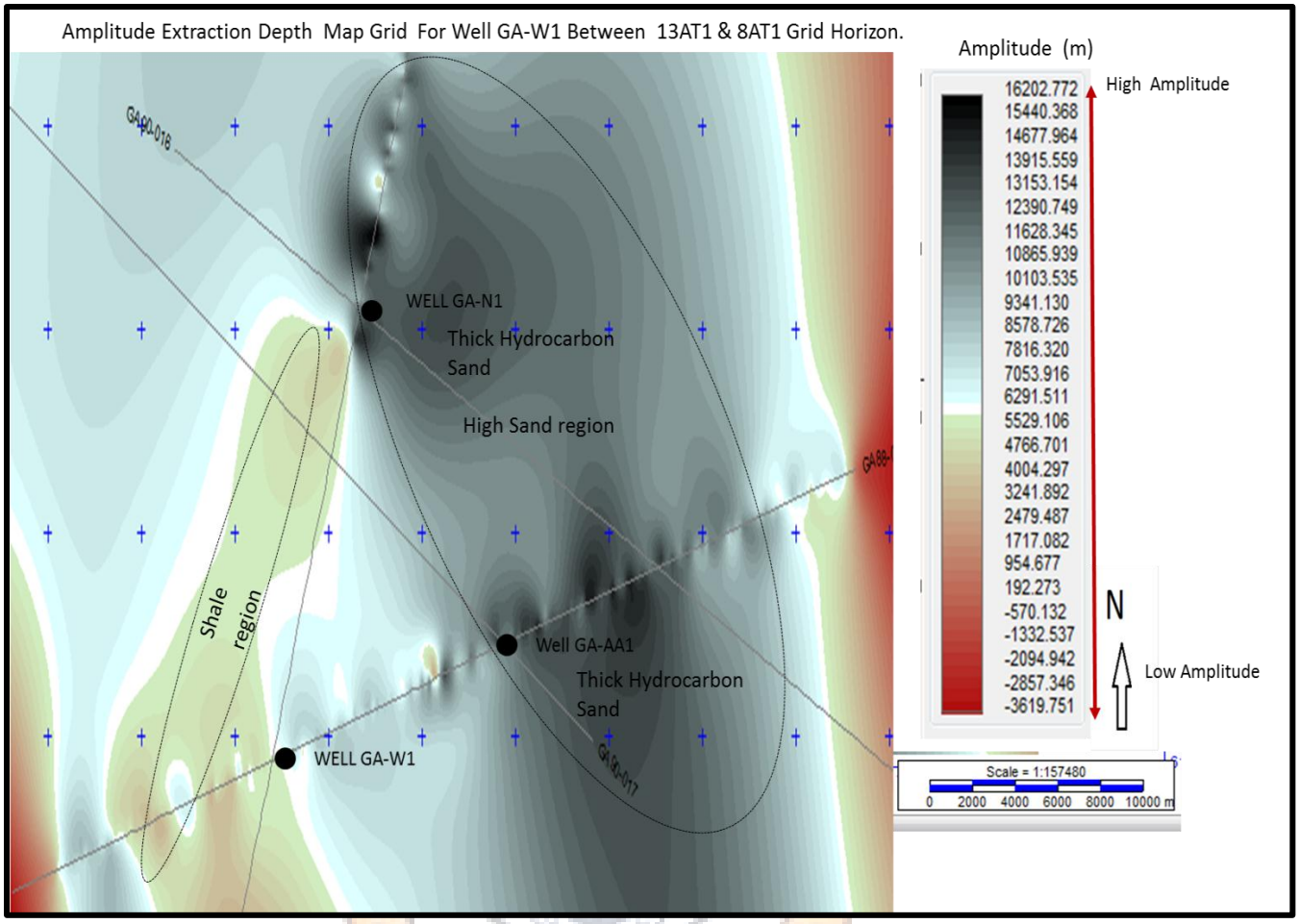

Figure 6.3 Amplitude extraction depth map grid of Well GA-W1, indicating thick hydrocarbon-bearing sand from 13AT1 & 8AT1 horizons grid generated from the 2-D seismic line.

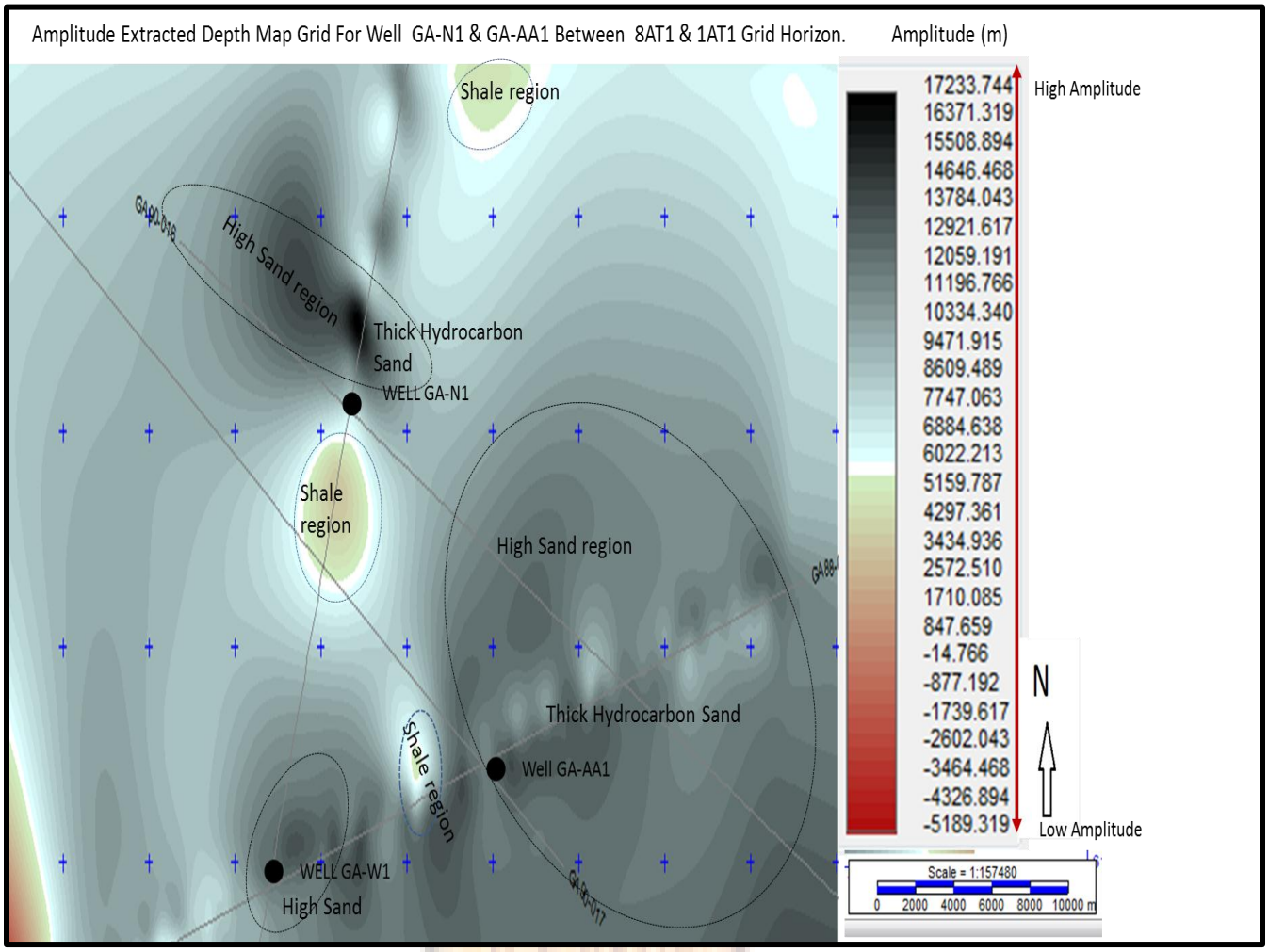

Figure 6.4 Amplitude extraction depth map grid of Well GA-N1 and GA-AA1, indicating thick hydrocarbon-bearing sand from 8AT1 & 1AT1 horizons grid generated from the 2-D seismic line.

6. 0. 2. 3. Discussion on Time -Depth Grid Map for Wells GA-W1, GA-N1 and GA-AA1:

The time-depth grid map was generated from the horizons 13AT1 & 8AT1 for well GA-W1 and horizons 8AT1 & 1AT1 for the wells GA-N1 and GA-AA1 from the 2-D seismic line (Figure 6.5). These correspond to the selected interval depths for the purpose of recording depth variation across the horizons, thus generating the subsurface geometry for structural interpretation. This is an indication that the horizons conform to a similar structural geometry. No faulting was observed within the selected interval on the map, therefore the hydrocarbon trap in the area are stratigraphic traps; the hydrocarbons are trapped in dual sandstones surrounded by shale, which prevent the hydrocarbon fluids from escaping. Horizons 13AT1 & 8AT1 for well GA-W1 and 8AT1 & 1AT1 for the wells GA-N1 and GA-AA1 are interpreted as being pinch-out traps. The observed lateral variation in the amplitude from the horizons confirms the interpretation of the lateral stratigraphic change.

The high amplitude (black colour, sand bodies) observed in the Northeast-Central and the Southeast-Central zone of horizon 13AT1 and 1AT1 for well GA-W1 as well as in the Southern and North-west of horizons 8AT1 and 1AT1 horizons for the wells GA-N1 andGA-AA1.

The sand bodies could be interpreted as submarine canyons cutting through the shape and abyssal plains as observed on time grid map of the seismic section, where the red colour indicates shale or high impedance and the black colour indicates the high amplitude and shows the highest stack of sand accumulations. However, it does not reveal the reservoir quality. The geological feature exposed by the high amplitude in the extraction map is interpreted to be a turbidite lobe which could be a regional sand pinch-out trap.

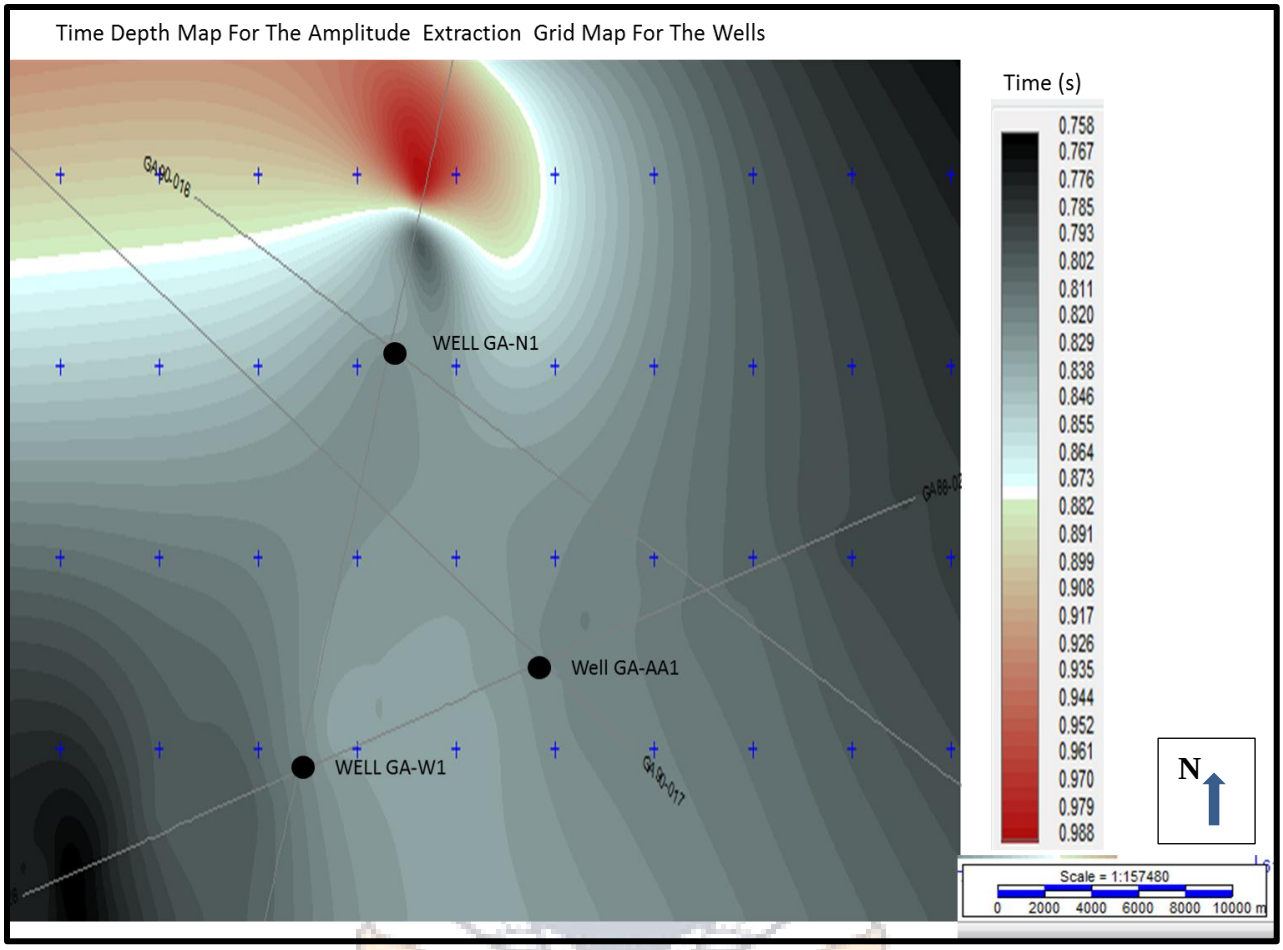

The figure 6.5. The time depth grid map of the wells GA-N1, GA-W1 and GA-AA1

6. 0. 2. 5 Reservoir Geometry and The Possible Hydrocarbon Traps

The reservoir geometry of the selected wells defines a basin pattern without much variation due to the absence of faults cutting across the horizons which are laterally continuous reflectors. The sediments have a relatively smooth character and the whole reservoir geometry conforms to the shape as indicated in the amplitude extraction grids maps. In addition, the commercially most promising hydrocarbon prospects may be found beneath 8AT1 and 1AT1 horizons which are indicated by the high amplitude (black colour). That defining thick hydrocarbon-bearing sand bodies of potential reservoir quality in wells GA-W1 and GA-AA1 on the amplitude extraction grid maps.

Furthermore, due to some area occupied by pitfall anomalies related to dim spots as found in amplitude extraction grid map horizons 13AT1 and 8AT1 a large volume of wet gas may be present which may be found beneath these horizons giving way to another commercial hydrocarbon prospects in the region. Based on the interpretation that the depositional environment of the sediments in the basin is a deep-marine to submarine Canyon-fill, it is expected that the sand bodies would be relatively thin bedded with intermediate shale coupled with a gentle structural deformation in the area. It is therefore suggested that most of the traps are indeed stratigraphic in nature.

CHAPTER SEVEN

7.0: Conclusions and Recommendations:

The pore pressure prediction of the reservoir units encountered in wells GA-W1, GA-N1 and GA-AA1 was comprehensively investigated and predicted using two appropriate methods: (a) Eaton's resistivity method with depth-dependent normal compaction trendline and (b) Eaton's sonic velocity method with depth-dependent normal compaction trendline. However, the direct hydrocarbon indicator (DHI) of the wells was also carefully studied in order to delineate the possible of the hydrocarbon prospects in the basin through the identification of bright spots, flat spots and dim spots as well as sand regions by means of horizons picking reflector using poststacks surface seismic amplitude analysis.

7.1 Deduction:

The objectives were achieved and the following deduction can be made in concluding this thesis.

The three studies wells (GA-W1, GA-N1 and GA-AA1) of lower Cretaceous of Early Aptian to Hauterivian age (112 to 117.5 Ma), fall within the transitional rift-drift phase or pre-drft phase (13AT1 to 1AT1) of the Pletmos Basin. The depositional environment of the studies reservoir was interpreted as a deep marine abyssal plain and submarine canyon which deposits from lowstand progradating wedges.

The pore pressure prediction of the reservoir units encountered in the three drilled wells GA-W1, GA-N1 and GA-AA1 were comprehensively investigated and predicted by means of using two appropriate methods such as Eaton's resistivity method with depth-dependent normal compaction trendline and Eaton's sonic velocity method with depth-dependent normal compaction trendline from seismic data. The results obtained were not only precise but also relatively similar for the various methods used. The total reservoir interval depths section for the wells has a relatively close maximum mud weight obtained from the two methods used, such as 1.98 g/cm3, 2.12 g/cm3 and 2. 16 g/cm^3, respectively. These values were predicted to

be required to maintain the stability of the holes. Drilling records show that no mud loss or lost circulations were experienced during the drilling, as a result of accurate mud weight used, but if the excess mud weight was used the reservoir may be damage by causing pipe stucking, lost circulation. Conversely, if the mud weight is too low it will have a hydrostatic pressure that is less than the formation pressure. This will cause pressurized fluid in the formation to flow into the wellbore and make its way to the surface. This is referred to as a formation "kick" and can lead to a potentially deadly blowout if the invading fluid reaches the surface uncontrolled.

Also the effective stress of the wells ranges from -5.76 g/cm3, -7.28 g/cm3 and -9.46 g/cm3 across the interval depth selection which also enhanced the detection of the over pressure and normal pressure formations of the wells' interval depth section.

The predicted pore pressures calculated for the entire interval depth of the sections for the wells from the two methods ranges from 3,401 psi to 3,621 psi (GA-W1), 4,098 psi to 4,120 psi (GA-N1), and 5,074 psi to 5,083 psi (GA-AA1) and are predicted to be encountered within the interval depths of the wells during the drilling.

The tomography extraction grid map was also generated from the seismic data for the wells GA-W1, GA-N1 and GA-AA1 in order to delineate the depth imaging of the pore pressure conditions of respectively the overpressure formation and normal pressure formation. This method also confirmed the presence of an overpressure formation in well GA-W1 with low value of the interval velocity volume ranges between 4,582.367 m/s to -3,619.751 m/s. Likewise a normal pressure formation was also confirmed in wells GA-N1 and GA-AA1 with high value of the interval velocity volume ranges between 14,151.506 m/s to 9,366.937 m/s

It is thus concluded that using IP and the methods outlined above from seismic data is a reliable tool for the prediction of pore pressure in wells.

The Direct Hydrocarbon Indicator (DHI) was carried out using post stack surface seismic amplitude analysis characteristic such as bright spots, flat spots and dim spots as well as sand bodies' deposits to delineate the possible hydrocarbon prospects of wells GA-W1, GA-N1 and GA-AA1, through amplitude extraction grid map from the horizons reflection.

High amplitude extraction interpreted as a large thick hydrocarbon-bearing sand deposit of possible commercial hydrocarbon prospects was found on seismic section beneath horizons 8AT1 and 1AT1 well GA-N1 and GA-AA1. While, the pitfalls anomalies relatively to dim spot that associated with gas-sand reservoir as a result of decreased in amplitude extraction reflection was found beneath the horizons 13AT1 and 8AT1 well GA-W1 which can be interpreted as wet gas. This finding was the same with the well report.

Thus, concluded that well GA-N1 and GA-AA1 may contain little amount of hydrocarbon in their respective borehole, where well GA-W1 might be a wet gas reservoir with no hydrocarbons due to the relative anomalies related to dim spot observer on the seismic section of the well. No bright spot, dim spot and flat spot was indicated on seismic section except thick hydrocarbon-bearing sand deposits.

7.2 Recommendation and Future work:

Additonal improvement on this study will shed more light in understanding the pore pressure prediction, safe drilling operation and Direct hydrocarbon indicator (DHI) of the Pletmos Basin. The list below suggests some fact for futher investigation.

I. High mudweights should not be used to fracture the formation of the wells in order to avoid lost circulation. Using these methods to predict pore pressure will guide the to mudweight will help to reduce the problem encountered during the drilling and enhance the depth at which casing is set. This should aid in improving the well designed which will lead to an improvement in the enhancement of the production of hydrocarbon prospects for any future well of the area.

II. Taking the direct pressure measurements of the permeable formation of the wells and combined with the methods used in this study in order to actually know the true pore pressure prediction will be of greater advantage for the benefit of the future works as most of the pressure data measurement such as, Repeat Formation Test (RFT) and Drill Stem Test (DST), for these wells was not performed during the drilling operation.

III. By using different techniques methods to investigate the pore pressure prediction of Pletmos basin in order to understand the uncertainty in each method used will help to know the better method suitable for the Pletmos Basin. The methods used in this study provides a complementary result (seismic and wireline logs methods).

IV. Additional methods such as amplitude variation with offsets analysis (AVO), seismic forward modelling, as well as an acoustic and elastic impendance version to investigating Direct Hydrocarbon Indicators (DHI) will be an added advantange to delineate the hydrocarbon prospects zones of the Pletmos Basin.

APPENDIX

Appendix A: Review of Seismic Data Survey:

Seismic survey are usually the key component carried out in an exploration of hydrocarbon and in the production phase which are widely used around the world to produce detailed image beneath the earth's surface, which can be used to locate well and help to reduce or minimize land disturbance.

The pre-drill estimate of pore-pressure are usually derived from seismic data, such as seismic velocities from two dimensional (2D) and three dimensional (3D) seismic survey are used to predict pore pressure. The accuracy of the seismic velocities is normally assessed by using comparison with interval velocities which calculated by upscaling sonic logs and by inverting time/depth pairs from the checkshots measured in wells. Seismic velocities are important geophysical parameters and tool in which Velocity and density constrasts allow to image reservoirs. Velocities can be used indirectly through their influence on coefficient and amplitude for a purpose as a direct hydrocarbon indicator.

In addition, to calibrate the velocities to pore pressure transform, pressure test and drilling mud weights must be available in order to estimate formation pore pressure. This technique method is capable of optimize drilling operations, such as to avoid unnecessary kicks, develop casing points, and assist in reservoir development by evaluating pressures compartments.

Appendix B: Review of Seismic Relection Theory:

Wave propagation through the earth is the fundamental basis of the seismic exploration method. Wave propagation depends on the elastic properties of the rocks and the fluid contained within them. The difference measure at which the rocks resist the change are noted and interpreted as geological structure, lithology and fluid through the travel time, phase, frequency and amplitude domain. In general, seismic reflections are function of acoustic impedance (velocity time density) and are influenced by reservoir pressure. However, the type of reservoir fluid impacts on sonic velocities, shear waves (Vs) and compressional waves (Vp) respond differently to various reservoir fluids as well as to reservoir pressure. Two major

practical methods are applied for this phenomenon such as; prediction of abnormal pressure from seismic before drilling, mapping reservoir fluid movement and dynamic change of reservoir pressure using time lapse (4-D seismic).

Appendix C: Review of Seismic Pore Pressure Prediction:

The concept of pore pressure prediction from the acoustic data was explored in the 1960's. Pennebaker (1968) was among the pioneer's men to describe the method of predicting pore pressure from sonic data. Eaton (1975) also showed a mathematical expression that related to sonic travel times to pore pressure. Reynolds (1970) described how pore pressure can be derived from seismic data using velocities. All these methods takes to account because sonic velocities depend on the effective pressure, and hence the pore pressure. The relation between effective pressure and velocity depend much on the mineral composition and texture of the rock. For instance, P-wave (compressional-wave) velocities vary significantly with effective pressure for unconsolidated sandstone (Domenico, 1977). When unconsolidated sand exerted by external load, the individual grains contacts becomes stronger. Thus the stiffness of the sand increases, thereby leads to an increased P-wave velocity. However, velocities of the consolidated rocks may also vary significantly with pressure, as this not related to the strengthening of grain contacts, but due to microscopic cracks in the rock. The cracks tend to close when external pressure is being applying thereby creating contacts at the crack surface. Due to this, P-wave velocity increases. However, for consolidated rocks with little cracks, the velocities may not vary much with pressure. It can be notice that a granular rock cemented gain contacts have no pressure dependence at all (Dvorkin et al).

Under-compaction is one of the major important geological processes for buildup of abnormal high pore pressure. Due to under-compaction the porosity of the sediments is preserved showing that under-compacted sediments are more porous than compacted sediments. Thus, porosity is the major factors that determine the velocity of the rock. However, both theoretical and experiments showed that seismic velocities decrease with increasing porosity. Therefore, under-compacted sediments seem to possess lower velocities than compacted sediments.

P-wave and S-wave (Compressional wave, V_P, & Shear wave V_S) velocities are the key parameters for seismic pore pressure prediction. Pore pressure prediction depend directly or indirect on relationship between pore pressure and either P-wave or S-wave as well as both. Thus, accurate velocity information from seismic data is crucial to estimate pore pressure.

Appendix D: Review of P- wave Velocity and S- wave Velocity:

Seismic wave can be referred to as elastic waves, due to the oscillation of the medium particles which occur as a result of interaction between the stress gradient against the elastic forces (Suprajitno, 2000). The compressional wave applied to rock units, the rock change in volume and shape, while changing in shape only applicable to rock units when shear wave applied, as shown in figure

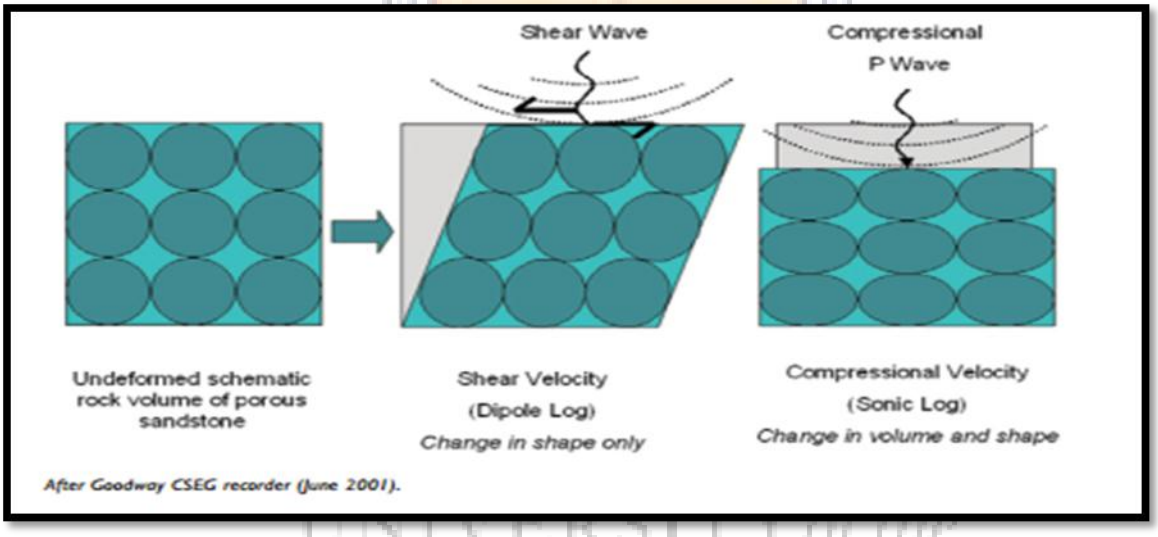

Figure showing rock deformation schemas against of P-wave and S-wave on rock units, (Goodway, 2001).

There are two types of waves depending on how the seismic wave velocity travels and propagated through a medium. They are longitudinal wave and transverse wave.

Longitudinal wave is the wave in which the displacement particle of the medium travels parallel to the direction of wave propagation. Simply oscillate back and forth about their individual equilibrium position, this wave usually occurred in a compressed region (i.e a pressure wave), which move from left to right. This wave type is also referred to as compressional wave or P-wave, and travels faster in a medium. **Transverse wave** is a wave in

which the oscillation or direction of the particles of the medium is perpendicular to the direction of propagation. The particles simply oscillate up and down about their individual equilibrium position. This type of wave is also referred to as Shear wave (S-wave) or rotational wave, has the tendency to travel in a slow pace do arrive after compressional wave (P- wave). The equation to show the relationship between P-wave and S-wave are shown below.

$$V_P = \sqrt{\frac{\lambda + 2\mu}{\rho}}$$

$$V_S = \sqrt{\frac{\mu}{\rho}}$$

(Goodway, 2001).

Where: coefficient = k+ 2/3μ

K = Bulk modulus

μ = Shear modulus

ρ = Density

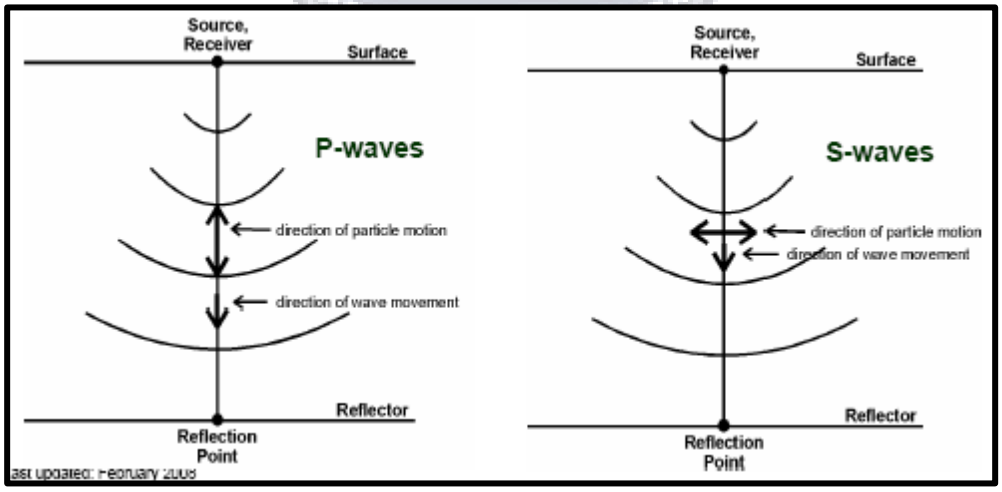

Figure showing the particles wave movement motion of P- wave and S- wave. (Russel, 1999).

Poisson ratio (σ) equation can be represented by ratio between the Vp and Vs as follow:

$$\sigma = \frac{\gamma - 2}{2\gamma - 2} \quad \text{and} \quad \gamma = \left({}^{Vp}/_{Vs} \right)^2$$

However, the empirical relationship between Vp and Vs wave for watersaturated clastic silicate rocks, is known as Mudrock Line which was derived by Castagna (1985) and shown in the figure. Vp = 1.16Vs + 1.36 km/s Figure 2.25. (Russel, 1999), Mudrock Line Relationship between Vp and Vs.

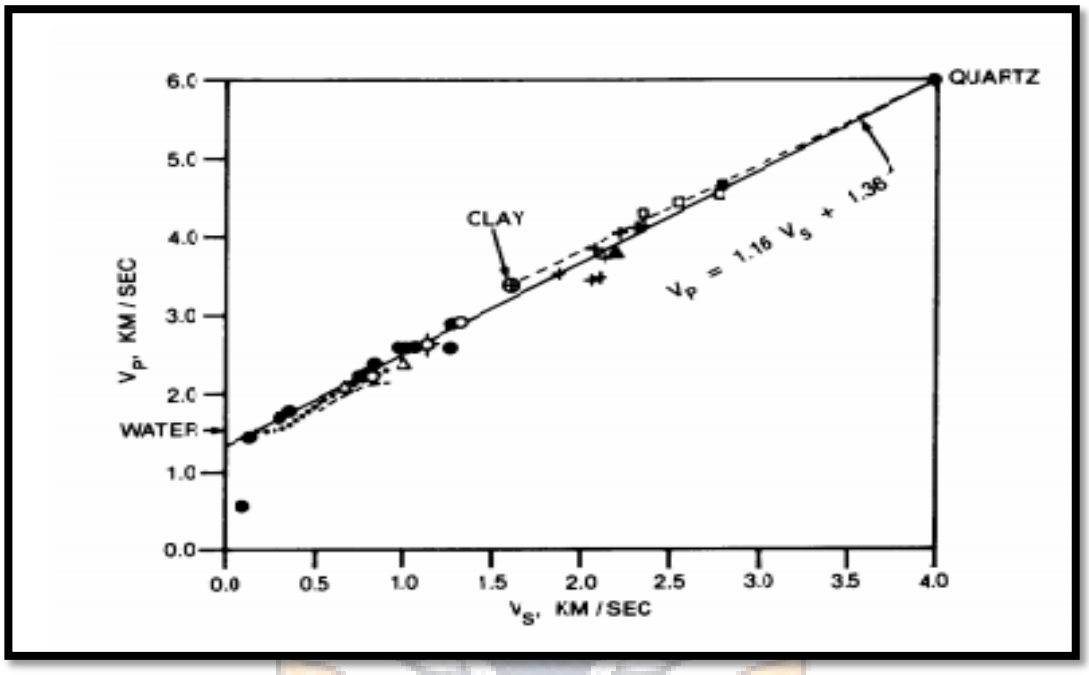

Figure showing Mudrock Line Relationship between Vp and Vs. (Russel, 1999),

The mud rock line is only valid for the water- saturated clastic silicate rock and used to calculate Shear wave (Vs) velocity. The weakness of this relationship is where the value of Shear wave (Vs) is underestimated for soft consolidated sands and some clean sands.

However, the ratio value of Vp/Vs is also used as a lithology indicator as well as isotropic parameters indicator (Pickett, 1963; Nation, 1974 ;) Clay can sometime have higher Vp/Vs ratio than sandstone.

The value of Vp/Vs by mean of AVO (amplitude variation with offset) can also be used as Direct Hydrocarbon Indicator, since Shear wave (Vs) does not sensitive to fluid and Vp-wave does sensitive to both lithology and fluid changed. Therefore, Vp/Vs is a function of lithology and fluid change. (Eastwood and Castagna, 1983; Castagna et al., 1985) studied shows that Vp/Vs

sensitive to gas in most elastics sediments, also (Gregory, 1977; Tatham, 1982; Ensley, 1984, 1985) states its variable response to gas in carbonates rocks.

Appendix E: Review of Bright spot, Dim spot and Flat spot:

Studies show that the presence of gas in soft sand show a dramatic increases in the compressibility of the rocks, the amplitude decreases and the velocity drops thereby producing a negative polarity, which is known as ''bright spot'' which signifies as strong reflector, a high amplitude impedance i.e. increasing the reflection coefficient. However, in a relatively hard sand saturated with brine may induce a bright spot anomaly and the gas –filled sand may be transparent thereby producing what is known as ''dim spot'', a very weak reflector. Dim spot occur when the shale have lower acoustic impedance than both water and oil/gas as a result of compaction which causes the acoustic impedance of sand and shale to increase according to the depth and age but in an uniformly manner (younger shale usually have higher acoustic impedance than the younger sand, but interms of depth related, older shale has lower acoustic impedance than the older sands. In addition, "flat spot" occur when phase change by lowering of impedance due to presence of gas and flattening of seismic events due to gas-water contacts. The figure shows the lower impedance of sand which produces amplitude improve above the crest structure of present hydrocarbon, with this kind of ''bright spot'' situation, ''flat spot'' can be obtained at the hydrocarbon-water contacts. This is a hard reflector (impedance increase) and has to be at the same TWT relatively to the changing in amplitude. Assumed both oil and gas are present, it indicates of two distinct flat spots, such as gas-oil contacts and oil-water contact at deeper.

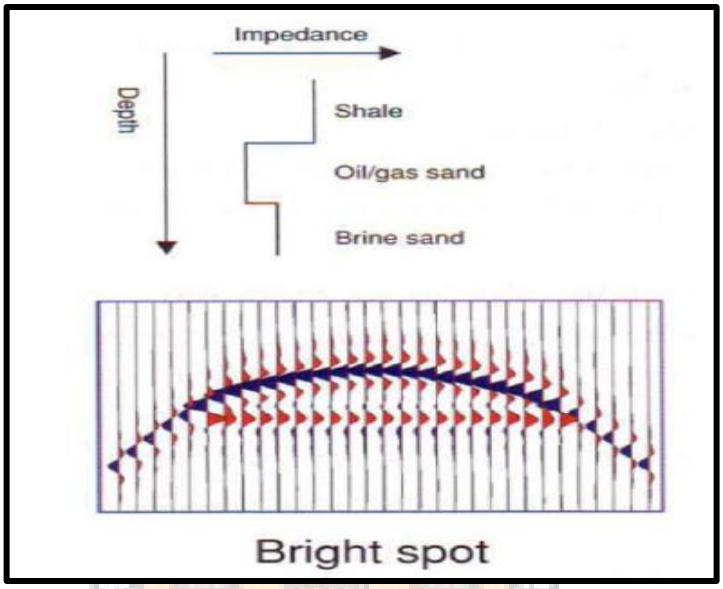

Figure showing the schematic model of bright spot for oil/gas brine sand response (from Bacon et al., 2009). The red colour indicates hard loop (Impedance increase) and the blue colour indicate soft loop (Impedance decrease).

Flat spot occur at the reflective boundary between different fluids, either gas-oil, gas-water or water-oil contacts. All these are easily detected in area where there is tilted stratigraphy background as the flat spot will stick out. However, if the structure more flat, the fluids related to the flat spot cannot be easily discovered. Quantitative methods such as AVO analysis can be used to constitute the difference in or between the fluid-related flat spot from the flat-lying lithostratigraphy. However, proper observation should be clearly made when considering flat spot as DHI as several pitfalls (false flat-spot) may arise such as volcanic-sill, paleo-contacts, sheet-flood deposits and flat bases of lobes and channels, also flat spots can be related to diagenetic events that are depth dependent. The boundary between opal-A and opal-CT indicate an impedance increase in the same way for fluids contacts, and dry wells have been drilled on digenetic flat spots. If the larger scale structure is tilted clinoforms can appear as flat feature.

Appendix F: Review of Seismic anomaly on Bright and dim spots:

The behaviour of hydrocarbon presence on seismic profile does not actually produce a standard seismic imaging, is often change as a function of impedance contrasts along the contacts. Showing in the figure, an oil/gas brine sand model can have different impedance contrasts: for brine sand with relative to the overlying shale and soft hydrocarbon saturated sand in figure (A) the shale/gas sand contacts will have decrease impedance with polarity inversion, while the gas/brine sand contacts have an increase impedance with polarity inversion, which often hard to interpret. In some cases minor faulting may affected the structures. In hard brine sand relative to the shale, and hydrocarbon sand relative to the shale figure(B) "dim spot" can be observed or where the amplitude decrease at the top reservoir. Dim spot is very hard to see as result of a very near-offset reflector may have correspond to strong far-offset reflectors, which conform to the structure and to the TWT of flat spot.

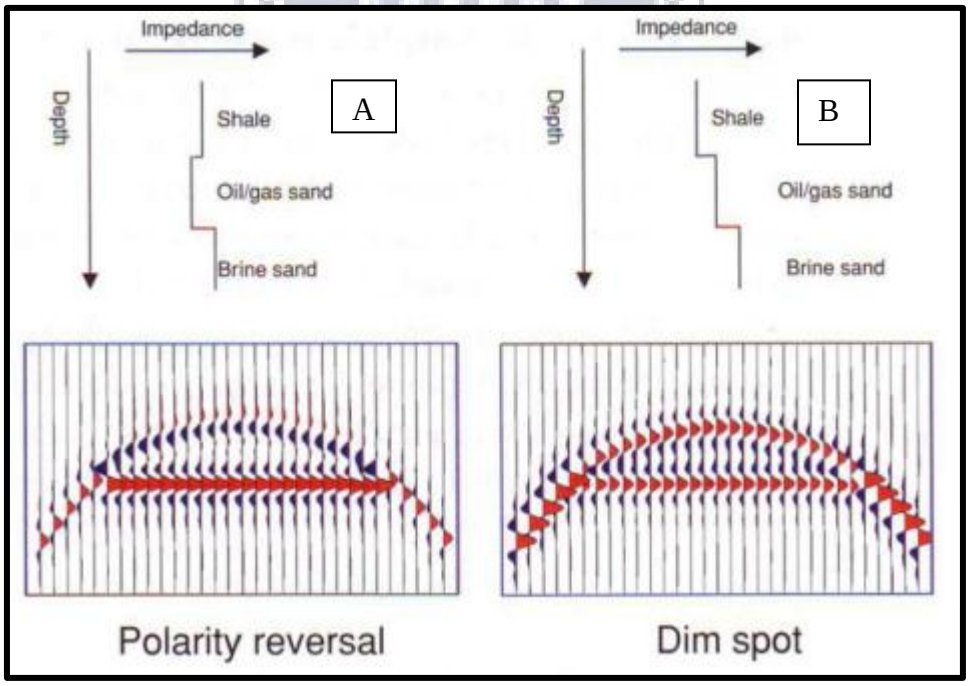

Figure a, b: showing schematic model of polarity reversal and dim spot for different oil/gas brine sand responses (Bacon et al., 2009). The red colour indicates hard loop (impedance increase) and the blue colour indicate soft loop (impedance decrease).

Therefore, the other areas to consider during the interpretation of a seismic data are many and the acoustic result of a gas accumulation usually depend on: the porosity, the depth, the overlying materials, Watersaturation and the reservoir configuration. Therefore, only amplitude anomaly observation might not enough to ascribe a hydrocarbon origin; thereby very significant to consider other effect produced by gas/oil presence on the seismic signal, mostly its components which are not only amplitude, but also frequency and phase.

However, many criteria have been proposed for the recognition of a gas accumulation in using them as direct hydrocarbon detection, an analysis of some of the criteria proposed by Anstey (1977) for hydrocarbon detection with the integration of recent literature data, in order to enable schematic structure use during the interpretation of a potentially gas-related seismic anomaly are discusses as below:

Appendix G: Review of gas-liquid contact seismic anomaly:

The gas-liquid contacts are the flat boundaries between the gas and water saturated sediments, usually seen at the compressed horizontal scale. The flat spots are easier to detect in tilted structure than in sub-horizontal succession, also indicating the feature that is hard to interpret. In seismic data of TWT (Two Way Time), flat spots are not really flat as a result of pull-down effect of the overlying gas sediments, characterized by lower velocity. In addition flat spots are more sensitive to diagenetic events which are depth dependent. This reflector may not be flat with the presence of minor faulting or change in permeability nature.

Appendix H: Review of Seismic Anomalous Reflection Frequency Coefficient:

The anomalous reflection coefficient related to the frequency content (low-frequency) and with the application of specific gain functions on the seismic signal. Abnormal amplitude also related with the interference and tuning effects which caused by the thin layered reservoir, at the points of the interference between the seismic and the pulse, constitute the top of the reservoir and the seismic pulse from the base of the present reservoir. Such example shown in figure (a) 6-60Hz bandwidth wedge model of material increasing in thickness from 0m to 30m with 0.3m increment (Bacon et al., 2009). The wedge materials are softer compared to the material below and above it. At the left sides of the figure where there is no sand, weak negative reflection occurs as a result of impedance contrast between the sand and the shale. The top of the sand was marked by a strong bleak loop (green line), and a white negative loop (blue line) at the base of the sand on the right of the figure. In situation like this, the top and the base of the wedge are obviously detectable for subsequence picking. As the sand becomes thinner, the separation between the top and the base of the loops got to a near constant value with thickness about 13m (as indicated by the yellow box) known as tuning thickness. Later on, the separation remain constant and any decrease in sand thickness will result in gradual amplitude decrease, due to the interference between the reflection at the sand top and base; these reflections overlap being a reverse polarity, they partially cancel each other (destructive interference). Below the 13m, both top and base are not visible as separate events as a result of insufficient vertical resolution.

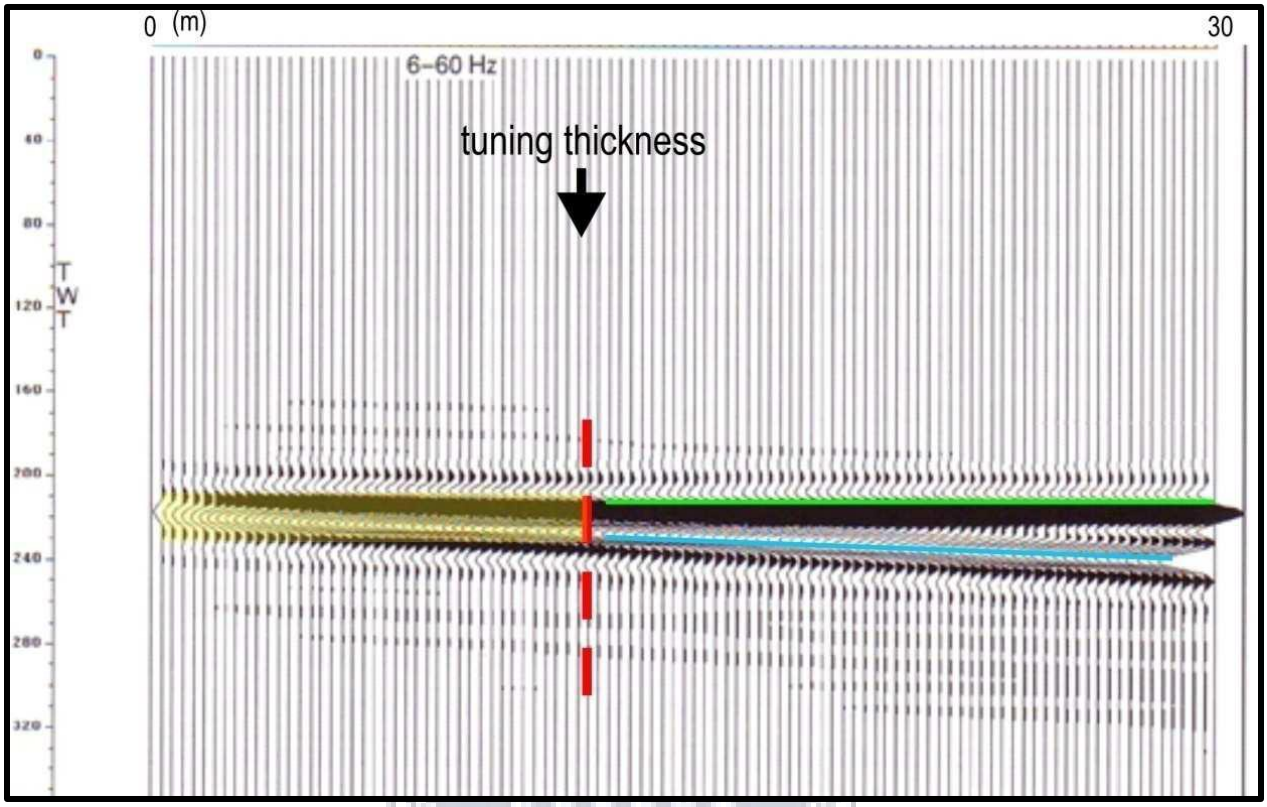

Figure showing the example of a wedge model for bandwidth 6-60 Hz, the red dashed line displays the tuning thickness point, while the green line constitute the top sand and the blue line its base (modified from Bacon et al., 2009).

On seismic sections retuning effect produces amaximum amplitude that could constitute a complication in the study of the amplitudes. Where the sand is saturated with gas, this situation complicates the quantitative measures of the sand thickness. The figure showing the gas sand as evidence; the amplitude of the gas bearing sand reflection is highest (yellow) on the flanks of the structure, at the points of clear tuning between the top sand and the base of decrease on the crest of the structure where the gas column should be greater (Bacon et al, 2009).

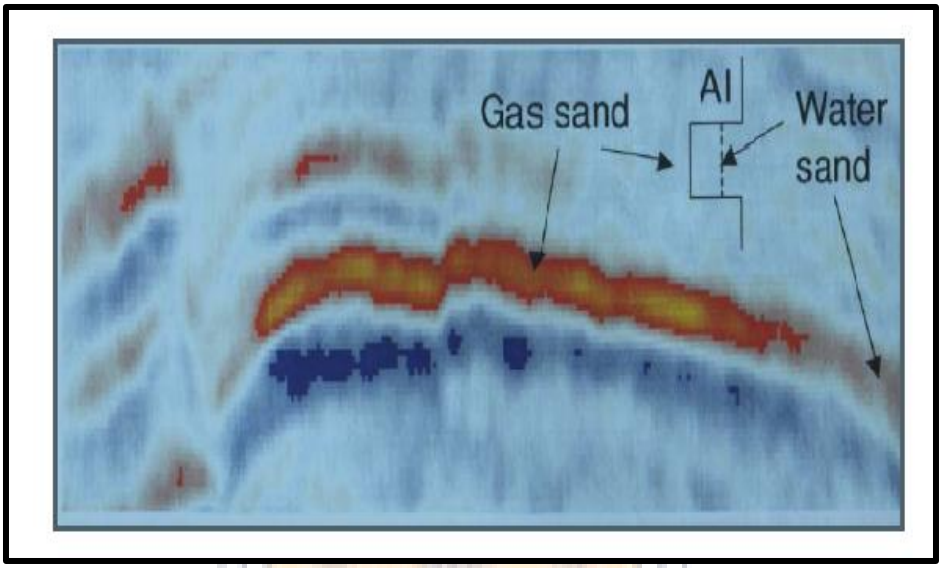

Figure showing seismic section indicating the seismic response on the flanks of structure with gas accumulation (Bacon et al., 2009)

However, there are some geological features of the amplitude anomaly that could be wrongly ascribed as a gas related bright spot; (Avseth et al, 2005). Such as:

- Top of salt diapirs
- Coal beds
- Overpressure sand and shale
- Low-porosity heterolithic sand
- Magmatic intrusion and volcanic ashes
- Highly-cemented sand, often calcite cement and thin pinch-out zone.

The first three features cause the same polarity of gas sand; and the last three features cause what is known as“hard kick” amplitude. However, once the polarity of the data is determined, it would be easier to assess the difference in or between associate bright spot from “hard kicks” anomalies. AVO (amplitude variation with offset) analysis is normally used to differentiate hydrocarbon from coal, salt or overpressured sand or shale.

Appendix I: Review of Shadows Anomalous Reflection Coefficient:

Reservoir filled with gas creates higher frequency-dependent seismic attenuation than similar rocks sufficiently saturated with brine. However, high frequency drop-off components are usually caused by oil and gas, and generate a low frequency zone (shadow) just at the base of the hydrocarbon saturated horizons. Seismic data usually indicate a decrease of high frequency contents in terms of late times acquisition, sometimes denoted by high frequency noises.

Castagna et al, (2002) proposed and display the result of spectral decomposition as seismic section represented as instantaneous amplitudes at specific frequencies. Figure shows the instantaneous amplitude sections at frequencies of 30 Hz and 60 Hz, in Gulf of Mexico gas reservoir, shows that below the reservoir top, the reflections are more attenuated at high frequency compared to low frequency. This kind of attenuation is normally observed in reservoir that has thickness sufficiently to accumulate significant attenuation, as the seismic energy travels up and down through the reservoir to ignore complications as a result of an interference top and base reflection (tuning).

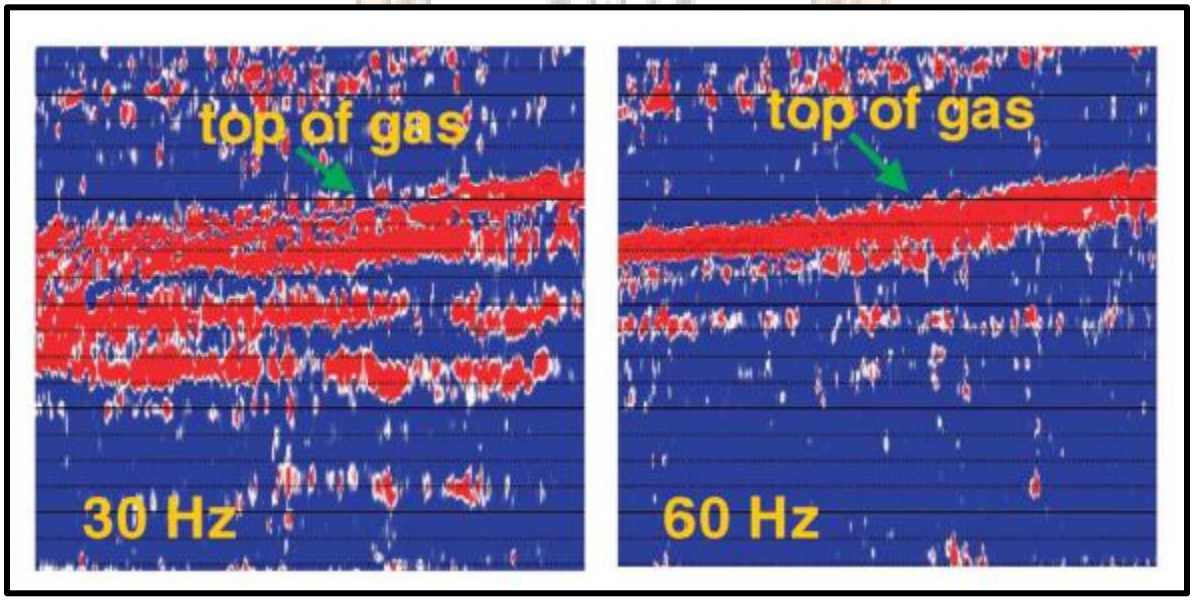

Figure showing Comparison between a 30 Hz and 60 Hz instantaneous amplitude seismic section over a gas reservoir in the Gulf of Mexico (Castagna et al., 2002)

The shadow presumed to relate with the additional energy occurring at low frequency, compared with higher frequency of attenuation. Figure shows the reservoirs that has high energy zone at frequency of 10 Hz, while higher energy zone absent at frequency of 30 Hz

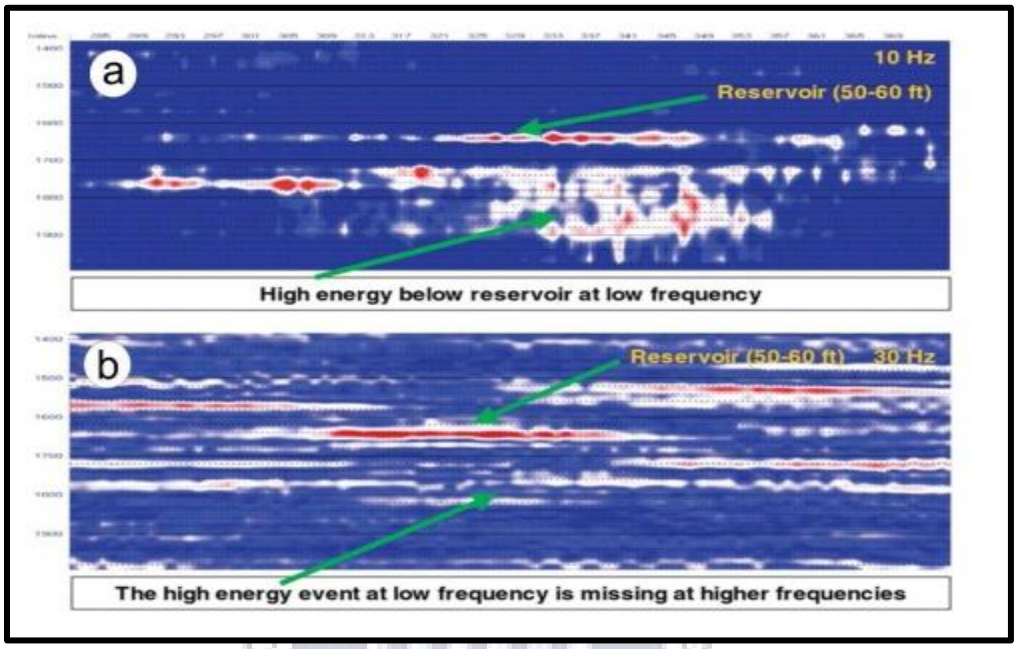

Figure showing Instantaneous Amplitude seismic section at (a) 10 and (b) 30 Hz, where the high energy at low frequency is more evident than higher frequency (Castagna et al., 2002)

Appendix J: Diffractions Anomalous Reflection Coefficient:

Diffractions are usually caused by acoustic impedance with strong contrasts, which are associated with a gas reservoir area of thickness and trapping fault mechanism. Also, absent in lenticular sand, with decrease thickness smoothly to zero in all direction. Sometimes, reef may be indicated and generating diffraction along the side only.

Finally, the compatibility among these points constitutes the last conditions proposed by Anstey; (1990) that the best option to conclude the analysis of the amplitude anomalies is to verifying the correlation of these aspects with the generating of potential geological subsurface model.

Appendix K: Gas seepage and sea-bed structures:

The presence of faults or micro-fracture system, constitute mode of migrating of fluids to the shallower sediments and the sea-bed. The mobility of gas/ hydrocarbon reveal a special feature on the seismic reflection data that could be related as direct hydrocarbon indicators, such as **gas chimney, pockmarks and particular carbonate/coral mounds.**

Appendix L: Gas chimney as gas seepage structure:

Gas chimney usually occurs majorly along the fault plane where there is relatively a gas movement from the deeper levels into the overburden, which is mainly constitute by shale with limited permeability (Bacon et al., 2009). Diffuse cloud of gas-bearing materials is usually the result, typically with low saturations also possibilities of little high-amplitude gas sand reflection at the top or within the body of the cloud showing in figure. But, the amplitude reduced at the base and within, it due to absorption and scattering. Thus rendered the amplitude measurements result meaningless. However, there is often a pull down velocity effect below the cloud, as a result of the velocity decrease in the gas –bearing layer; this can result in difficulty accurate structural mapping in depth.

Gas present in sediment usually not affected by shear-wave data, it can act as the best methods to image the horizontal below the cloud. This is not quite important, thou the gas within the chimney are very low to add any effect to the economic value, thereby, the present of chimney can reflect the area possible present of a leaking trap just at the base.

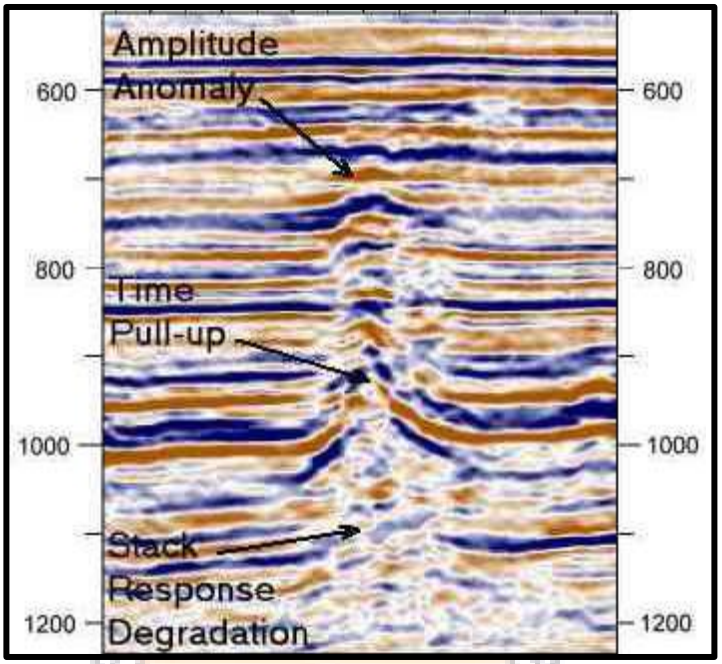

Figure showing the example of seismic imaging of a typical gas chimney: (Taken from http://www.explorationist.com)

Appendix M: Pockmarks as gas seepage structure:

Pockmarks are the structures formed when the escarpment of light hydrocarbon (e.g methane) pullout of sea bed, thereby formed a void from collapse sediments. This structure usually found along the continental margins, broad and irregular crater-like depressions in soft, fine grained sediments of the sea bed, thus attributed to episodic and catastrophic fluid expulsion (Hovland and Judd, 1988). However, pockmarks depend on two main factors such as:

- Sub-bottom hydrology I.e., hydraulically active conditions, as a result of presence of shallow gas or pressurised pore-water.
- A pockmarkable seabed made up of fine-grained sand, silt or clay.

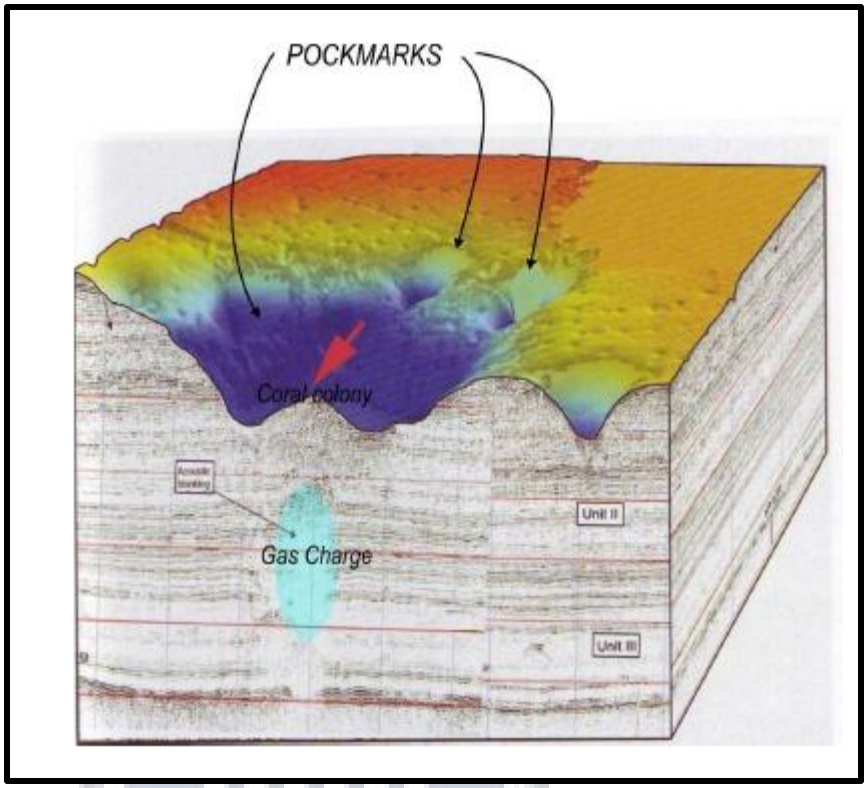

Figure showing example of pockmarks of Troll gas field (Norway) where coral colonies inside the main depression are evidenced; the seismic data displays a gas accumulation just below the sea bottom structures (modifies from Hoyland, 2008).

Appendix N: Carbonate or Coral Mounds as Gas seepage structure:

Carbonate or coral mounds are sometime develop well in water depth of low temperature that located at bottom sea pockmarks. Coral colonies as ''Lophelia Pertusa'' and ''Palagorgia''are absolutely related to gas seepage and normally found in gas field, such as in Norway offshore. However, in 1992, shallow seismic data showed prolific emission of gas through the seabed, with the presence of large patches of corals, sponges and bacteria masses, with geochemical samples showing evidence of high hydrocarbon. (Judd and Hovland, 2007).

Other gas-seepage that could be seen as sea-bed related structures are constituted by carbonate mounds which are produce by carbon precipitation with extremely large dimensions. They are characterised by a semi-transparent seismic facies as indicated in figure such examples are found in Ireland offshore, ''Lophelia'' has founded as giant carbonate mounds, up to

kilometre across their base and height as 400m and others are Holland mounds, Belgical mounds etc on the Atlantic margin.

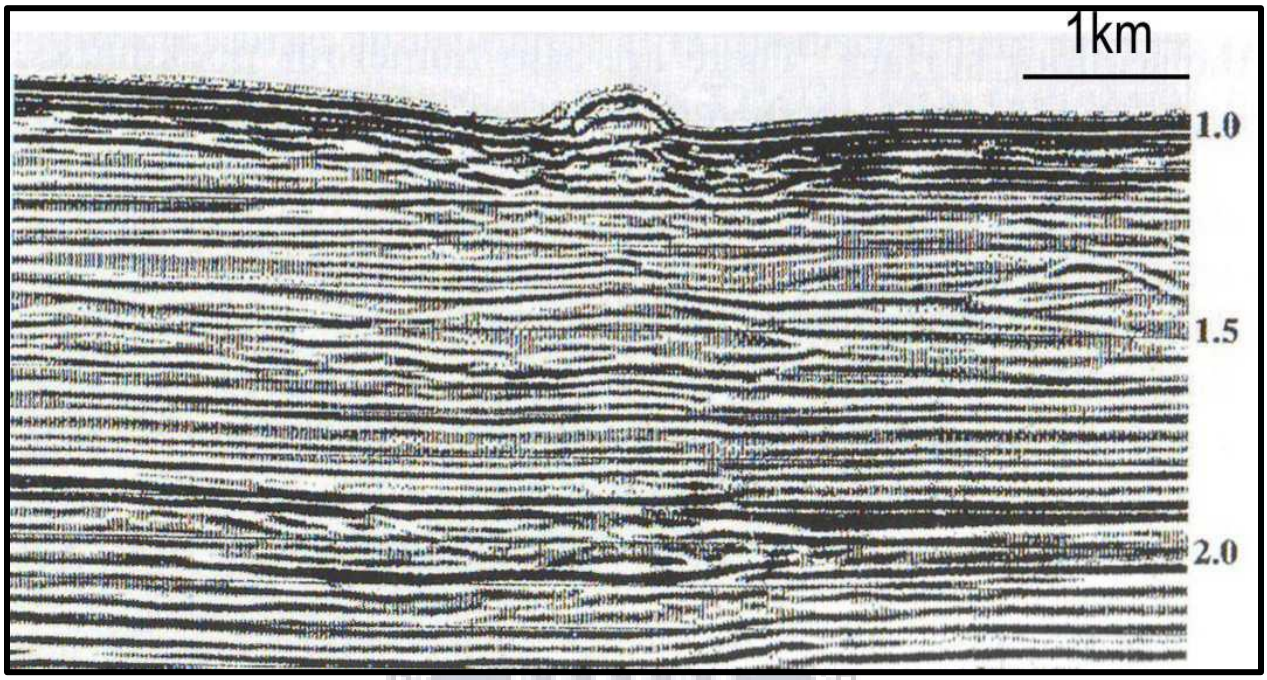

Figure showing Acoustic response of a carbonate mound from the Vulcan Sub Basin, off northwest Australia (modified by Hovland, 2008).

REFERENCES

Alberty, M.W., & McLean, M.R., (2003). Emerging trend in pressure prediction. Offshore Technology Conference, Paper 15290, 1-7.

Adeoye, T. O., and Enikanselu, P.A., (2009). Hydrocarbon Reservoir Mapping and Volumetric Analysis Using Seismic and Borehole Data over "Extreme" Field, South western Niger Delta; Ozean Journal of Applied Sciences 2(4).

AGIP, (1980). The wellsite geological activity in hydrocarbon exploration, Handbook. S. Donato Milanese: Agip-Milan

Ahmed, W., (2008). Contrast in clay mineralogy and their effect on reservoir properties in sandstone formations. Bulletin of Chemical Society of Ethiopia, 1, 41 - 65.

Aki, K., and Richards P.G., (1980). Quantitative Seismology. W.H. Freeman and Co.

Anstey, N. A., (1990).The seismic pulse – Its generation and transmission: GP 202 Exploration Geophysiscs Series, IHRDC.

Anstey N.A., (1977). Seismic Interpretation: the Physical Aspects. International Human Development Corporation, Boston. ISBN: 1-934634-01-7, pp. 625.

Athy, L.F., (1930). Density, pororsity, and compaction of sedimentary rocks. AAPG Bulletin, 14, 1-24.

Avseth P., Mukerji T., and Mavko, G., (2005). Quantitative seismic interpretation. Cambridge University Press, 359 pp.

Avseth, P.D., (n.d). Rock physics diagnostic of North Sea sand: Link between microstructure and seismic properties. Geophysical research letter, 27 (17), 2761 – 2764.

Babu, S., and Sircar, A., (2011). A comparative study of predicted and actual pore pressure in Tripura , India. Journal of Petroleum Technology and Alternative Fuels Vol 2(9), pp. 150 – 160.

Bacon, M., Simm, R., and Redshaw T., (2009). 3-D Seismic Interpretation. Cambridge University Press. Pp. 221.

Bally, A.W., Burbi, L., Cooper, L., Ghelardoni R., (1986). Balanced sections and seismic reflection profiles across the Central Apennines. Mem. Soc. Geol. Ital., 35, 257-310.

Barker, C., (1972). Aquathermal pressuring-role of temperature in development of abnormal-pressure zone. AAPG Bulleting, 80, 2068 – 2071.

Bate, K.J. and Malan, J.A., 1992, Tectonostratigraphic evolution of the Algoa, Gamtoos and Pletmos Basins, offshore South Africa *in :*De Wit, M.J. and Ransome, I.G.D. (Eds.), Inversion Tectonics of the Cape Fold Belt, Karoo and Cretaceous Basins of Southern Africa. A.A. Balkema, Rotterdam, 61 – 73.

Ben, E. L., (1994). Abnormal Pressure in Hydrocarbon Environments: AAPG Memoir, 70.

Braide, (2012). Petroleum development geology, lecture notes. Unpublished material.

Broad, D.S., (2000). Petroleum exploration offshore South Africa: Journal of African Earth Science, 31(1), 50 - 51.

Broad, D., (2004). South Africa activities and opportunities, an unpublished Power Point Presentation to PetroChina**.**

Broad, D.S., et al., 2006, Offshore Mesozoic basins. In Johnson, M.R., Anhaeusser, C.R., and Thomas, R.J. (Eds). The Geology of South Africa. Geological Society of South Africa. Johannesburg/Council for Geoscience Pretoria, 553-571

Brown, L.F. Jr., Benson, J.M., Brink, G.J., Doherty, S., Jollands, A., Jungslager, E.H.A., Keenan, J.H.G., Muntingh, A. and Van Wyk, N.J.S., (1996). Sequence stratigraphy in offshore South Africa divergent basins. An atlas on exploration for Cretaceous Lowstand traps by Soekor (Pty) Ltd American Association of Petroleum Geologist Studies in Geology, 41**,** 184.

Bjorlykke, K. & Hoeg, K., (1997). Effects of burial diagenesis on stress, compaction and fluid flow in sedimentary basins. Marine and Petroleum Geology, 14, pp. 267-276.

Bjorlykke, K., (1998). Clay mineral diagenesis in sedimentary basin: a key to the prediction of rock properties: examples from North Sea Basin. Clay Mineral, 33., pp 15 – 34.

Bourgoyne Jr, A. T., Millheim, K. K., Chenevert, M. E., & Young Jr, F. S., (1986). Applied drilling engineering. Volume 2.

Bowers, G.L., (1994). Pore pressure estimation form velocity data: accounting for overpressure mechanisms besides undercompaction. In: Proceeding of the 1994 lADC/SPE drilling Conference, 27488, pp. 515 - 530.

Bower, G., (1995). Pore pressure estimation from velocity data: Accounting for overpressure mechanisms besides undercompaction. SPE drillin & Completion,. 10 (2), pp 89 – 95.

Bowers, G.L., (1999). Pore pressure estimation form velocity data: accounting for overpressure mechanisms beside undercompaction: SPE Reprint Series, 49, pp.78 – 84.

Bowers, G.L., (2001). Determining an appropriate pore-pressure estimation strategy. Offshore Technology Conference, paper OTC 13042

Bowers, G.L., (2002). Detecting high pressure. The Leading Edge, 21, 174 - 177.

Bowers, G. L., and Katsube, T. J., (2002). The role of shale pore structure on the sensitivity of wireline logs to overpressure. In: A. Huffman and G.Bowers (Eds.), Pressure regimes in sedimentary basins and their prediction. AAPG Memoir 76, pp. 43 - 60.

Brace, W., (1972). Pore pressure in geophysics. Flow and fracture of rocks, 265-273.

Broad, D.S., (2000). Petroleum exploration offshore South Africa: Journal of African Sciences, 31(1), 50-51.

Brooks J. and Thusu B., (1977). Oil-source rock identification and characterization of the Jurassic sediments in the northern North Sea. Chem. Geol. 20 (1977), 283-94; Elsevier Scientific Publishing Company, Amsterdam [Originally, Publication No. 79 of the Continental Shelf Institute, Trondheim, Norway].

Brown, A. R., (2010). Dim Spots in Seismic Images as Hydrocarbon Indicators; Search and Discovery Article #40514.

Bruce., C. H., 1984, Smectite dehydration its relation to structural development and hydrocarbon accumulation in northern Gulf of Mexico Basin: AAPG Bulletin, Vol. 68, no 6, pp. 673 – 683.

Buffin, A., (2010). Petrophysic and pore pressure: Pitfall and perfection. Search and Discovery, Vol., 40654.

Burst, J.F., (1969). Diagenesis of gulf coast clayey sediments and its possible ralation to petroleum migration. AAPG Bulletin, 53, 73-93.

Carcione, J.M., and Helle, **H.B.,** (2002). Rock physics of geopressure and prediction of abnormal pore fluid pressure using seismic data: CSEG Recorder, Vol. (27/7), pp. 8-32.

Castagna, J.P., Sun, S., and Siegfried, R.W., (2002). The Use of Spectral Decomposition as a Hydrocarbon Indicator. GasTIPS, 24-27.

Castagna, J.P. and Swan, H.V., (1997). Principles of AVO crossplotting. The Leading Edge,

16, pp. 337-342.

Castagna, J.P, Swan H.W., and Foster D.J., (1998). Framework for AVO gradient and intercept interpretation. Geophysics, 63 (3), 948-956.

Castagna, J.P., Batzle, M.L., and Eastwood, R. L., (1985). Relationships between compressional-wave and shear-wave velocities in clastic silicate rocks: Geophysics, 50, 571-581.

Cibin, P., Pizzaferri, L., & Martera, M. D., (2008). Seismic Velocities for Pore- pressure prediction. 7th International Conference and Exposition on Petroleum Geophysics.

Chiburis, E., Leaney, S., Skidmore, C., Frank, C., & McHugo, S., (1993). Hydrocarbon detection with AVO. Oilfield Review, 5, pp 42-50.

Cheli, E., Brancato, Calogero. & Vagnoux, J.P., (1995). Woodie: A tool to support overpressure detection. SPE/IADC 29346.

Chilingar, G. V., Serebryakov, V. A., & Robertson, J.O., (2002). Origin and prediction of abnormal formation pressures. Developments in petroleum science, Elsevier.

Chopra, S., and Huffman, A., (2006). Velocity determination for pore pressure prediction: Leading Edge, Vol. (25/12) pp. 1502-1515.

Chopra, S., and Marfurt, K. J., (2005). Seismic Attributes-A historical perspective. Geophysics, 70(5), 3SO-28SO.

Colton-Bradley, V.A.C., (1987). Role of pressure in smectite dehydration - effects on geopressure and smectite to illite transition. AAPG Bulletin, 71, 1414-1427.

Daniel, R., (2001). Pressure prediction for a Central Graben wildcat well, UK North Sea. Marine and Petroleum Geology, 18, 235-250

Daines, S.R., (1982). Prediction of fracture gradient for wildcat wells. J. Petroleum Technol., Vol. (34) 4, 863 - 872.

Daw Robert N., Mercer, Richard F., & Myers, Donald L., (1975). Overpressure detection and control at IMP Immerk B-48 using wellsite mud gas detector. SPWLA, Annual Symposium.

De Swardt, A.M.J. and McLachlan, 1982, Petroleum exploration in the South African offshore: the geological framework and hydrocarbon potential *in* Proceedings of the 12th CMMI congress, Johannesburg (H.W. Glen, Ed.): Geological Society of South Africa, p. 17- 161

Dickinson, G., (1953). Geological aspects of abnormal reservoir pressure in Gulf Coast Louisiana. AAPG Bulletin, 37, pp. 410-432.

Dingle, R.V, Siesser, W.G., & Newton, A.R., (1983). Mesozoic and Tertiary Geology of Southern African. A.A. Balkema/Rotterdam. pp. 99 - 106.

Dix, C.H., (1955). Seismic velocities from surface measurements. Geophysics, 20, 68-86.

Domenico, S. N., (1977). Elastic properties of unconsolidated porous sand reservoirs. Geophysics, 42,1339-1368.

Domenico, S.N., (1984).Rock lithology and porosity determination from shear and compressional wave velocity. Geophysics, 49, 1188 - 1195.

Dutta, N. C., (2002). Geopressure prediction using seismic data: Current status. Geophysics, Vol.(67), No 6, pp 2012 -2041

Dutta, N. C., (2002). Deepwater geohazard prediction using prestack inversion of large offset P-wave data and rock model. The leading edge pp 193 – 198.

Dutta. (1987).

Eaton, B.A., (1975). The equation for Geopressure prediction from well logs: SPE 5544, 11 p.

Eaton, B. A., (1969). Fracture gradient prediction and its application in oil field operations. J.eTechnol., petroleum Vol.(21), 1353-1360.

Evers, J.F., & Ezeanyim, R., (1983). Prediction of abnormal pressure in Wyoming sedimentary basins using wireline logs. SPE-AIME, Meeting 11859, 363-374.

Fertl, W. H., & Timko, D.J., (1971). Parametrs for identification of overpressure formation. SPE 3223, pp. 125-131.

Forgotson, J., (1969). Indication of proximity of high pressure fluid reservoir, Louisana and Texas Gulf Coast". AAPG, 53, pp. 171-173.

Finetti, I.R., Ed. (2005). CROP Project: Deep seismic Exploration of the Central Mediterranean and Italy. Atlases in Geoscience 1, Elsevier, Amsterdam**.**

Frewin, J., Grobbler, N., & Feddersen, J., (2000). The Oribi and Oryx oil fields: geological characterisation of a deep-marine channel-lobe system, Block 9, Bredasdorp Basin, offshore South Africa. Journal of African Sciences, 31(1), 22.

Gardner, G.H.F., Gardner, L.W., and Gregory, A.R., (1974). Formation velocity and density:

the diagnostic basics for stratigraphic traps. Geopgysics, 39, 770-80.

Greenberg, M. L., and Castagna, **J. P.,** (1992). Shear-wave velocity estimation in porous rocks: Theoretical formulation, preliminary verification and applications: Geophysical Prospecting, 40, 195-210.

Goulty, N.R., (2004). Mechanical compaction behaviour of natural clays and implications for pore pressure estimation. Petroleum Geoscience, 10, 73-79.

Gregory, A.R., (1977). Aspects of rock physics from laboratory and log data that is important to seismic interpretation. In: Payton, C.E. (Ed.), Seismic stratigraphy - applications to hydrocarbon exploration. AAPG Memoir 26, pp. 15-45.

Goodway, B., Chen, T., and Downton, J., (1997). Improved AVO fluid detection and lithology discrimination using lame petrophysical parameters: ''λρ'', "μρ", and "λμ'' fuid stack'', from P and S inversions, CSEG Expanded Abstracts, 148 – 151.

Hammond, A.L., (1974). Bright spot: better seismological indicators of gas and oil. Science, 185(4150), 515-517.

Haq, B.U., Hardenbol, J., and Vail, P.R., (1988) Mesozoic and Cenozoic chronostratigraphy and eustatic cycles of sea-level change. In: The geology of South Africa edited by M.R Johnson, C.R Anhaesser and R.J Thomas. 2006.

Hilterman, F., (1998). Rock property framework for comprehending deep-water seismic response. Proceedings GSH, 1998 spring aa symposium, Ann. SEG Gulf Coast Tech. Mtg. Society of Exploration Geophysics.

Hilterman, F., (2001). Seismic amplitude interpretation: SEG, EAGE

Hottman, C.E., & Johnson, R. K., (1965). Estimation of formation pressure from log derived shale properties. Journal of Petroleum Technology, 717-722.

Hovland, M., (2008). Deep-Water Coral Reefs, Unique Biodiversity Hot-Spots. Springer Ed. pp.278.

Hovland, M., and Judd A.G., (1988). Seabed Pockmarks and Seepages-Impact og Geology, Byology and Marine Environment. Graham & Trotman Ed., London, pp. 293.

Hovland M., and Thomsen E., (1997). Cold water corals: Are they hydrocarbon seep related?. Marine Geology, 137, 159-164.

IHS Basin Monitor, 2010, Outeniqua Basin, South Africa.

Issler, D.R., (1991). A new approach to shale compaction and stratigraphic restoration,Beaufort – Mackenzie Basin and Mackenzie Corridor, Northern Canada. AAPG Bulletin, 76, 1170 – 1189.

Jiang, S., (2012). Clay Minerals from the Perspective of Oil and Gas Exploration.

Jikelo, N.A., (2000)**.** The natural gas resources of southern Africa: Journal of African Sciences, 31(1), 34.

Jungslager, E.H.A., 1999a, Petroleum habitats of the Atlantic margin of South Africa. *In:* Cameron, N.R., Bate, R.H. and Clure, V.S. (Eds.), The Oil and Gas Habitats of the South Atlantic. Spec. Publ. Geol. Soc. London, 153, 153 – 168.

Johansen, H., (1998). Kaolinite-to-dickite conversion series in sandstone reservoirs. Clay Minerals, 33, 297 - 316.

Jordden, J.R., & Shirley, O.J., (1966). Application of drilling performance data to overpressure detection. 1387-1394.

Judd A.G. and Hovland M., (2007). Submarine fluid flow, the Impact on Geology, biology, and the Marine Environment. Cambridge University Press, Cambridge, UK, pp. 475.

Katahara, K., (2003). Analysis of overpressure on the Gulf of Mexico shelf. Offshore Technology Conference, Paper 15293, 1-10.

Katahara, K., (2006). Overpressure and shale properties: stress unloading or smectite-illite transformation? 76th SEG Annual Meeting, Expanded Abstractss,, (pp. 11520-1524).

Knobloch, C., (1982). Pitfalls and merits of interpreting colour displays of geophysical data: 52nd Annual International Meeting, SEG, session S8.8.

Lahann, R.W., McCarty, D.K., & Hsieh, J.C.C., (2001). Influence of clay diagenesis on shale velocity and fluid-pressure . OTC 13046, Offshore Technology Conference.

Lahann, R., (2002). Impact of smectite diagenesis on compaction modelling and compaction equilibrium. In: Huffman, A.R. & Bowers, G.L. (eds) Pressure Regimes in Sedimentary basins and their Prediction. AAPG, Tulsa, 61-72.

Lahann, R.W., & Swarbick, R.E., (2011). Overpressure generation by load transfer following shale framework weakening due to smectite diagenesis. Geofluids, 11, 362-375.

Larsen, M. J., (1989). Geological Well Completion Report of borehole GA-AAs. Petroleum Agency/SoeKor (Pty) Ltd. South Africa.

Lesage, M., Hall, P., Pearson, J.R.A., & Thlercelln, M. J., (1991). Pore-pressure and fracture-gradient predictions. JPT/SPE, 652-654.

Luton. L. C., & Prieto., C., (2000). Accurate depth conversions reduce risk.

Luo, M., & Vasseur, G., (1992). Contribution of compaction and aquathermal pressuring to geopressure and the influence of environmental conditions. AAPG Bulletin, 76, 1550-1559.

Lopez-Solis, V., Pemex, Velazquez-Cruz, D., (2006). Normal resistivity trend for geopressure analysis, in Mexican Offshore Wells.

Magara, K., (1975). "Effect of Aquathermal Pressuring Effect in Gulf Coast". AAPG Bulletin 59, 10, 2037-2045.

Mallon, A.J., & Swarbrick, R.E., (2002). A compaction trend for non-reservoir North Sea Chalk. Marine and Petroleum Geology, 19, 527-539.

Martin, A.K., S.W. Goodlad, C.J.H. Hartnady and Du Plessis., A. 1982, Cretaceuous palaeopositions of the Falkland Plateau relative to southern Africa using Mesozoic sea-floor spreading anomalies. Geophys. J. R. astr. Soc 71:567-579.

Mathews, M., (2004). Uncertainity - shale pore pressure from borehole resisitivity. ARMA/NARMS Paper04-551.

Mathews, W.R., & Kelly, J., (1967). How to predict formation pressure and pressure gradient. Oil and Gas Journal, Vol. (65)8, 92-106.

Massaferro, J.L., Anselmetti, F.S., Eberu, G.P., Baechle, G.T., Bracco-Gartner, G. and Sun, Y. F., (2002). Effects of pore types on velocity and permeability in carbonates. Shell Exploration and Production Newsletter (EPNL), Special Issue "Seismic Petrophysics", Nov 2002.

McAloon, W., Barton, K., Egan, J., & Frewin, J., (2000) Pre-development characterisation of a marginal deep-marine channel/lobe-system reservoir: block 9, the Bredasdorp Basin, offshore South Africa. Journal of African Earth Sciences, 31, 47.

McLachlan, I.R., & Broad, D.S., (2000): Petroleum exploration offshore South Africa: Journal of African Sciences, 31(1), 50-5.

Mello, Ulisses T., & Karner, Garry D., (1996). Development of sedimentary overpressure and its effect on thermal maturation: Application to the Gulf of Mexico Basin. AAPG Bulletin,Vol. (80)9, 1367-1396.

Mocnik, A., (2011). Processing and Analysis of Seismic Reflection Data for Hydrocarbon Exploration in the Plio-Quaternary Marine Sediments. PhD Thesis, UNIVERSITÀ DEGLI STUDI DI TRIESTE.

Morris, K.A., & Shepperd, (1982). The role of clay minerals in influencing porosity and permeability characteristics in the Bridport sands of Witchy farm, Dorset: Clay Minerals*,* 17**,** 41 – 54.

Mouchet. J, P., & Mitchell., A. F., (1989), Abnormal pressures while drilling: Origins, Prediction, Detection, Elf Aquitaine Edition, Evaluation Techniques Manual Vol. 2, pp.225

Nations, J.F., et al. (1974). Lithology and porosity from acoustic shear and compressional wave transit time relationships. 15"' Ann. Symp. Soc. Prof. Well Log Analysts, McAllen, Texas.

Norton, I.Q., and Sclater, J.G., 1979, A model for the evolution of the Indian Ocean and the breakup of Gondwanaland. *J.* Geophys. Res. 85:6803- 6830.

Nietzsche, F., Common techniques for quantitative seismic interpretation.

Oyvind, K., (2005, January). Pore pressure estimation from single and repeated seismic data. PhD. Thesis.

Osborne, M. J., & Swarbricks, R. E., (1997). Mechanisms for generating overpressure in sedimentary basin: AAPG Bulletin, Vol. 81, pp. 1023 – 1041.

Ostrander, W.J., (1984). Plane wave reflection coefficients for gas sands at non-normal angles of incidence. Geophysics, 49, 1637-1648.

Pennebaker, E. S., (1968). Seismic data indicate depth and magnitude of abnormal pressure, World Oil, Vol. 166, 73 – 82.

Petroleum Agency SA (2004/005/006/2007). Petroleum exploration information and opportunities: Petroleum Agency Brochure.

Petroleum Agency SA Bronchures (2000-2005): South African Exploration Opportunities, Pp. 28, published by the South African Agency for Promotion of Petroleum Exploration and Exploitation, Cape Town.

Pilkington, P., (1999). Uses of pressure and temperature data in exploration and new development in overpressure detection. Pore Pressure and Fracture Gradients. SPE Reprint, 49, pp. 64-70.

Pickett, G.R., et al., (1963: 1974). Acoustic character logs and their applications in formation evaluation: 1. Can. Petr. Tech. 15, pp. 659 - 667.

Pironon, B. and Champanhet, J.M., (1992). Evaluation of Pliocene bright spots in the Adriatic Sea, Italy-volcanic ash or gas. First Break, 10(7).

Powers, M.C., (1969). Fluid realease mechanism in compacting marine mudrocks and their importance in oil exploration. AAPB Bulletin, 51, 1240-1254.

Prasad, M., Manghnani, M.H., (1997). Effect of pore and differential pressure on compressional wave velocity and quality factor in Berea and Michigan sandstones. Geophysics, 62, 4, pp.1163- 1176.

Øygard K., (2005). Risk assement, principle and Experiences. SINTEF Petroleum Research.

Rabia. H., Well Engineering and construction.

Raiga-Clemenceau, J., Martin, J.P. & Nicoletis, S., (1986). The concept of acoustic formation factor for more accurate porosity determination from sonic transit time data. SPWLA 27th Symposium, 1-14.

Ramdhan, A.M., & Goulty, N.R., (2010). Overpressure generating mechanisms in the Peciko Field, the Lower Kutai Basin. Petroleum Geoscience, 16, pp.367-376.

Ramdham, A.M., & Goulty, N.R., (2011)**.** Overpressure and shale compaction in the Lower Kutai Basin, Indonesia - a radical reappraisal. AAPG Bullettin, 95, pp. 1725-1744.

Ramseyer, K., & Boles, J. R., (1986). Mixed-layer illite/smectite minearals in Tertiary sandstones and shale, San Joaqui basin, Clays Clay Miner, 34, pp 115 – 124.

Rider, M., (2002). The geological interpretation of well logs. Second edition revised. Pp 26 – 30.

Roux, J., 1997, Soekor E andP: Potential Outlined in Southern Outeniqua Basin, off S. Africa, Oil and Gas Journal, July 21.

Russell, H., (1999). Theory of the Strata Program, Hampson-Russell Software Services.

Rutherford, S.R., and Williams, R.H., (1989).Amplitude-versus-offset variations in gas sands. Geophysics, 54, 680-688.

Ryan W. B.F., Hsü K.J., Cita M.B., Dumitrica P., Lort J., Maync W., Nesteroff W. D., Pautot G., Stradner H. and Wezel F. C., (1973). Boundary of Sardinia Slope with Balearic Abissal Plain – sites 133 and 134. In: Deep Sea Drilling Project, Vol. XIII, doi:10.2973/dsdp.proc.13.114.1973.

Sayer, C. M., Johnson, G. M., & Denyer, G., (2002). Predrill pore- pressure prediction using seismic data. Geophysic, 67 (4) 1286 – 1292.

Schlumberger, 1989, Log Interpretation Principle / Applications: Schlumberger Wireline and Testing, Houston, SMP-7017.

Schroot, B. M., & Schuttenhelm, R. T. E., (2003). Expressions of shallow gas in the Netherlands North Sea. Netherlands journal of Geosciences 82 (1), pp 91-105.

Selly, C. R., (1985). Elements of Petroleum Geology, W.H. Freeman and Co. New York.

Serra, O., (1986). Development in Petroleum Science: Fundamentals of Well Log Interpretation 2. The Interpretation of Logging Data, New York, Elsevier Science Publishing Company Inc., 15B, 684.

Shaker, S., (2007). Calibration of geopressure predictions using the normal compaction trend: Perception and pitfall. Geopressure Analysis Service (G.A.S) , East Stroudsburg, Pennsylvania, USA, pp 30 – 35.

Shokir, E. M., Detection and Prediction of the Abnormal Pressure value before, while and during drilling. Powerpoint: Available at, **Shuey, R. T.,** (1985). A simplification of the Zoeppritz equations: Geophysics, 50, 609-614.

Slotnick, M. M., (1936). On seismic computation with applications. Geophysics 1, pp 9-22.

Smith, G. and Gidlow, P.M., (1987). Weighted stacking for rock property estimation and detection of gas. Geophys. Prosp., 35, pp. 993-1014.

Sukmono, S., (2002). An Introduction to Seismik Reservoar Analysis, in Seismic Inversion and AVO Analysis for Reservoar Characterization, Department of Geophysical Engineering ITB, Bandung.

Suprajitno, M., (2000). Physical Aspect of Exploration Seismology, Geophysics Program of Mathematics and Science Department UI, Depok.

Swarbrick, R.E., Osborne, M.J., Grunberger, D., Yardley, G.S., Macleod, G., Aplin,

A.C., Larter, S.R., Knight, I. & Auld, H.A. (2011) Integrated Study of the Judy Field (Block 30/7a); an Overpressured Central North Sea Oil/Gas Field. Marine and Petroleum Geology, Elsevier. Oxford. 17**,** 993-1010.

Swarbrick, R.E., (2002). Challenges of Porosity-based Pore Pressure Prediction: CSEG Recorder, pp. 4.

Swarbrick, R.E. & Osborne, M.J., (1998). Mechanism that generate abnormal pressures: An overview. AAPG Memoir, 70, 13-32.

Swarbrick, R.E., Osborne, M.J., & Yardley, G.S., (2002). Comparison of overpressure magnitude resulting from the main generating mechanisms. In: Huffman, A.R. and Bowers, G.L. (eds), Pressure Regimes in Sedimentary Basins and their Prediction: AAPG, Tulsa,, 1-12.

Taner, M. T., and Sheriff, R. E., (1977). Application of amplitude, frequency, and other attributes to stratigraphic and hydrocarbon determination, In: C. E. Payton, ed., Applications to hydrocarbon exploration: American Association of Petroleum Geologists Memoir 26, 301–327.

Taner, M. T., (2001). Seismic attributes: Canadian Society of Exploration Geophysicists Recorder, 26, no. 9, 48–56.

Tatham, R.T., (1982). Vp/Vs and lithology. Geophysics, 47. Pp. 336 - 344.

Terzaghi, K., & Peck, R. B., (1948). Soil Mechanics in Engineering practice, John Wiley and Son.

Terzaghi, K., & Peck, R.B., (1967). Soil Mechanics in Engineering Practice 2nd Edition. New York. Pp.729 : John Wiley & Sons.

Tingay, M.R.P., Hillis, R.R., Swarbrick, R.E., Morley, C.K., & Damit, A.R., (2009). Origin of overpressure and pore-pressure prediction in the Baram province, Brunei. AAPG Bulletin, 83,, 51-74.

Tissot, B.P., & Welte, D.H., (1984). Petroleum Formation and Occurrence. Berlin, Springer-Verlag, 518.

Turner, J.R., Grobbler, N., & Sontundu, S., (2000). Geological modelling of the Aptian and Albian sequences within Block 9, the Bredasdorp Basin, offshore South Africa: Journal of African Sciences, 31(1), 80.

Vail, P.R., (1987). Seismic stratigraphy interpretation procedure. In: Bally, A.W. (Ed.), Atlas of Seismic Stratigraphy, American Association of Petroleum Geologists 27, 1 - 10.

Van der Spuy, D., (2000). Potential source rocks and modelled maturity levels in the southern Outeniqua Basin, offshore South Africa.

Walsh, J. B., (1981). Effect of pore pressure and confining pressure on fracture permeability. In: International Journal of Rock Mechanics and Mining Sciences & Geomechanics Abstracts Vol. (18), No. 5, pp. 429-435. Pergamon.

Wang, Z., (2001). Fundamentals of seismic rock physics: Geophysics, 66, 398-412.

Wayne D., Pennington, (2001). Reservoir Geophysics, In: Geophysics, vol. 66, no. 1 (January - February 2001); pp. 25–30.

Webster, M., O'Connor, S.A., Pindar, B. & Swarbrick, R.E. (2010). Overpressures in the Taranaki Basin: Distribution, Causes and Implications for Exploration. Proceedings of the AAPG GTW, Singapore.

White, R. S., Smith, L. K., Roberts, A. W., Christie, P. A., Kusznir, N. J., ISIMM Team., Roberts, A. M., Healy, D., Spitzer, R., Chappell, A., Eccle, J, D., Fletcher, R., Hurst, N., Lunnon, Z., Parkin, C. J., & Tymms, V, J., (2008). Lower –Crustal intrusion on the North Atlantic continental margin. Journal of nature, vol. 452, pp.460 – 464.

Wood, E.M., (1995) Oil and gas development potential in Block 9, the Bredasdorp Basin, offshore South Africa. Oil & Gas Journal, 27th June, 2010.

Yassir, N., & Addis, M.A., (2002). Relationship between pore pressure stress in different tectonic setting, in pressure regimes in sedimentary basin and their prediction, In: Alan R.; Huffman & Bowers, G., (Eds) America Association of petroleum Geologists Publication.

Yoshida, C., Ikeda, S. & Eaton, B.A., (1996). An Investigative Study of Recent Technologies Used for Prediction, Detection, and Evaluation of Abnornal Formation Pressure in North and South America. IADC/SPE.

Yilmaz, O.z., (2001). Seismic data analysis: processing, inversion, and interpretation of seismic data. Society of Exploration Geophysicists, investigations in geophysics No.10,Tulsa, OK, USA, 1/2, pp. 2027.

Zhang, J., & Roegier J.C., (2005). Double porosity finite element method for borehole modeling. Rock mechanics and rock Engineering. Vol. 38, no 3. pp. 217-242.

Zhang, J., (2011). Pore pressure prediction from well logs: methods, modification, and new approaches. Earth-Science Reviews, 108(1), pp 50-63.

Zoeppritz, R., (1919). On The Reflection and Propagation of Seismic Waves, Erdbebenwellen VIIIB; Gottinger Nachrichten l, 66-68.

Electronic References:

http://www.explorationist.com: accessed on: 10th/April/2013

http://infohost.nmt.edu/~petro/faculty/Engler370/fmev-chap10-neutronlog.pdf Access on 18/August/ 2013.

tp://faculty.ksu.edu.sa/shokir/PGE472/Lectures/Abnormal%20pressure.pdf. Access on 15th April, 2013.

http://www.spwla.org/library_info/glossary) Access on 18th /April, /2013.

http://infohost.nmt.edu/~petro/faculty/Engler370/fmev-chap10-neutronlog.pdf Access on 18/August/ 2013.

http://www.ge-enegy.com/

energy.com/products_and_services/products/wireline_systems/compensated_neutron_log.jsp

Accessed on 18th /august/2013.